PRECISE NULLING OF ATTITUDE AND MOTION ERRORS OF A SPACECRAFT USING A PHASE SPACE AUTOPILOT

by

MARY LOUISE KELLOGG

B.S.E., Princeton University

(1976)

SUBMITTED IN PARTIAL FULFILLMENT

OF THE REQUIREMENTS FOR THE

DEGREE OF MASTER OF SCIENCE

at the

MASSACHUSETTS INSTITUTE OF TECHNOLOGY

September, 1978

Signature of Author Signature redacted
Department of Aeronautics and Astronautics

Approved by Signature redacted
Technical Supervisor, CSDL

Certified by Signature redacted
Thesis Supervisor

Accepted by Signature redacted
Chairman, Departmental Graduate Committee

PRECISE NULLING OF ATTITUDE AND MOTION ERRORS
OF A SPACECRAFT USING A PHASE SPACE AUTOPILOT

by

Mary Louise Kellogg

Submitted to the Department of
Aeronautics and Astronautics on June 20, 1978,
in partial fulfillment of the requirements for
the degree of Master of Science

ABSTRACT

A phase space autopilot is designed for the control problem of the precise nulling of the residual attitude and motion errors of a reaction-jet controlled spacecraft following a maneuver. The phase space technique, which coordinates control for all six degrees of freedom of the vehicle, produces alternating periods of coasting and jet firing to rapidly converge on an end state of constant commanded attitude and constant commanded translational velocity. IMU measured velocity and attitude data is processed by a rate estimator while the vehicle is coasting. This estimator provides inputs to a control law which combines these inputs with commanded attitude and rates to generate a six-dimensional "rate change request vector". The request vector, in turn, is used by a jet selection routine which selects and commands firing times for jets to produce the changes requested in angular and translational velocities.

Two jet selection algorithms are compared. One, called the "pseudo inverse" method is based on a matrix manipulation procedure which provides an optimization of the jet selection process. The other jet selection procedure uses predetermined combinations of jets to satisfy each component of the rate change request vector and requires significantly less computation time than the pseudo inverse method while providing comparable performance.

Two alternative jet firing policies were studied. One initiates all jet firings simultaneously and terminates individual firings when commanded firing times have elapsed. The other policy divides some of the shorter firing times into several segments which are distributed within the interval of the longest firing jets in a manner to reduce excursions in attitude and rate.

Simulation results of the phase space autopilot and its alternative features are presented.

Thesis Supervisor: David G. Jansson
Title: Assistant Professor of
Aeronautics and Astronautics

ACKNOWLEDGMENTS

For their invaluable assistance with this project, I would like to express my deep gratitude to the following people: to Ed Bergmann, whose earlier studies served as a foundation for this thesis; to Dick Goss, whose careful editing helped give clear expression to the ideas and material contained in this thesis; and especially to Gil Stubbs, without whose advice, assistance, concern, and constant good humor, this thesis simply would not have been possible.

This report was prepared at The Charles Stark Draper Laboratory, Inc., under Contract F04704-78-C-0002 with the Space and Missile Systems Organization of the Air Force Systems Command.

Publication of this report does not constitute approval by the Draper Laboratory or the U.S. Air Force of the findings or conclusions contained herein. It is published for the exchange and stimulation of ideas.

TABLE OF CONTENTS

Table of Contents (Cont.)

LIST OF FIGURES

List of Figures (Cont.)

List of Figures (Cont.)

LIST OF TABLES

CHAPTER 1

INTRODUCTION

The problem of achieving a desired end state in minimum time for a reaction-jet-controlled spacecraft will be investigated and used as a basis for developing and evaluating new concepts in the group of control techniques known as "phase space control". For this study, the spacecraft is to be controlled to achieve desired terminal conditions of constant attitude and constant translational velocity. It is assumed that initial errors in these quantities have resulted from a prior attitude and/or translational maneuver. The initial errors in attitude and attitude rate are expected not to exceed 1 deg and 1 deg/sec about each of the body axes. The initial errors in translational velocity are typically 2 ft/sec along each of the body axes. However extreme cases were investiagted in which maximum initial translational velocity errors were as large as 6 ft/sec. The nulling of these state errors in minimum time can be a difficult problem if the precision required for the end state approaches the limits of measurement accuracy of the inertial measurement unit (IMU) and uncertainties in jet control. The time required to reach the desired end state with a specified precision is strongly influenced by the manner in which the vehicle state is estimated from measurements and by the manner in which these estimates are processed to generate jet-firing commands. The conventional approach[1,2] to this control problem is to employ independent roll, pitch and yaw control channels, whose jet-firing commands are determined by some function of the errors in attitude, angular

rate and translational velocity. This approach implements rotational control in terms of a phase-plane representation of angular-rate error versus angular error for each axis. The estimated position in this phase plane, in relation to switching boundaries and/or control regions, is used to determine the jet-firing commands for rotational changes. The firing commands for rotational and translational control can be in the form of on-off commands issued to each jet every control cycle period, or they can be in the form of total firing times computed for each jet (as determined from predicted phase-plane trajectories which will result from these firing times). The selection of the jets which will be employed by each channel is most often done by a "table look-up", in which the jets assigned to translational and rotational control in each channel are predetermined as a function of the variable mass properties of the vehicle and the maneuver to be performed.

In the conventional phase-plane approach, the coupling effects between control channels and between the rotational and translational control modes are treated as disturbances which are to be nulled out in the process of feedback control. Unfortunately, the timing and magnitude of these disturbances in any one control channel cannot easily be predicted because of the assumed independence of the three channels and because of the separation of translational and rotational controls in each channel. These disturbances also complicate the problem of including jet-firing effects in estimating the angular rate and translational velocity for each autopilot channel.

The conventional procedure of committing certain individual jets or groups of jets to rotational and translational control on a per-axis basis may also be inefficient in applications where the jets are not conveniently located relative to the control axes. Moreover, this procedure may turn out to be cumbersome in applications where

alternate sets of jets must be tabulated to accommodate variable mass properties or to compensate for the inhibiting of jets because of failures or operational constraints.

The foregoing difficulties of the phase-plane method seem to be largely overcome by the use of a new "phase space" control approach developed originally by E. Bergmann.[3] The term "phase space" refers to the fact that this autopilot uses "rate" and "position" vectors in place of the "rate" and "position" scalars of the phase plane approach. These vectors, which can include body-axis components of both translation and rotation, form the basis for a control approach that can conveniently coordinate rotation and translation for all the three body axes, simultaneously.*

The development and evaluation of a modified phase space approach for application to the particular problem of precisely achieving a constant attitude and constant translational velocity in minimum time will be the object of this thesis. The modified phase space approach, resulting from this effort has some options which offer new performance capabilities and other options which offer a more efficient utilization of flight computer time than even the relatively crude phase-plane control approach.

---

* The generalized phase space autopilot developed by Bergmann employed a six-dimensional phase-space control law—and a linear programming jet selection. The autopilot was tested in a simulation of the NASA Space Shuttle. Also, the phase space autopilot was compared with the exisiting phase plane autopilot for the shuttle and shown to require 35.4% fewer words of core memory, 20.5% less average CPU time, up to 65% fewer firings, and consume up to 25.7% less propellant for the cases tested. It also proved capable of maintaining control in the presence of a large number of jet failures.

CHAPTER 2

PHASE SPACE CONTROL

2.1 General Formulation

The phase space autopilot concept generates a "rate change request" vector based on the magnitudes and directions of error vectors in "rate" and "position" similar to a phase-plane autopilot concept which determines jet firing-time commands based on achieving a certain change in angular rate, according to the phase-plane relationship between angular rate error and angular error. As mentioned previously, the "rate" error vector, in general, includes three body-axis components of angular rate error and three body-axis components of translational velocity error. Similarly, the "position" error vector, in general, includes body-axis components of angular error and position error. When certain specified limits on these rate and position vectors are exceeded during the autopilot operation, the vectors are examined in relation to each other in a control law to generate the rate change request vector. This request vector, composed of three angular rate components and three translational velocity components (all referred to body axes) is then employed by a jet selection routine to determine the separate firing times for the individual reaction control jets.

In addition to the benefits of combined three-axis, six degree-of-freedom control offered by the phase-space approach, this method offers a very useful feature of allowing relatively long coasting periods between jet firings. These coasting periods can be employed

to great advantage in estimating angular rate and translational velocity by allowing the use of simple averaging methods to reduce the effects of measurement noise.

The phase space approach permits a considerable degree of flexibility and generality in its jet selection, since the rate request vector indicates the net effect required from all jet firings. Various schemes have been developed to select the jets to be fired and to compute their firing times based on the rate request vector. Two of these schemes are covered in this thesis.

2.2 New Formulation and Concepts

A simplified version of the original phase space autopilot will be presented in this thesis. The basic elements and organization of this simplified version are shown in the block diagram of Figure 2.1 and in the flow chart of Figure 2.2. The basic variables of the autopilot are defined in Table 2-1.

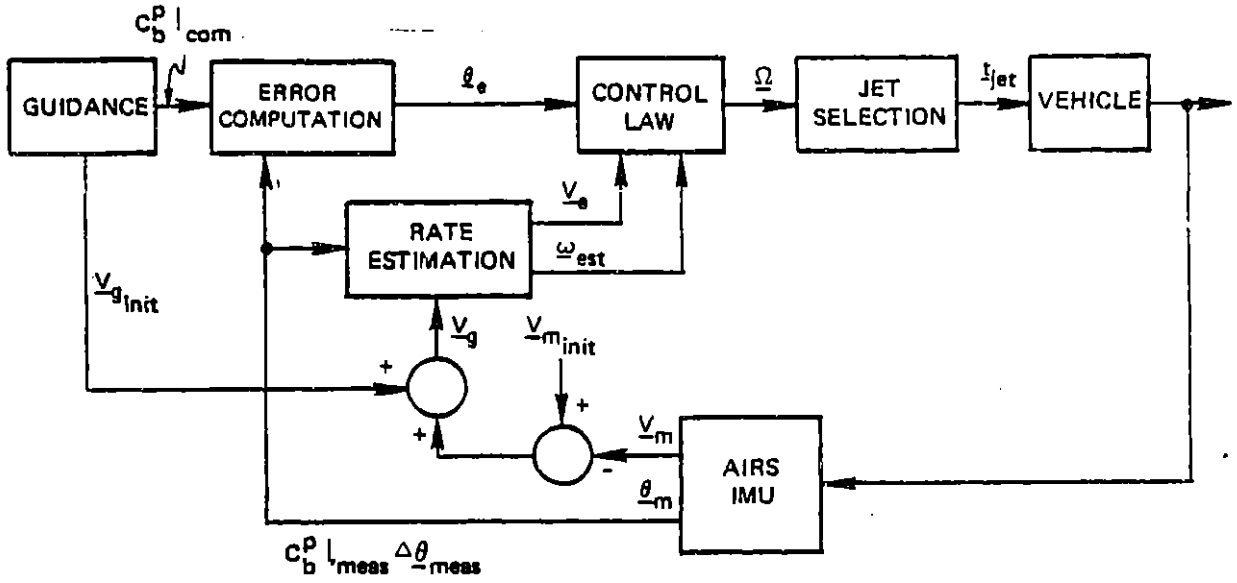

Figure 2.1. Functional block diagram of the phase space autopilot.

Table 2-1. Definition of basic variables of the phase space autopilot.

Variable	Definition
$C_b^p\|_{com}$	Platform-to-commanded-body-axes transformation
$C_b^p\|_{meas}$	Measured platform-to-body-axes transformation
$\underline{\Delta\theta}$	Body-angle increment vector, computed from measured AIRS band-angle increments
$\underline{\theta}_e$	Measured attitude error vector (angular components about body axes)
$\underline{\omega}_{est}$	Estimated angular rate vector (rate components about body axes)
$\underline{V}_{g_{init}}$	Initial value of the velocity-to-be-gained vector (platform coordinates)
$\underline{V}_{m_{init}}$	Initial measured velocity (platform coordinates)
$\underline{V}_m$	Current measured velocity (platform coordinates)
$\underline{V}_g$	Current velocity-to-be-gained (platform coordinates)
$\underline{V}_e$	Estimated velocity error at the center of mass (body coordinates)
$\underline{\Omega}$	Rate change request vector (body coordinates)
$\underline{t}_{jet}$	Commanded jet-firing-time vector

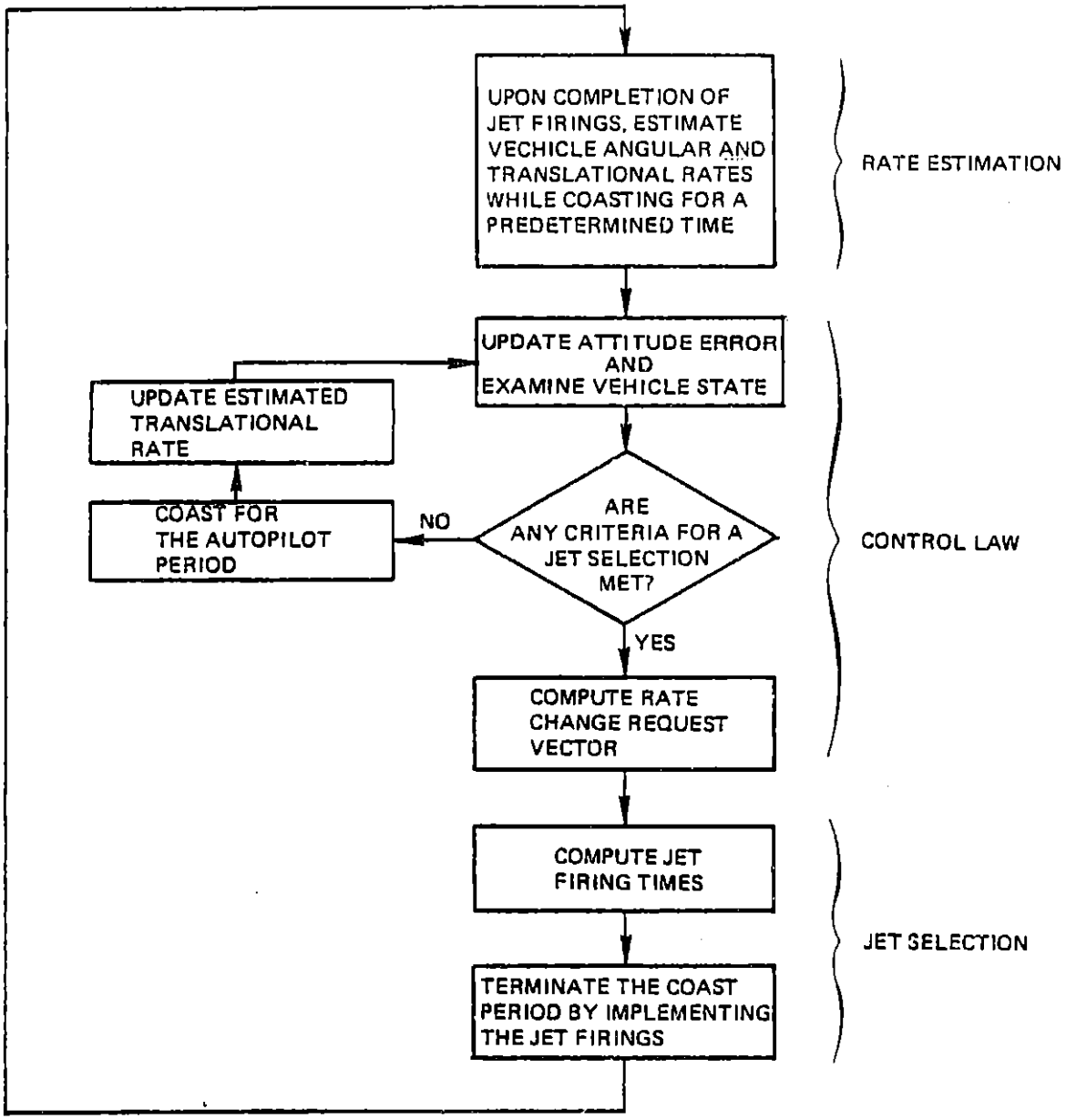

Figure 2.2. Sequence of operations of the phase space autopilot.

Like the original phase space autopilot the new version performs rate estimation, control law computations and jet selection. However, the implementation of these functions is quite different than in the original autopilot.

The simplified phase space autopilot has several major features which are outlined below and discussed in detail in subsequent chapters on this thesis.

2.2.1 Simplified Computation of Rate Change Request

The generation of the rate change request vector by the general phase space control law takes into account the fact that the requested changes in angular rate and translational velocity will also impact the angular position and translational position. However, for the particular control problem considered in this thesis there is no translational position requirement. Therefore, the simplified autopilot does not consider the translational position effects of the translational velocity changes but merely uses the translational velocity errors directly in the six-dimensional rate change request vector (shown as $\underline{\Omega}$ in Figure 2.1). The angular rate components of this vector, on the other hand, are computed by considering both an estimated angular rate error vector, $\underline{\omega}_{est}$, and an estimated angular error vector, $\underline{\theta}_e$.

2.2.2 Jet Selection Alternatives

Two alternative jet selection procedures are investigated in place of the linear programming jet select algorithm which was employed in the original approach and tested in the Space Shuttle simulation. Linear programming is the most general algorithm known for linearized fuel or time optimal jet selection in systems with many jets, significant variations in mass properties or a need for maximum fault tolerance. Its benefits are clear. However, in systems with few jets, and nearly

static mass properties, the computational burden of the linear jet select algorithm in comparison to simpler algorithms (such as those investigated in this thesis) may be too great to justify its use.

The two jet selection routines considered in this thesis compute the total firing times, $\underline{t}_{jet}$, for all the jets based on the six-dimensional rate change request vector $\underline{\Omega}$, as shown in Figure 2.1.

One of the two jet selection methods considered in the thesis is the "pseudo inverse" method, based on a matrix manipulation procedure. This method is not as suitable as linear programming for a large number of jets but does provide an optimization of the jet selection process for the limited number of jets considered in this thesis.

The second jet selection procedure which was investigated is a simple fixed selection routine involving (1) the initial computation of firing times to meet the translational velocity change request and (2) the subsequent computation of jet firings to meet the angular rate change request, taking into account the effects of translational jet firings on angular velocity.

The first of these jet selection approaches provides efficient use of the jets at the expense of relatively long computation time, while the second approach is relatively inefficient in its jet utilization but requires much less computation time.

2.2.3 "Parceling Out" of Jet Firings

Another basic revision to the original phase space concept is the addition of an alternative to the original concept of starting all jet firings simultaneously and terminating each jet firing according to its jet-selection-determined firing time. This alternative policy fires the shorter-firing jets more than once during the interval of the longest-firing jet. The total impulse determined by the jet selection routine for each jet is retained in computing the separate firings. The objective of this "parceling out" of jet firings is to reduce the attitude changes which can, in some cases, result from drastically different firing times.

2.2.4 Rate Estimation During Coast

The original phase space autopilot performed rate estimation continually, which required that the effects of the jet firings be included in the rate estimator. The new approach avoids the uncertainties and complexity of incorporating jet firing effects by estimating the angular rate and translational velocity only while coasting.

2.2.5 No-Interrupt Feature

The new phase space concept differs also in that there is no provision for interrupting either the rate estimation coast period or the execution of jet firings. The duration of the uninterrupted sequence of jet firings is determined by the jet selection routine, and the duration of the rate-estimation coast period following these firings is predetermined by the accuracy requirements of the particular estimation.

These and other features of the control law, jet selection and rate estimation are developed and discussed in detail in Chapters 3, 4 and 5, respectively. All of these elements are combined for evaluation in a simulation. This is discussed in Chapters 6, and 7. Conclusions are presented in Chapter 8.

CHAPTER 3

THE CONTROL LAW

3.1 Introduction

The phase space control law is developed here for a specific spacecraft control problem in which it is required to achieve in a minimum time and with relatively high precision a constant commanded attitude, a constant commanded translational velocity, and zero angular rate. These requirements are assumed to be specified by the guidance system. For this study the specified tolerance for the magnitude of the attitude error vector is 0.5 degrees. The tolerance for the attitude rate is 0.1 deg/sec for each component of the rate vector expressed in body coordinates. The tolerance for the translational velocity if 0.05 ft/sec for each component of the velocity error vector expressed in body coordinates. For this application, the control law is designed to allow uninterrupted periods of coasting to be used for the estimation of angular rate and translational velocity. Estimation during coasting avoids the necessity of modeling jet-produced accelerations during jet firings and substantially decreases the computer burden compared to a policty which requires estimation during jet firings. However, there is a trade-off between reduced computation time and increased time required for achieving the commanded state.

The next section (3.2) presents the equations used in generating a six-dimensional rate change request vector which specifies desired corrections to the vehicle's trajectory. In the last section (3.3), the control decisions which determine when and how the corrections will be computed and implemented are discussed.

3.2 Computation of the Rate Change Request Vector

3.2.1 General

One function of the control law is to generate a six-dimensional rate change request vector, $\underline{\Omega}$

$$\underline{\Omega} = \begin{bmatrix} \Delta\underline{\omega}_c \\ \cdots\cdots \\ \underline{V}_e \end{bmatrix} \tag{3.1}$$

Three components of the request vector $\underline{\Omega}$ are requested changes in translational velocity along the body axes. These components comprise the vector $\underline{V}_e$, which is determined from the velocity-to-be-gained vector supplied by the guidance system. The other three components of $\underline{\Omega}$ are requested changes in angular rates about the three body axes. These components comprise the vector $\Delta\underline{\omega}_c$, which is computed by the control law.

3.2.2 Requested Change in Translational Velocity

The velocity-to-be-gained vector, $\underline{V}_g$, represents an error in the translational velocity of the IMU which must be nulled out by the action of the control system. This vector is initialized by the guidance system and then updated by the control system to incorporate the effects of changes in the IMU—sensed velocity. (It is assumed that the guidance system already compensates for gravity effects, so that gravity-produced changes in velocity need not be included in this updating process.)

Since the IMU is not located at the vehicle center of mass, the nulling of $\underline{V}_g$ can be accomplished by any combination of translational velocity at the vehicle center of mass and vehicle rotational velocity which would yield the desired velocity at the IMU. However, since the vehicle angular rate is to be nulled independently of any $\underline{V}_g$ requirement, it is convenient to delete from $\underline{V}_g$ the effects of the velocity

at the IMU resulting from vehicle rotation rates. This deletion amounts to determing a translational velocity-to-be-gained at the vehicle center of mass, which is the vector $\underline{V}_e$ used in the control law.

The computation of $\underline{V}_e$ involves first the determination of an estimated velocity-to-be-gained, $\underline{V}_{g_{est}}$, based on averaging the coast-period computations of $\underline{V}_g$ (performed every autopilot cycle). The value of $\underline{V}_{g_{est}}$ is computed no more than twice during a coast period: first, immediately upon the completion of an angular rate estimation, and possibly once more if there is additional coasting before performing a jet selection. Each time $\underline{V}_{g_{est}}$ is computed it is transformed to body coordinates and the effects of angular motion deleted through the use of the coast-period estimation of angular rate, $\underline{\omega}_{est}$. The resulting vector is $\underline{V}_e$, which is the translational portion of the rate change vector $\underline{\Omega}$.

The steps for computing $\underline{V}_e$ are summarized as follows in terms of the mathematical relationships which must be implemented:

1. At the end of each rate estimation period and subsequently if the coast period is extended, generate an estimated velocity-to-be-gained, $\underline{V}_{g_{est}}$, according to the relationship

$$\underline{V}_{g_{est}} = \underline{V}_{g_{init}} - \frac{1}{k}\sum_{i=1}^{k} \underline{V}_{m_i} + \underline{V}_{m_{init}} \qquad (3.2)$$

where

$\underline{V}_{g_{init}}$ = initial velocity-to-be-gained vector, supplied by the guidance system at the beginning of the control system's nulling operations

$\underline{V}_{m_{init}}$ = initial value of the measured velocity, $\underline{V}_m$, (at the instant when $\underline{V}_{g_{init}}$ is supplied)

$\underline{V}_{m_i}$ = IMU accelerometer—measured velocity, sampled at the i^{th} autopilot sampling time during the coast period

k = number of autopilot cycles in the coast period

2. Transform $\underline{V}_{g_{est}}$ from IMU platform coordinates to body coordinates and delete the effects of angular rotation using the angular rate estimation $\underline{\omega}_{est}$ which was computed from coasting period data. The resulting vector is $\underline{V}_e$

$$\underline{V}_e = C_b^p \underline{V}_{g_{est}} - \underline{\omega}_{est} \times \underline{R}_{IMU} \qquad (3.3)$$

Here, C_b^p is the measured platform-to-body transformation matrix and $\underline{R}_{IMU}$ is a vector which represents the position of the IMU with respect to the center of mass of the vehicle.

It should be pointed out that if translational position control were required it would be necessary to determine a translational rate change request vector $\underline{V}_e$ which is a function of both positional errors and translational velocity errors. However, for the purposes of this thesis it was assumed that position control was not required in which case the translational velocity changes required (and requested) are merely the translational velocity errors. By contrast, both the angular position and the angular rates must be considered in the determination of the rotational portion of $\underline{\Omega}$, which leads to the more complicated formulation described in Section 3.2.3.

3.2.3 Requested Change in Angular Velocity

The attitude control problem has two conflicting goals. First, the vehicle attitude vector, $\underline{\theta}$ must be driven to the commanded vector $\underline{\theta}_c$. This requires a non-zero vehicle angular rate vector, $\underline{\omega}$. Second, the vehicle angular rate must be driven to a desired terminal value of

zero. The phase approach provides a means for iteratively homing in on both of these goals by using a variable coefficient equation to determine the commanded angular rate $\underline{\omega}_c$ which is employed in the computation of the angular rate change request $\Delta\underline{\omega}_c$. This equation gives precedence to the attitude goal when the attitude error vector $\underline{\theta}_e$ is large in magnitude and then gives an increasing emphasis to the zero angular rate goal as $|\underline{\theta}_e|$ approaches zero. This error vector $\underline{\theta}_e$ is initialized and updated every 15 autopilot cycles in terms of off-diagonal elements of the measured-body-axes-to-commanded-body-axes transformation matrix, as described in Section 6.4. In every autopilot cycle between these updates, $\underline{\theta}_e$ is updated incrementally by subtracting the measured body-angle increment vector from $\underline{\theta}_e$:

$$\underline{\theta}_e = \underline{\theta}_e - \underline{\Delta\theta} \tag{3.4}$$

The angular rate change request $\Delta\underline{\omega}_c$ is the difference between the commanded angular rate $\underline{\omega}_c$ and the estimated angular rate $\underline{\omega}_{est}$

$$\Delta\underline{\omega}_c = \underline{\omega}_c - \underline{\omega}_{est} \tag{3.5}$$

where the commanded angular rate is determined from the attitude error $\underline{\theta}_e$ by the simple relationship

$$\underline{\omega}_c = c\ \text{Unit}(\underline{\theta}_e),\ c \geq 0 \tag{3.6}$$

This relationship commands the vehicle to rotate at an angular velocity c about an axis that would result in all the components of $\underline{\theta}_e$ being reduced to zero at the same time if the actual rate $\underline{\omega}$ were equal to the commanded rate $\underline{\omega}_c$. The "convergence factor" c is made a function of the magnitude of $\underline{\theta}_e$, with c decreasing as $|\underline{\theta}_e|$ decreases and with c reducing to zero when $|\underline{\theta}_e|$ becomes less than a "deadband" level.

This variation of c with $|\underline{\theta}_e|$ gives the proper emphasis to the commanded attitude goal for large $\underline{\theta}_e$ and then allows the zero rate goal to dominate when the attitude error has reached the deadband.

Details of the manner in which the convergence factor c is varied with changes in the magnitude of the attitude error $\underline{\theta}_e$ are described and discussed in Section 3.3.

There are three assumptions made in using equations (3.4) to (3.6) to generate $\Delta\underline{\omega}_c$: (1) It is assumed that the attitude of the vehicle is sufficiently close to the commanded attitude that the difference between commanded and actual attitude can be represented by three angular errors about the three body axes, to form a vector $\underline{\theta}_e$. (2) Rotations of the vehicle to null out $\underline{\theta}_e$ are assumed to be sufficiently small to be commutative, so that any set of body-angle increments represented by a vector $\Delta\underline{\theta}$ can be merely subtracted from $\underline{\theta}_e$ to obtain a new $\underline{\theta}_e$, independently of the sequence of rotations which produced the attitude increment $\Delta\underline{\theta}$. (3) It is assumed that the direction of the error vector $\underline{\theta}_e$ does not change while $\underline{\omega}$ is being driven to the desired rate $\underline{\omega}_c$. To the extent that this assumption is valid, the direction of the new $\underline{\theta}_e$ will still be such that it can be nulled by the angular rate $\underline{\omega}_c$. In practice the angular rate must be driven to the desired rate by means of finite jet firing times, during which the magnitude - and more importantly, the direction - of $\underline{\theta}_e$ may change. If the new error is different in direction from the original $\underline{\theta}_e$, then the acquired angular rate will not drive all components of $\underline{\theta}_e$ to zero simultaneously.

It is possible, at least in principle, to compensate the control law for anticipated changes in $\underline{\theta}_e$ based on some prediction of the effects of the jet firings. Such compensation is not considered in this thesis but recommended for future study.

3.3 Phase Space Control Law Decision Policies

For the purposes of control law computations, the three-dimensional attitude error space is divided into four regions defined

by three concentric spheres of radii R_1, R_2, and R_3 as shown in two dimensions in Figure 3.1. The magnitude of the attitude error vector, $|\underline{\theta}_e|$, is compared to R_1, R_2, and R_3 to determine the region in which the attitude error lies. The determination of the region in which the attitude error lies is made immediately following estimation of the vehicle's angular and translational rates. In the flow chart of autopilot operations shown in Figure 2.2 this determination is made at the point at which the vehicle state is examined to see whether any criteria for jet selection are met.

Region 4 was designed to define a "larger error" region in which it is desired to initiate thrusting as soon as possible to reduce the attitude error. To insure only a small delay in thrust initiation in this region, the coasting period for rate estimation is chosen to be of smaller duration than in the other regions. The trade-off for the reduction in thrust initiation time is a reduced accuracy in rate estimation in Region 4.

Region 3 was established as a "buffer" region between Region 4 and Regions 1 and 2. In Region 3 vehicle angular rates are to be estimated with sufficient accuracy so that they may be reduced to acceptable levels after a single burn. The convergence rate for reducing the attitude error during coasting is sufficiently small in Region 3 to allow the longer coasting period required for accurate rate estimation. (A discussion of the way in which convergence rate is reduced is given below). The distinction between Regions 3 and 4 lies only in the difference in the rate estimation coasting periods. The control decision criteria are identical for the two regions. The radius, R_3, of the sphere which defines the boundary between Regions 3 and 4 was chosen to be 1.25 degrees.

Before describing the roles of Regions 1 and 2, it is useful to define the term "deadband region" as applied to the present control problem. The deadband region is defined as the region in which a convergence rate of 0 is specified. If jets are fired in the deadband region it is for the purpose of directly reducing attitude rate (and

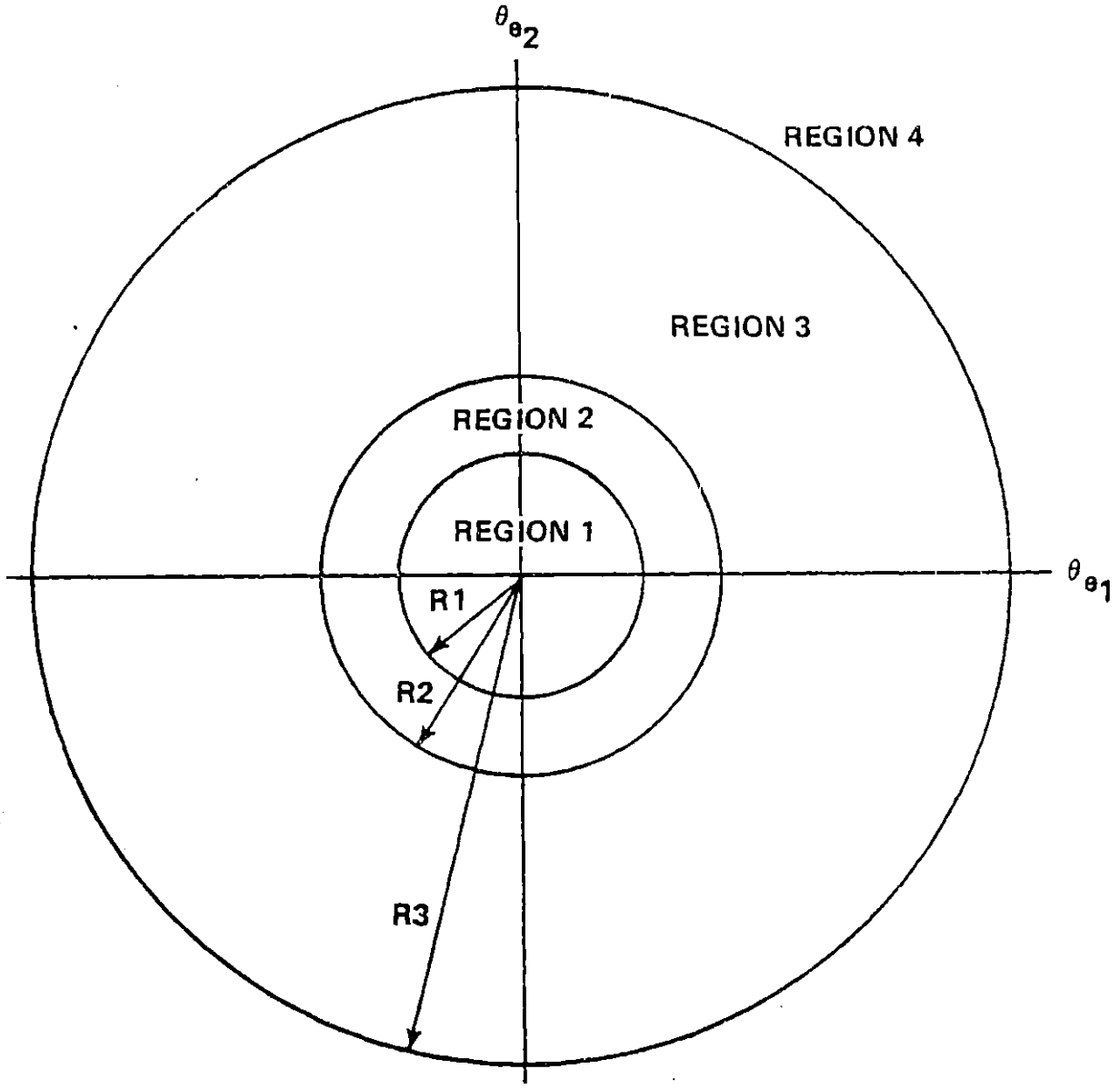

There are four attitude error switching regions defined by three spheres:

$$\underline{\theta}_e = \underline{\theta}_{command} - \underline{\theta}_{measured}$$

REGION 1: $|\underline{\theta}_e| < R1$

REGION 2: $R1 \leq |\underline{\theta}_e| < R2$

REGION 3: $R2 \leq |\underline{\theta}_e| < R3$

REGION 4: $R3 \leq |\underline{\theta}_e|$

R1 = 0.3 deg

R2 = 0.5 deg

R3 = 1.25 deg

Figure 3.1. Attitude error switching regions.

$\underline{V}_e$) to within acceptable tolerances and not for establishing a convergence rate for further reduction of $\underline{\theta}_e$. The deadband radius must be sufficiently small so that the magnitude of attitude errors in the region are within the specified tolerance. In the present design the deadband region includes Region 1 and may under certain conditions be expanded to include Region 2. If $\underline{\theta}_e$ lies in Region 2, the decision on whether or not Region 2 is a deadband region depends on the particular path by which $\underline{\theta}_e$ entered Region 2. This is illustrated by Figure 3.2.

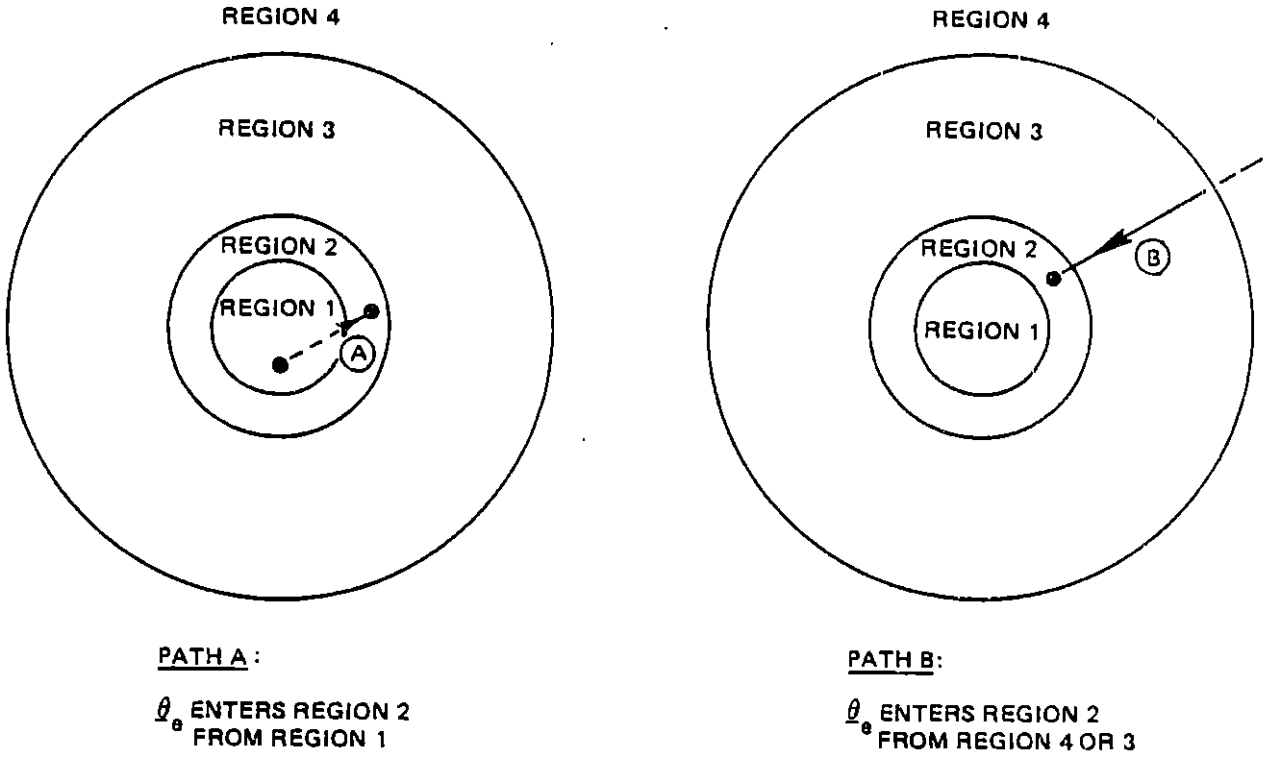

Figure 3.2 Two possible paths by which $\underline{\theta}_e$ may enter Region 2.

If $\underline{\theta}_e$ is determined to have followed a path described by Path A, then the deadband region includes both Regions 1 and 2. In this case, no distinction is made between Regions 1 and 2 in terms of control policy. If $\underline{\theta}_e$ is determined to have followed a path described by Path B, then the deadband region is "shrunk" to be Region 1. In this case, Region 2

is equivalent to Regions 3 and 4 in terms of control policy. Region 2, therefore, can be considered as a "hysteresis" region. The radius, R_2, of the sphere which includes Regions 1 and 2 is 0.5 degrees. This is the tolerance specified for achieving the commanded attitude. After a burn is made in the deadband region, a coast period follows in which attitude rate is estimated. It is desired that during the burn and rate estimation periods the attitude error not drift into Region 3. The motivation for establishing the dual deadband design is based on this requirement. In selecting the value of the radius, R_1, there are two conflicting requirements which must be considered. From the point of view of maximizing the probability that the coasting attitude error trajectory will intersect Region 1, a large value of R_1 should be chosen. From the point of view of minimizing the probability of the attitude error trajectory drifting into Region 3 from Region 1 during rate estimation, a small value of R_1 should be chosen. Simulation results indicate that a good compromise to satisfy these two requirements is obtained with a value of R_1 = 0.3 degrees. It was not attempted to select R_1 based on a theoretical analysis of the probability distribution of the solution time (i.e., the time required to achieve the desired state).

For implementation of the control law the regions are used for two purposes:

1. They are used for deciding among the following three alternative control policies (described in Figure 3.3.)
   a. The control law signals that the desired terminal state has been achieved.
   b. The control law requires the vehicle to continue coasting.
   c. The control law commands jet firings based on a computed rate change request vector.

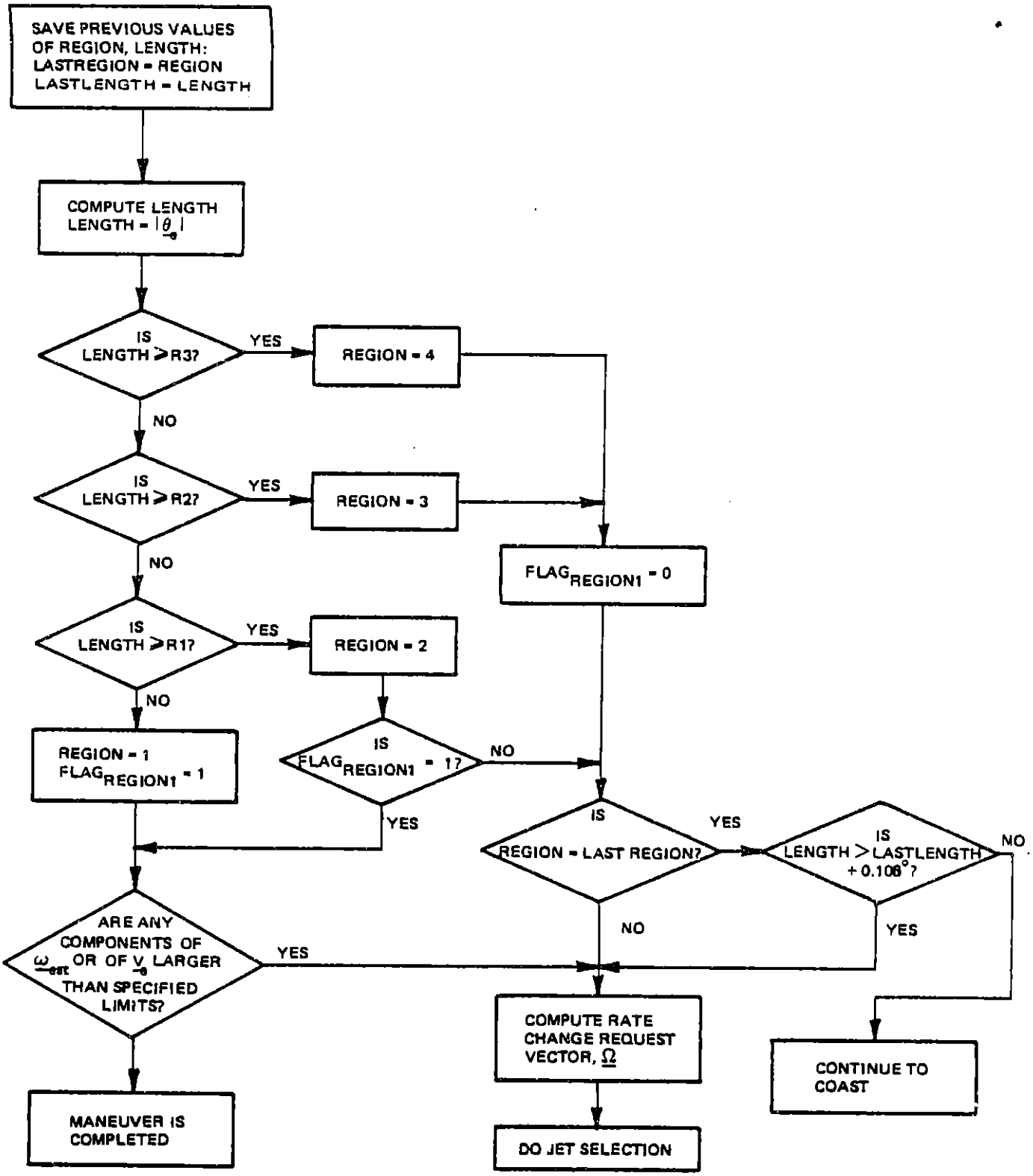

Figure 3.3. Flow chart of control law decisions.

2. The regions are used in determining the appropriate value of the convergence rate, c, which is used to compute the angular rate components of the rate change request vector.

As shown in the flow chart in Figure 3.3, the vehicle will continue to coast unless conditions for performing and implementing a jet selection are met. These conditions are dependent on the region in which the attitude error lies. There are two cases to be considered:

Case 1: $\underline{\theta}_e$ lies in the deadband region—i.e., $\underline{\theta}_e$ is in Region 2 as a result of having followed a path described by Path A in Figure 3.3 or $\underline{\theta}_e$ is in Region 1.

Control Policy: If any of the components of $\underline{\omega}_{est}$ or $\underline{V}_e$ exceeds its specified limit, command jets to reduce these quantities to zero. If $\underline{\omega}_{est}$ and $\underline{V}_e$ are within the desired tolerances, then the control maneuver is complete.

Case 2: $\underline{\theta}_e$ lies outside the deadband region—i.e., $\underline{\theta}_e$ is in Region 2 as a result of having followed a path described by Path B in Figure 3.3 or $\underline{\theta}_e$ is in Regions 3 or 4.

Control Policy: Command jets to be fired to achieve the computed rate change request vector if, (1) The current region is different from the region computed just previously to the current one. Or (2) $|\underline{\theta}_e|$ has increased by more than a specified amount since the previous computation of $|\underline{\theta}_e|$.

A special policy is followed at the beginning of the control maneuver. Upon completion of the initial estimation period, jets are commanded to be fired to achieve a desired convergence rate unless $\underline{\theta}_e$ is in Region 1 and all components of $\underline{\omega}_{est}$ and $\underline{V}_e$ are within the specified limits.

The convergence rate c used in Eq. (3.4) for generating the requested incremental angular rates was chosen to be proportional to the

distance of $\underline{\theta}_e$ from the origin of the attitude error space. This form for the convergence rate was chosen to satisfy the requirements that,

1. For attitude errors in Region 4, the convergence rate should be sufficiently large so that the time required to achieve the desired terminal state does not exceed a specified value.

2. For attitude errors in Region 3, the convergence rate should be sufficiently small so that the attitude error does not reach the vicinity of the origin before rate estimation is completed.

For a given rate estimation period in Region 3, requirement 2 establishes an upper bound on the value of the proportionality constant, K, by which $\underline{\theta}_e$ is multiplied. To determine this value, assume that $|\theta_e|$ will "coast" to the origin in the time, T_{est}, it takes to complete rate estimation. It is assumed that a burn has been commanded to achieve the convergence rate c. Therefore, the time required for $\underline{\theta}_e$ to coast to the origin (assumed here to be T_{est}) is given by the equation

$$T_{est} = \frac{|\theta_e|}{c} \tag{3.7}$$

But, c is chosen to satisfy the equation

$$c = K|\theta_e| \tag{3.8}$$

From these two relationships, therefore, K is determined to have the value

$$K = \frac{1}{T_{est}} \tag{3.9}$$

This expression for K is based on the assumption that the convergence rate, c, is exactly and instantaneously achieved. Since in practice these ideal conditions are not realized, the attitude error will not coast directly to the origin and indeed may coast through the deadband region in the time required for estimation. To minimize this possibility, the convergence rate, c and therefore the value of K, should be reduced. The amount by which K is reduced is based on the expected deviations in the vehicle state from the ideal state during this coasting period. The value of k used in this autopilot design is 0.8 sec^{-1}. This value corresponds to T_{est} = 1.25 sec, which is slightly longer than the maximum rate estimation period of 1.14 sec. The choice of this and the other estimation periods is discussed in Chapter 5.

CHATPER 4

JET SELECTION

4.1 Introduction

Assuming a rigid vehicle with constant mass properties, the vehicle equations of motion may be expressed as

$$\underline{\tau} = \frac{d\underline{H}}{dt} + \underline{\omega} \times \underline{H} \qquad (4.1)$$

and

$$\underline{f}_I = M \frac{d\underline{V}_I}{dt} \qquad (4.2)$$

where

$\underline{\tau}$ = 3-dimensional torque vector whose elements are the net jet torques about each of the three body axes

$\underline{f}_I$ = 3-dimensional force vector whose elements are the net jet forces along three orthogonal inertial references axes

$\underline{\omega}$ = 3-dimensional angular velocity vector whose elements are the angular velocities about the three body axes

$\underline{H}$ = 3-dimensional angular momentum vector

$\underline{H}$ = I $\underline{\omega}$, where I is the inertia tensor of the vehicle

$\underline{V}_I$ = 3-dimensional translational velocity vector whose elements are the translational velocity components along three inertial reference axes

M = vehicle mass

The above equations can be simplified as follows for the particular problem of achieving an end state of constant attitude and constant translational velocity.

First, the angular velocities comprising $\underline{\omega}$ can be assumed to be small enough that the term $\underline{\omega} \times \underline{H}$ can be neglected, resulting in

$$\underline{\tau} \cong I \frac{d\underline{\omega}}{dt} \tag{4.3}$$

(Here, it may be noted that the elements of $\underline{\omega} \times \underline{H}$ are called "angular velocity coupling terms". These terms will be neglected in the autopilot implementation but included in the vehicle simulation.)

Second, the effects of angular rotation on the direction of the translational acceleration resulting from the jet forces can be neglected, so that Eq. (4.2) can be rewritten in terms of the body-axis force vector, $\underline{f}$, and body-axis translational velocity, $\underline{V}$

$$\underline{f} \cong M \frac{d\underline{V}}{dt} \tag{4.4}$$

(This approximation is employed only in the autopilot implementation, not in the vehicle simulation.)

Both Eqs. (4.3) and (4.4) can be solved for the angular and translational acceleration vectors

$$\frac{d\underline{\omega}}{dt} \cong I^{-1} \underline{\tau} \tag{4.5}$$

$$\frac{d\underline{V}}{dt} \cong \frac{1}{M} \underline{f} \tag{4.6}$$

The jet selection routine of the phase space autopilot computes a set of firing times such that the elements of the change in $\underline{\omega}$, as obtained by integrating Eq. (4.5)

$$\Delta\underline{\omega} \cong I^{-1}\int_0^t \underline{\tau}dt \qquad (4.7)$$

and the elements of the change in $\underline{V}$, as obtained by integrating Eq. (4.6)

$$\Delta\underline{V} \cong \frac{1}{M}\int_0^t \underline{f}dt \qquad (4.8)$$

are equal to the corresponding elements of the rate change request vector $\underline{\Omega}$. This computation of firing times is a two-step procedure in which the firing-times are first computed assuming constant jet forces and the times are subsequently adjusted to compensate for the transient build-up and decay of jet forces (which results in a nominal force-impulse versus firing-time curve).

The phase-space jet selection represents the firing time of each of m jets as an element of an m-dimensional vector, $\underline{t}_{jet}$. If the forces of the jets are constant over their respective firing times, then it can be shown from Eqs. (4.7) and (4.8) that the changes in $\underline{\omega}$ and $\underline{V}$ resulting from the firing times are merely equal to the products of the firing times and the associated elements of $I^{-1}\ \underline{\tau}$ and $\frac{1}{M}\ \underline{f}$. These elements are represented by a constant 6-dimensional vector $\underline{a}_i$ for the i^{th} jet

$$\underline{a}_i \cong \begin{bmatrix} I^{-1}\ F\ \underline{r}_i \times \underline{u}_i \\ - - - - - - - \\ F\ \underline{u}_i/M \end{bmatrix} \qquad (4.9)$$

where I^{-1} is the inverse of the inertia tensor, F is the constant force assumed for each jet (which is here assumed to be the same for all jets),

M is the vehicle mass, $\underline{r}_i$ is the position vector of the i^{th} jet with respect to the vehicle center of mass and $\underline{u}_i$ is a unit vector in the direction of the force produced by firing the i^{th} jet. The acceleration vectors $\underline{a}_i$ of the m jets for constant jet forces may be incorporated into a 6 × m acceleration matrix A

$$A = \begin{bmatrix} \uparrow & \uparrow & & \uparrow \\ \underline{a}_1 & \underline{a}_2 & \cdots & \underline{a}_m \\ \downarrow & \downarrow & & \downarrow \end{bmatrix} \tag{4.10}$$

The product of this A matrix and the jet firing time vector, $\underline{t}_{jet}$, yields a 6-dimensional vector, whose first three elements represent changes in elements of $\underline{\omega}$ and whose second three elements represent changes in elements of $\underline{V}$ resulting from the constant-force firings. Setting this matrix-vector product equal to the rate change request vector $\underline{\Omega}$ gives

$$\underline{\Omega} = A\,\underline{t}_{jet} \tag{4.11}$$

In general, there will not be a unique solution of Eq. (4.11) for $\underline{t}_{jet}$. Since negative jet firing times are not realizable, all solutions having one or more negative components must be rejected. Additional criteria for selecting $\underline{t}_{jet}$ from the set of solutions will be discussed in Section 4.2.

The two jet selection procedures presented in this chapter compute required firing times based on constant thrust jets. As mentioned previously, the thrust is not actually constant but takes a finite time to build up to and decay from the rated value. The firing times computed by the jet selection algorithms must therefore be modified to account for this effect. New adjusted firing times must be computed which will deliver the same total impulse as would have been delivered

by constant thrust engines firing for the originally computed times. This is discussed in more detail in Section 4.4.

4.2 Pseudo Inverse Jet Selection[4]

The jet selection procedure must find a solution $\underline{t}_{jet}$ to the set of linear equations given by

$$\underline{\Omega} = A\,\underline{t}_{jet} \tag{4.12}$$

where A is n × m. If the number of independent equations is equal to the number of unknowns (i.e., n=m), then the solution is found by multiplying $\underline{\Omega}$ by the inverse of the A matrix

$$\underline{t}_{jet} = A^{-1}\,\underline{\Omega} \tag{4.13}$$

When the number of unknowns is not equal to the number of equations, an alternative operation is to multiply $\underline{\Omega}$ by an appropriate matrix, $A^{\dagger}$, called the "pseudo inverse"[5] of A

$$\underline{t}_{jet} = A^{\dagger}\,\underline{\Omega} \tag{4.14}$$

$A^{\dagger}$ has two forms depending on the relative dimensions of A. If A has more columns than rows (i.e., if the number of unknowns is greater than the number of equations), then the pseudo inverse, $A^{\dagger}$, is chosen to yield the solution vector, $\underline{t}_{jet}$ having minimum length. The pseudo inverse in this case is given by

$$A^{\dagger} = A^{T}(AA^{T})^{-1} \tag{4.15}$$

If A has more rows than columns (i.e., if the number of unknowns is less than the number of equations), then, in general, the equation

$\underline{\Omega} = A\,\underline{t}_{jet}$ cannot be satisfied. Therefore, for any vector, $\underline{t}_{jet}$, a non-zero error vector $\underline{\Omega} - A\,\underline{t}_{jet}$ will be produced. In this case, the pseudo inverse is chosen to minimize the length of the error vector and is given by

$$A^{\dagger} = (A^{T}A)^{-1}A^{T} \tag{4.16}$$

The spacecraft considered in this thesis has twelve jets, resulting in m=12. Therefore, since n=6 by definition, there are more columns than rows in A (i.e., m > n). For this case the pseudo inverse matrix, $A^{\dagger}$ is computed from the relationship given in Eq. (4.15) and $\underline{t}_{jet}$ is given by the equation

$$\underline{t}_{jet} = A^{T}(AA^{T})^{-1}\,\underline{\Omega} \tag{4.17}$$

If $\underline{t}_{jet}$ contains no negative components then the solution for jet firing times is complete. In general, however, $\underline{t}_{jet}$ will have negative components as well as positive ones, in which case the solution will be unacceptable. Two methods for obtaining an acceptable solution were investigated.

The first approach considered for dealing with the problem of negative firing times was to form a reduced A matrix using only the acceleration vectors, $\underline{a}_i$, of the jets having non-negative firing times (and assuming that the firing times of the rejected jets are zero). A new solution for $\underline{t}_{jet}$ was found using the appropriate form of the pseudo inverse. This solution was then examined for negative firing times and the process of eliminating all negative firing jets was repeated until a non-negative solution was obtained. However, when this approach was implemented it was found that a singular AA^{T} matrix occasionally resulted. The existence of this singular matrix indicates that the rate change request vector cannot be exactly satisfied with the particular jets chosen. Another approach was developed in an attempt to avoid this singularity problem.

Instead of eliminating all the jets with negative firing times from a given computation of $\underline{t}_{jet}$, the second approach eliminates only the single jet having the longest negative firing time, and continues the process of eliminating one jet at a time until the resulting elements of $\underline{t}_{jet}$ are all positive. This elimination procedure is described in the flow chart of Figure 4.1. The singularity problem was not avoided using this approach, but the occurrence of singularities was reduced. Further study is required to develop a modified jet selection procedure for these singular cases.

It should be emphasized that the pseudo inverse method of jet selection is a general one which does not need to be revised when vehicle mass properties change or when particular jets become unavailable due to failures or to operational constraints. It adapts to new mass properties by using the new jet acceleration vectors, $\underline{a}_i$, and it adapts to jet failures and constraints by omitting the corresponding jet acceleration vectors from the A matrix used in Eqs. (4.15) and (4.16). Moreover, the pseudo inverse method provides an exact, minimum length solution. The disadvantage to this method, in addition to the need to address the singularity problem, is that it involves matrix multiplications and inversions which may require substantial computation time. It may be possible to reduce the number of computations required by developing a scheme to eliminate unsuitable jets from the A matrix so that the first computation of $\underline{t}_{jet}$ results in a non-singular AA^T matrix and in a non-negative solution for $\underline{t}_{jet}$.

4.3 Fixed Jet Selection Routine

In the interests of reducing the computational load of the jet selection program, a simplified jet selection policy was investigated. This policy, called the "fixed jet selection routine", uses predetermined combinations of jets to satisfy each of the six components of the rate change request vector, $\underline{\Omega}$. The jet selection procedure is most easily

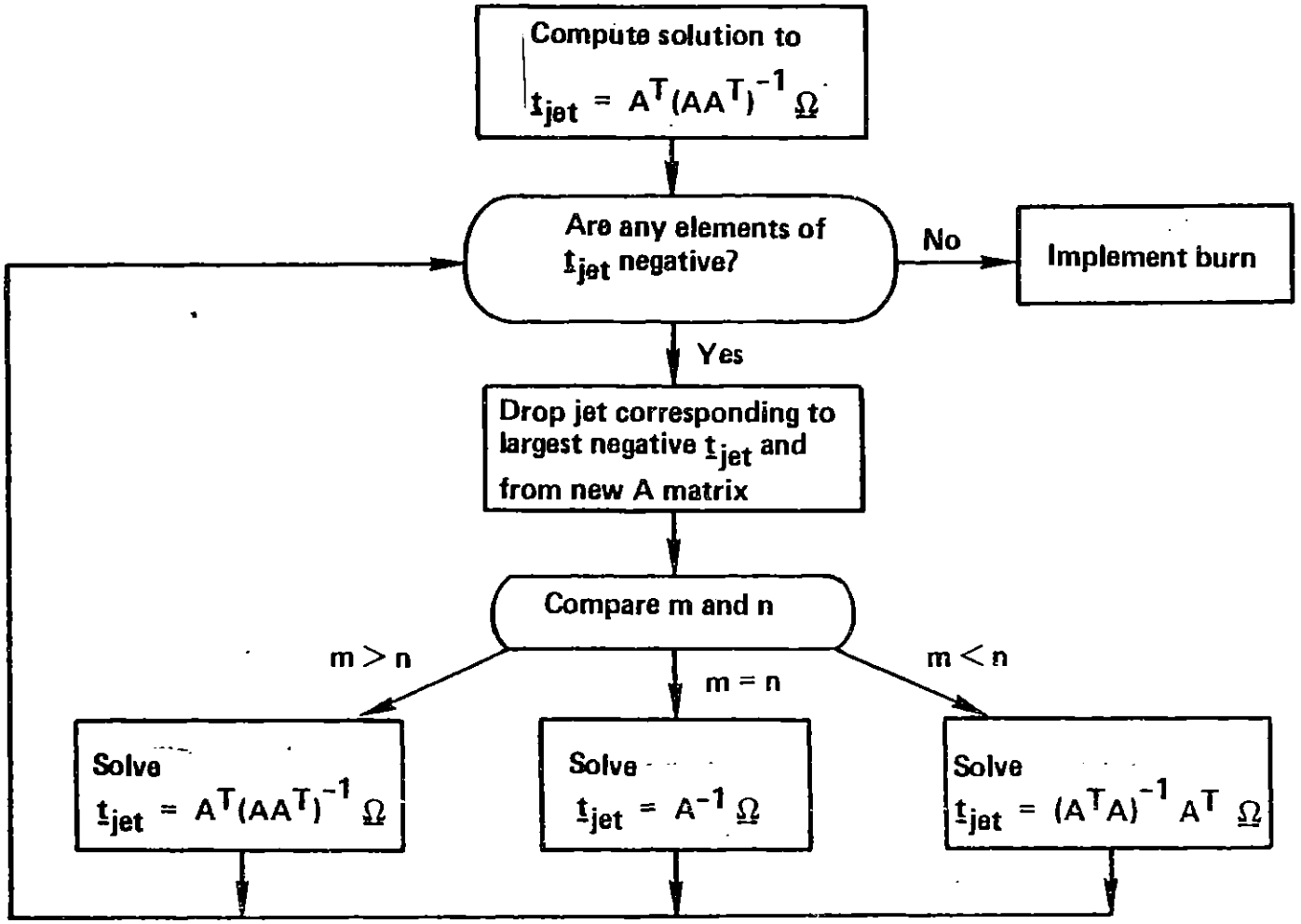

Figure 4.1. Pseudo inverse matrix solution for firing-time vector.

designed when the jet configuration is relatively simple and is particularly easy to design when there are pure jet couples available for producing torques about each body axis. As the jet configuration becomes more complex and the jets more skewed to each other, the design of this method becomes more difficult.

In general, the fixed jet slection procedure will not be as efficient as the pseudo inverse procedure in terms of fuel consumption or convergence time for reducing residual errors. It does have the advantage, however, that it places a relatively low burden on the flight computer, both in terms of storage and computation time.

The fixed jet selection procedure designed for this study is based on a spacecraft with a 12-jet configuration arranged in positive and negative couples in the x-y, x-z, and y-z body-axes planes as shown in Figure 4.2. The request vector, $\underline{\Omega}$, is composed of three incremental angular rates and three translational velocity errors in body coordinates.

$$\underline{\Omega} = \begin{bmatrix} \Delta\omega_{c_x} \\ \Delta\omega_{c_y} \\ \Delta\omega_{c_z} \\ V_{e_x} \\ V_{e_y} \\ V_{e_z} \end{bmatrix}$$

The fixed jet selection routine can be summarized as follows:

1. Determine the firing times to null out the y- and z-translational velocity errors using roll jets.
2. Determine the firing times to null out the x-translational velocity errors using pitch and yaw-jets.
3. Modify the angular velocity errors of the rate request vector by subtracting the angular rates produced by the translational firings from the desired angular rate changes.
4. Determine the firing times to null out the modified angular velocity errors using pure rotational jet couples. (Some of these jets will also have been selected in Steps 1 and 2. The firing times for these jets will be the sum of the firing times computed in Steps 1 and 2 and the firing times computed in Step 4.)

The detailed implementation of the procedure is given as follows:

1. Define new body axes y' and z' by rotating the y- and z-axes 45° in a positive direction about the x-axis. (The y' axis is parallel to the directions of the R2 and R4 jets, and the z' axis is parallel to the directions of the R1 and R3 jets).
2. Transform the components, V_{e_y} and V_{e_z} of the request vector to the y' and z' coordinate system as follows

$$\begin{bmatrix} V'_{e_y} \\ V'_{e_z} \end{bmatrix} = \begin{bmatrix} \cos(45°) & \sin(45°) \\ -\sin(45°) & \cos(45°) \end{bmatrix} \begin{bmatrix} V_{e_y} \\ V_{e_z} \end{bmatrix} \qquad (4.18)$$

3. Choose the appropriate roll jet, R2 or R4, to produce the requested velocity change, V'_{e_y}. If V'_{e_y} is positive, then R2 is fired for the time

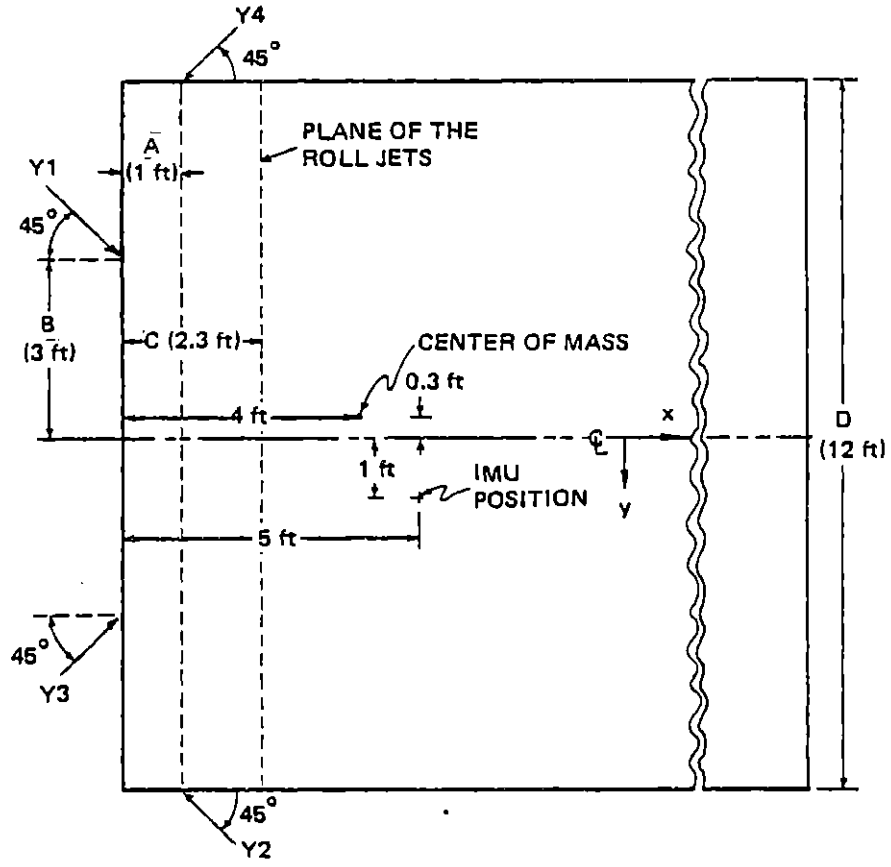

a. Top View

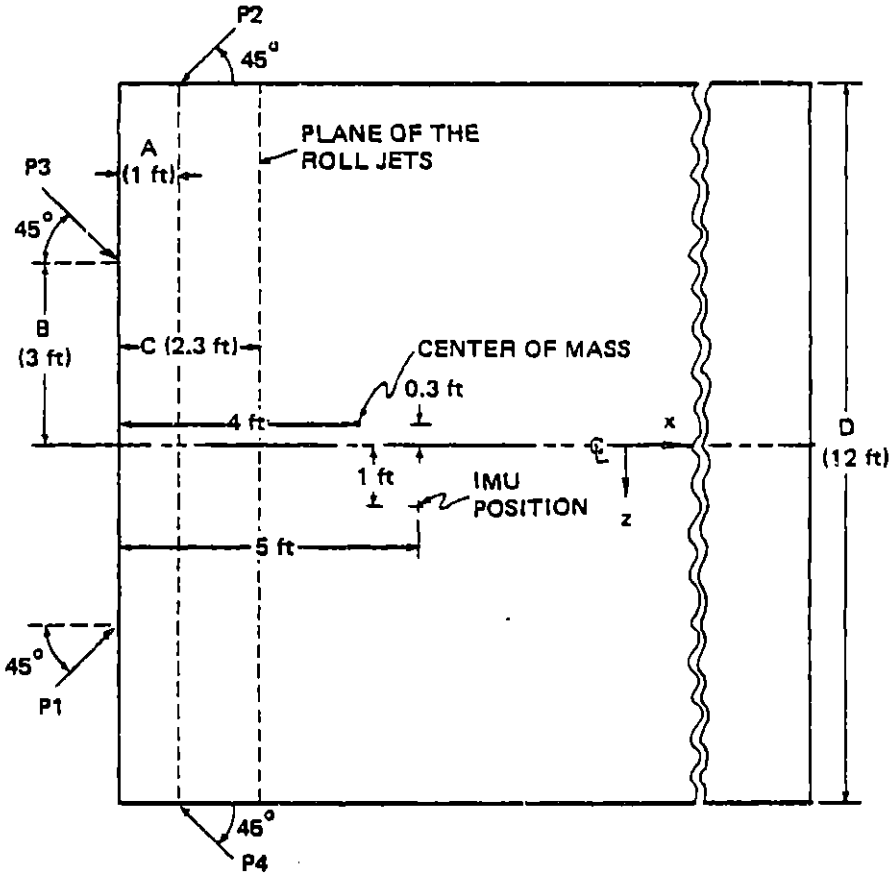

b. Side View

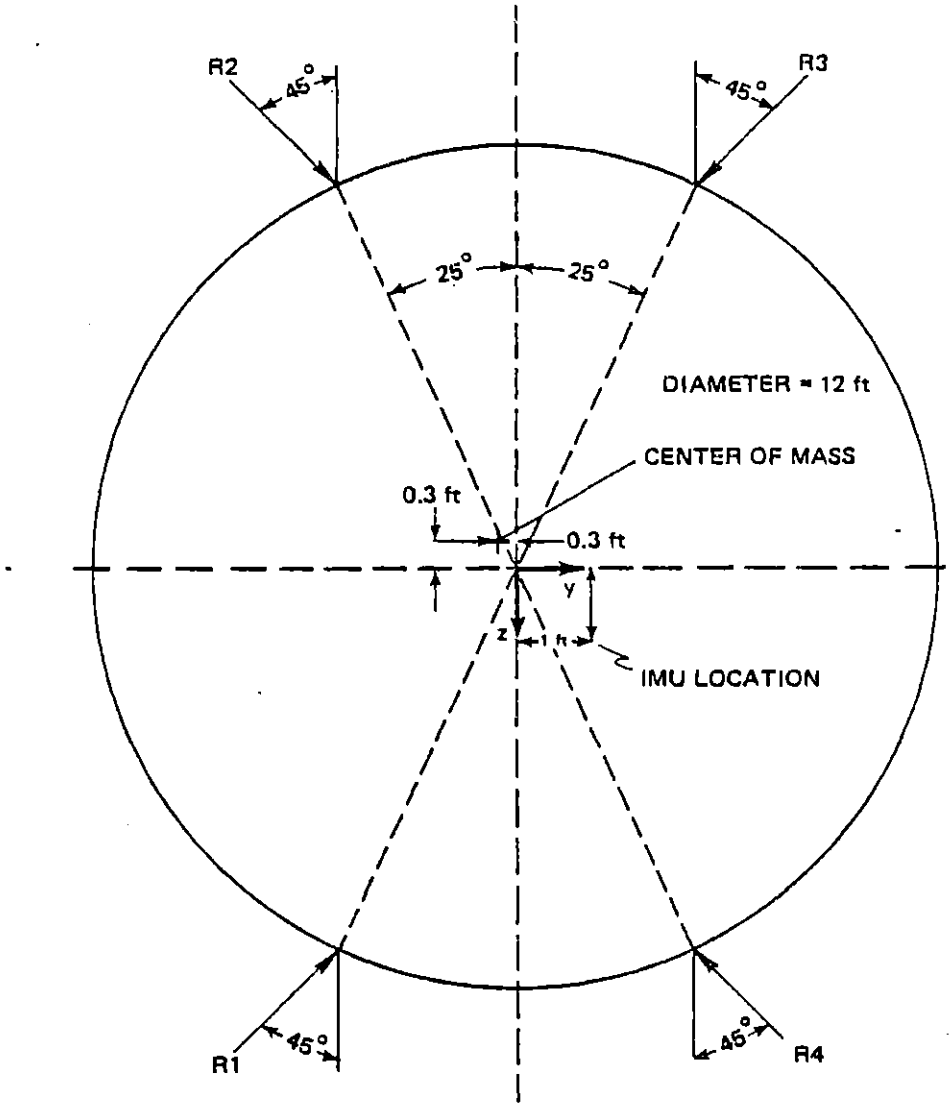

c. Rear View

Figure 4.2. Vehicle dimensions and jet configurations: top, side, and rear views.

$$t_{R2} = \frac{M}{F} V'_{e_y} \tag{4.19}$$

where M is the vehicle mass and F is the jet force. If V'_{e_y} is negative, then R4 is fired for the time

$$t_{R4} = -\frac{M}{F} V'_{e_y} \tag{4.20}$$

4. Choose the appropriate jet R3 or R1 to produce the requested velocity change V'_{e_z}. If V'_{e_z} is positive, then R3 is fired for the time

$$t_{R3} = \frac{M}{F} V'_{e_z} \tag{4.21}$$

If V'_{e_z} is negative, then R1 is fired for the time

$$t_{R1} = -\frac{M}{F} V'_{e_z} \tag{4.22}$$

5. Choose the appropriate jets to produce the requested x-axis velocity change, V_{e_x}. Two pitch and two yaw jets are used for x-translation. If V_{e_x} is positive, then jets P1, P3, Y1, and Y3 are used and the firing times are given by

$$t_{P1} = t_{P3} = t_{Y1} = t_{Y3} = \frac{M}{4 F \cos (45°)} V_{e_x} \tag{4.23}$$

If V_{e_x} is negative, then jets P2, P4, Y2, and Y4 are used and the firing times are given by

$$t_{P2} = t_{P4} = t_{Y2} = t_{Y4} = -\frac{M}{4 F \cos (45°)} V_{e_x} \tag{4.24}$$

6. Compute a modified rate change request, $\Delta\underline{\omega}_c'$. This is necessary to correct for the angular rate changes resulting from jet forces not acting through the center of mass. The modified request vector is determined by first computing the angular rate changes that will be produced by the translational firings and then subtracting these rates from the desired angular rate changes, $\Delta\underline{\omega}_c$

$$\Delta\underline{\omega}_c' = \Delta\underline{\omega}_c - I^{-1} F \sum_{1}^{m} (\underline{r}_i \times \underline{u}_i) t_{jet_i} \qquad (4.25)$$

Here, the t_{jet_i}'s refer to the firing times computed for the 12-jets (in Steps 3-5) to satisfy the translational velocity request. The $\underline{r}_i$ vectors are the position vectors of the jets relative to the center of mass and the $\underline{u}_i$ vectors are the unit thrust vectors of the jets. F is the jet thrust.

7. Compute the firing times for pure rotational jet couples to satisfy the modified request. For this purpose, assume that one jet couple per body axis is fired to produce the constant torques τ_x, τ_y, τ_z over the firing intervals Δt_x, Δt_y, Δt_z, resulting in the torque impulse vector

$$\int_0^{t_{max}} \underline{\tau}\, dt = \begin{bmatrix} \tau_x \Delta t_x \\ \tau_y \Delta t_y \\ \tau_z \Delta t_z \end{bmatrix} \qquad (4.26)$$

where t_{max} is the longest firing time of the jet couples. Integrating Eq. (4.3), it is seen that for a constant inertia tensor (I) this torque impulse vector produces an angular velocity change $\Delta\underline{\omega}$, according to

$$\int_0^{t_{max}} \underline{\tau}\, dt = I\, \Delta\underline{\omega} \qquad (4.27)$$

Equating (4.26) and (4.27), and replacing $\Delta\underline{\omega}$ by the requested angular velocity change $\Delta\underline{\omega}_c$

$$\begin{bmatrix} \tau_x\, \Delta t_x \\ \tau_y\, \Delta t_y \\ \tau_z\, \Delta t_z \end{bmatrix} = I\, \Delta\underline{\omega}_c \qquad (4.28)$$

If the inertia tensor I and the requested angular rate change vector $\Delta\underline{\omega}_c$ are expressed in terms of their components, the above vector equation may be written as three scalar equations

$$\tau_x\, \Delta t_x = I_x\, \Delta\omega'_{c_x} - I_{xy}\, \Delta\omega'_{c_y} - I_{xz}\, \Delta\omega'_{c_z} \qquad (4.29)$$

$$\tau_y\, \Delta t_y = -I_{xy}\, \Delta\omega'_{c_x} + I_y\, \Delta\omega'_{c_y} - I_{yz}\, \Delta\omega'_{c_z} \qquad (4.30)$$

$$\tau_z\, \Delta t_z = -I_{xz}\, \Delta\omega'_{c_x} - I_{yz}\, \Delta\omega'_{c_y} + I_z\, \Delta\omega'_{c_z} \qquad (4.31)$$

The jet selection routine solves these scalar equations for the firing times Δt_x, Δt_y, Δt_z, using values of τ_x, τ_y, τ_z that are determined by the product of nominal force times moment arm for each jet couple. The magnitudes of τ_x, τ_y, τ_z, are the same for each two opposing couples of the 12-jet spacecraft chosen as an example in this thesis. These magnitudes are expressed as follows in terms of the parameters of this spacecraft

$$|\tau_x| = F\ D \sin(20°) \tag{4.32}$$

$$|\tau_y| = F[\frac{D}{2} + B) \cos(45°) - A \sin(45°)] \tag{4.33}$$

$$|\tau_z| = F[\frac{D}{2} + B) \cos(45°) - A \sin(45°)] \tag{4.34}$$

8. If a jet selected in Step 7, was also selected in Steps 3-5, then the two firing times computed for that jet must be added to obtain the total firing time.

In these steps a set of jets has been selected and their firing times computed to produce the rate request vector, $\underline{\Omega}$. This approach takes advantage of the fact that for a constant mass properties, negligible angular motion, and negligible angular velocity coupling, the effects of separate translational jet firings and rotational jet firings can be superimposed to obtain the net angular and translational velocity vectors. This jet selection method reduces computation time by more than an order of magnitude compared to that required by the pseudo inverse method. It is also an exact solution but not necessarily optimal in any sense.

The choice of jet selection policy may have an appreciable effect on the size of the excursions in angular rate and the residual attitude errors which may be produced when the policy results in large alternating net torque impulses about an axis. Here, the residual attitude errors are of particular concern because of their possible effect on increasing the time to reach the desired state. The problem of large alternating torque impulses about an axis will generally arise when the translational jet firings requested produce moments about vehicle axes which are counter to the moments needed to satisfy the angular rate change request—and when these opposing moments are of unequal durations.

It is possible that the more efficient use of jets by pseudo inverse method may tend, in general, to minimize these adverse effects, but it is also possible to design the fixed jet selection method with a specific regard to minimizing these effects. Another solution will be discussed in Section 4.5. There, it will be shown that a procedure for "parceling out" the shorter jet firing times will significantly reduce both the rate excursions and the residual attitude errors.

4.4 Adjustment of Jet Firing Times

Both the pseudo inverse and the fixed jet selection procedures compute the jet firing times necessary to produce the requested rate change vector, $\underline{\Omega}$, based on the assumption that the force produced by each jet is constant. In practice, it takes a finite time after a jet has been turned on for the jet-produced force to build up to its maximum value and similarly it takes a finite time for the force to decay to zero after the jet has been turned off. These build-up and decay transients in the jet firings can result in a nonlinear curve of nominal jet impulse versus firing time, as shown in Figure 4.3.

The nominal impulse versus time curve of Figure 4.3 is approximated in the vehicle simulation by a curve with two constant slopes, F1 and F2, as shown in Figure 4.4. The autopilot adjustment of firing times is based on the same two-slope approximation of the nominal impulse curve. In addition the vehicle simulation provides for assumed biases in the nominal impulse curve as shown in Figure 4.4. The vehicle simulation superimposes, on the biased impulse curves, the effects of random variations in individual jet firings, as described in Chapter 6. Neither the biases nor the unpredictable random variations are included in the autopilot adjustment of firing times.

As a result of the dual-slope relationship of nominal impulse versus time it is necessary to fire each jet longer to attain a given impulse than would be the case if the jet force were constant at the rated level throughout its firing time. This adjustment in firing

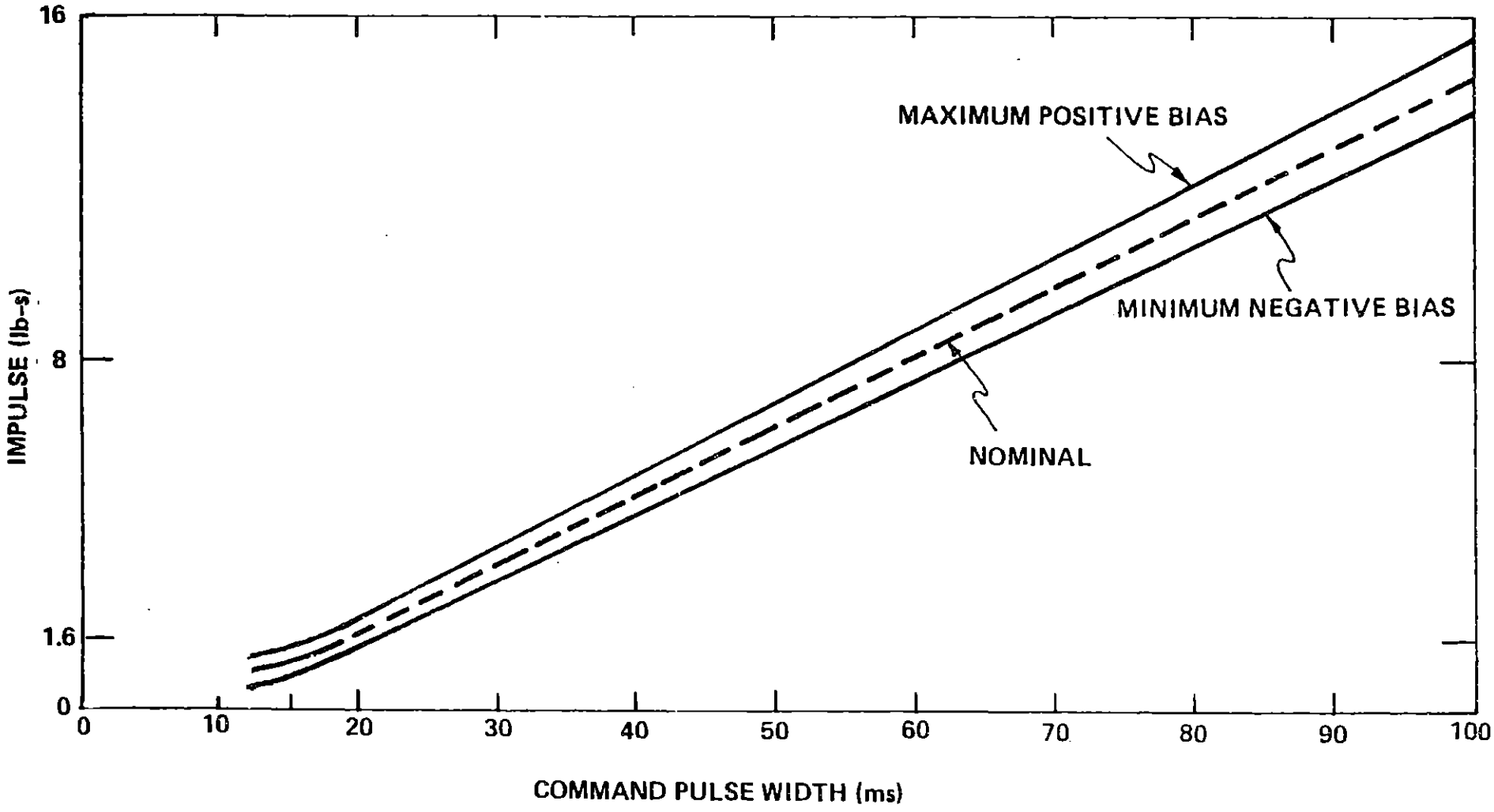

Figure 4.3. Impulse vs. command pulse width 160 lb thrust engine,

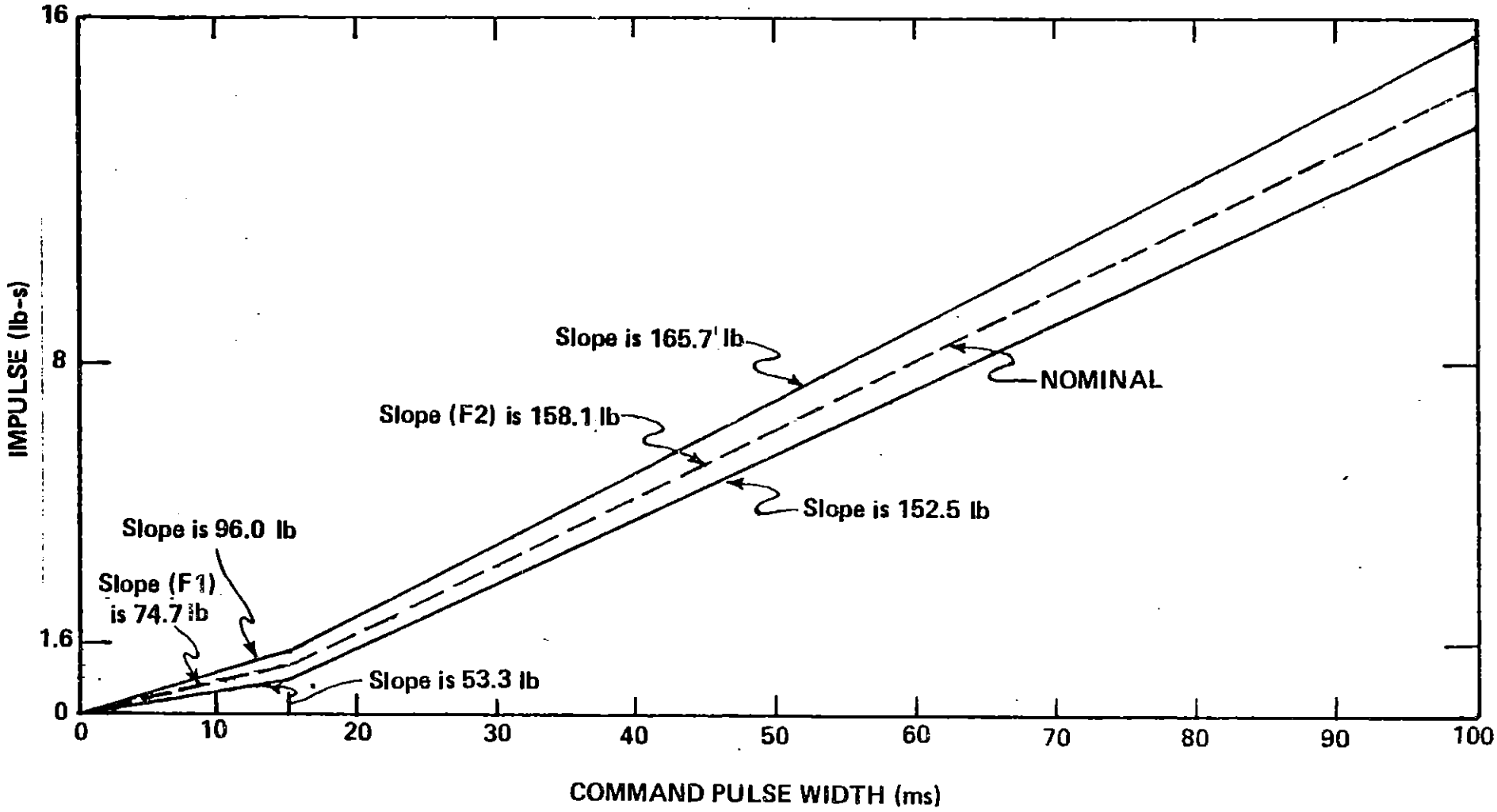

Figure 4.4. Simulation of jet bias effects; impulse variation vs. command pulse width 160 lb thrust engine.

times is made in the phase space autopilot following the initial constant-force computations of firing times by the two alternative jet selection routines. The adjustment is based on the assumption that a jet will produce a force F1 until it has fired for a time T1, after which time it will produce a force F2. The equations used to adjust the firing time of the i^{th} jet are:

If

$$t_{jet_i} \leq \frac{T1\ F1}{F}$$

then

$$t'_{jet_i} = t_{jet_i} \frac{F}{F1} \tag{4.35}$$

Otherwise, if

$$t_{jet_i} > \frac{T1\ F1}{F}$$

then

$$t'_{jet_i} = t_{jet_i} \frac{F}{F2} + T1 \frac{(F2 - F1)}{F2} \tag{4.36}$$

4.5 Implementation of the Commanded Jet Firing Times

4.5.1 General

Initial studies of the phase space autopilot, conducted for this thesis, were based on a jet firing policy in which all of the jets selected would be turned on at the same time and then turned off when their respective firing-time requirements were met. An alternative policy involving the "parceling out" of some of the firings into multiple time segments was later found to give significant improvements in the convergence to the end state (within specified error limits) from a given initial state.

The impact of the "parceled out" jet firings on the convergence time appears to be associated primarily with its reduction of adverse excursions in the attitude error. More specifically, this policy reduces the excursions in the components of the angular rate vector $\underline{\omega}$ which are caused by the differing jet firing times. This reduction, in turn, leads to a reduction in the magnitudes of components of $\underline{\theta}_e$ resulting from the integration of $\underline{\omega}$. The effects of this parceling out process will be examined below in terms of a simple example, following a detailed description of the "parceled out" jet firing policy.

4.5.2 Policy of "Parceled Out" Jet Firing Times

The "parceled out" policy fires each shorter-firing jet several times during the firing interval of the longest-firing jet, with these new times computed to achieve the same total force and torque impulses as originally requested by the jet selection procedure. This firing policy, which is illustrated in Figure 4.5 is implemented as follows:

The firing interval is subdivided into three divisions (or "parcels") by dividing the maximum jet firing time by three. The jet corresponding to the maximum jet firing time is fired continuously, (See jet #2 in Figure 4.5.) In practice it takes a finite time for the force delivered by a jet to build up to the maximum force. Therefore, in order to produce the same total force impulse as a jet which is fired continuously, a jet which is turned on and off several times must be fired for a longer total time. Each jet firing time is examined to see if it could be fired three separate times and still deliver the required impulse without exceeding the maximum jet firing time. If it cannot meet this constraint, then it is turned on at the beginning of the firing interval and fired continuously. (See jet #3 in Figure 4.5.)

If the jet can be fired three times without exceeding the firing interval of the maximum jet firing time, then its parceled time (i.e., the time in which the jet will deliver one third of the required impulse) is compared to the minimum allowable jet firing time. If the parceled

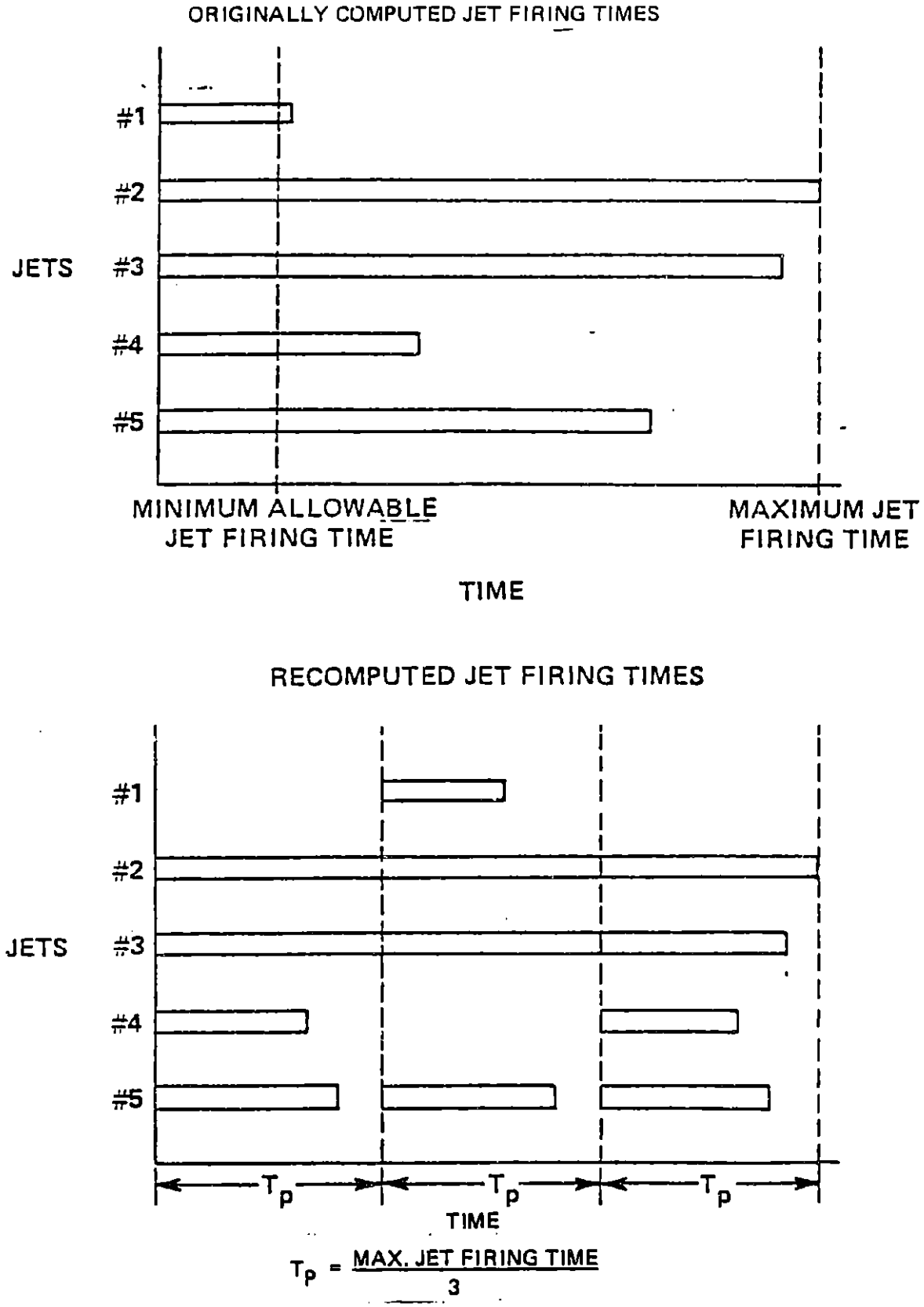

Figure 4.5. Illustrating the procedure employed for parceling out jet firing times.

firing time is greater than the minimum allowable jet firing time, then the corresponding jet will be fired three separate times during the firing interval. (See jet #5 in Figure 4.5.)

If the parceled time is less than the minimum allowable, then a new parceled time is computed which will deliver one half the total force impulse required from the corresponding jet. If this new parceled time is longer than the minimum jet firing time, then the corresponding jet is fired twice during the firing interval of the longest firing jet, in the first subdivision and in the last. (See jet #4 in Figure 4.5.)

If the parceled time which will deliver one half the total force impulse required from the corresponding jet is shorter than the minimum allowable jet firing time, then that jet will be fired only once during the middle subdivision. (See jet #1 in Figure 4.5.)

Consider a simple example which will illustrate the beneficial effects of jet parceling. Assume:

1. A vehicle whose center of mass is located on the x-body axis and whose products of inertia are zero.
2. The vehicle has a 12-jet configuration as shown in Figure 4.2
3. The jets are c nstant thrust.
4. The initial values of angular rate and attitude error are zero.
5. The rate change request vector has only one non-zero component, $\underline{V}_{e_z}$, which means that the final as well as the initial angular rates are to be zero.
6. The angular acceleration about the y-body axis produced by firing roll jets R2 and R3 simultaneously is denoted by $\dot{\omega}_R$ and the angular acceleration about the y-body axis produced by the pitch jet couple P3 and P4 is given by $-\dot{\omega}_P$. Let $\dot{\omega}_P = 2\dot{\omega}_R$.

Assume further that the fixed jet selection routine is employed. This routine will compute the jet firing times necessary for the roll jets R2 and R3 to satisfy the z-translational request. The firing time for roll jet R2 will be equal to the firing time for roll jet R3, which will be termed t_R. Firing the roll jets R2 and R3 simultaneously for a time t_R will produce an angular velocity, $\dot{\omega}_R\ t_R$. The requested change in angular velocity is zero, so the pitch jets P3 and P4 must be fired for a time t_P to null out the angular velocity which would be produced by firing the roll jets for t_R. Since $\dot{\omega}_P = 2\dot{\omega}_R$

$$t_P = \frac{\dot{\omega}_R}{\dot{\omega}_P} t_R = \frac{t_R}{2} \tag{4.37}$$

Consider now two alternative methods of implementing these jet-firing-time commands and compute the attitude errors which result from each method:

Method 1. - No Parceling—All four jets (R2, R3, P3, and P4) begin firing simultaneously and are turned off as they complete their respective commanded firing times. This firing sequence will produce a negative angular acceleration, $(\dot{\omega}_R - \dot{\omega}_P)$ for a time t_P and then produce a positive angular acceleration, $\dot{\omega}_R$, for the remainder of the firing interval. The dotted line in Figure 4.6. shows a plot of the angular velocity as a function of jet firing time. The angular error about the y-axis, $\Delta\theta_{e_{\text{Method 1}}}$ resulting from this burn is given by

$$\Delta\theta_{e_{\text{Method 1}}} = \frac{\left(\dot{\omega}_P - \dot{\omega}_R\right) t_P^2}{2} + \frac{\dot{\omega}_R \left(t_R - t_P\right)^2}{2} \tag{4.38}$$

Method 2. - Parceling—In the seond method of implementing the commanded firing times, the roll jets are fired continuously while the pitch jets are fired three separate times. The angular rate which will be produced during this firing sequence is shown by the solid line in Figure 4.6.

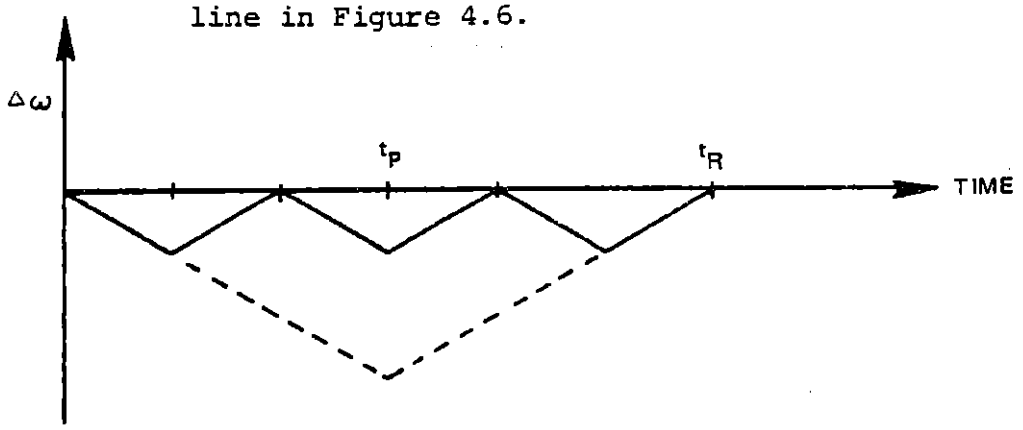

Figure 4.6. Effect of parceling the jet firing time.

The attitude error which results from this burn is

$$\Delta\theta_{e_{\text{Method 2}}} = \frac{1}{3}\left[\frac{\left(\dot{\omega}_P - \dot{\omega}_R\right)t_P^2}{2} + \frac{\left(\dot{\omega}_R t_R\right) - t_P}{2}^2\right] \qquad (4.39)$$

This simple example illustrates that the changes in attitude error resulting from excursions in attitude rate due to varying torques acting during a burn can be reduced by a factor of 3 where 3 is the number of subdivisions of a firing interval. This analysis can be extended to show that the reduction is by 1/n for n subdivisions. Three parcels were chosen for this autopilot design rather than two because of the symmetry it provided in handling different length firing times. A vehicle configuration with variable thrust jets was simulated to represent "infinite" parceling but the improvement in performance provided by the essentially infinite parceling for the vehicle parameters studied was not sufficient to justify increasing the complexity of the autopilot design by increasing the number of parcels.

CHAPTER 5

RATE ESTIMATION

5.1 General

The conventional approach to estimating angular rate and translational velocity of a jet-controlled spacecraft has been to utilize the estimated effects of the known-duration jet firings in a Kalman filter or some simpler, less accurate estimator.[1,2,6] The incorporation of the effects of these firings can be a complex and time-consuming process in the flight computer.

A much simpler and less time-consuming process of estimating angular rate and translational velocity while coasting is permitted by the phase space approach, which coordinates all jet firings to provide uninterrupted coasting periods. This estimation method is particularly well suited to the control goal of constant attitude and constant translational velocity. Furthermore, the accuracy of the estimations obtainable from coasting data alone has been found to be adequate for the achievement of this goal in terms of assumed system parameters.

In this thesis, random noise has been assumed to produce the largest errors in both the angular rate and translational velocity estimations, if there is no filtering in these estimations. It will be shown that significant reductions in the estimation errors are achieved by simple estimation schemes based on averaging measurements.

5.2 Angular Rate Estimation

In this thesis, three types of attitude measurement errors in the IMU are modeled: random noise, deterministic errors and quantization.

Only the random noise error was found to have a significant effect on the accuracy of estimated rate. It will be assumed that this is the case in the following discussion of rate estimation accuracy.

In estimating angular rate during a coasting period, it is assumed that the angular velocity coupling terms during the coasting period are sufficiently small that the resulting angular velocities about the three body axes do no change by a significant amount during the angular rate estimation time interval.

Table 5-1 compares the standard deviations of the rate estimated by three methods, for various numbers of samples (n) of an attitude angle θ while coasting. It is assumed that the errors in the measured values of θ are uncorrelated.

The largest errors listed for any particular value of n are obtained by using the two-point difference method in which the estimated angular rate ω_{est} is computed from

$$\omega_{est} = \frac{\theta(nT) - \theta(0)}{nT} \tag{5.1}$$

where T is the autopilot sampling period and nT is the rate estimation period. This estimation can be shown to produce a standard deviation in estimated rate, σ_ω, of

$$\sigma_\omega = \frac{\sigma_\theta \sqrt{2}}{nT} \tag{5.2}$$

where σ_θ is the noise-produced standard deviation of one sample of θ. A value of $\sigma_\theta = 0.05$ deg has been used to compute σ_ω values in the table.

The two-point rate estimation errors are shown to be reduced appreciably by taking the average of θ samples over the first n/2 autopilot periods (where n is chosen to be even), subtracting this from the

Table 5-1. Comparison of the standard deviations of ω = constant and uncorrelated noise in a ω which has a standard deviation of 180 sec (= 0.05 deg).

n = Total Number of Samples	nT = Measurement Time Interval (T = 0.03 s)	Standard Deviations of Rate Estimations (deg/s)		
		$\omega_{est} = \frac{\Delta\theta_n}{nT}$	$\omega_{est} = \frac{\overline{\Delta\theta}_{n/2 \text{ samples}}}{(n/2)T}$	ω_{est} From Kalman Filter
10	0.3	0.2357	0.2108	0.1589
20	0.6	0.1179	0.0745	0.0601
30	0.9	0.0786	0.0406	0.0335
40	1.20	0.0589	0.0264	0.0220
50	1.50	0.0471	0.0189	0.0159
60	1.80	0.0393	0.0143	0.0121

average over the second n/2 autopilot periods, and dividing the difference by nT/2. This second rate estimation approach may be expressed as

$$\omega_{est} = \frac{1}{\frac{nT}{2}}\left[\frac{1}{n/2}\sum_{i=n/2+1}^{n}\theta(iT) - \frac{1}{n/2}\sum_{i=1}^{n/2}\theta(iT)\right] \tag{5.3}$$

or it may be represented symbolically as in Table 6.2

$$\omega_{est} = \frac{\Delta\bar{\theta}_{n/2\ Samples}}{(n/2)T} \tag{5.4}$$

The standard deviation of the rate estimation for this n/2-average estimator is given by

$$\sigma_{\omega} = \left(\frac{2}{\sqrt{n/2}}\right)\left(\frac{\sigma_{\theta}\sqrt{2}}{nT}\right) \tag{5.5}$$

where it will be noted that the second factor is the value of σ_{ω} for a two-point rate estimator.

The best rate estimation obtainable from coast-period samples is that which would be provided by a Kalman filter. The σ_{ω} values listed for this filter in the last column of Table 5-1 are only slightly smaller than those listed for the n/2-average rate estimator, with the percentage difference between the σ_{ω}'s of the two estimators diminishing with increasing n.

It was decided that the n/2-average rate estimator provides an acceptable compromise between the conflicting goals of simplicity and accuracy, especially, since its accuracy is so close to that of a Kalman filter. The n/2-average filter is employed in all of the simulation runs of the phase space autopilot in this thesis.

5.3 Translational Velocity Estimation

The IMU accelerometers which measure translational velocity in the phase space autopilot have been assumed to have only two error sources, quantization and random noise. If the standard deviation of the random noise is appreciably greater than the level of quantization, then it is possible to significantly reduce the errors in sampled velocity by merely averaging these samples over the same period in which the angular rate is estimated. This is the approach which has been employed in the simulation results reported in Chapter 7.

5.4 Selection of the Estimation Periods

As indicated previously rate estimation is done during coasting periods (i.e., periods when jets are not firing). For a given IMU the accuracy with which vehicle attitude and translational rates can be estimated is a function of the number of measurements and the smapling interval at which measurements are taken. For the estimation technique selected for this design, this function is given in Eq. (5.5). In Figure 5.1, the standard deviation is plotted versus the number of attitude measurements for the specified parameters of 0.03 sec sampling period and 0.05 deg standard deviation for attitude measurement error.

For the attitude phase space control system, the attitude rate estimate is a more critical parameter than the translational velocity estimate. The length of the estimation period, therefore, is determined by the need for obtaining sufficiently accurate knowledge of attitude rate to allow the control system to effectively drive the attitude error into its deadband. For this purpose, three different estimation periods have been selected as shown in the following table. These are shown along with the respective standard deviations of the attitude rate estimate in Table 5-2. In selecting the estimation periods for each of these cases it was necessary to consider the direct impact of the duration of the estimation period on total convergence time and the indirect impact of the estimation accuracy (in terms of the total number of

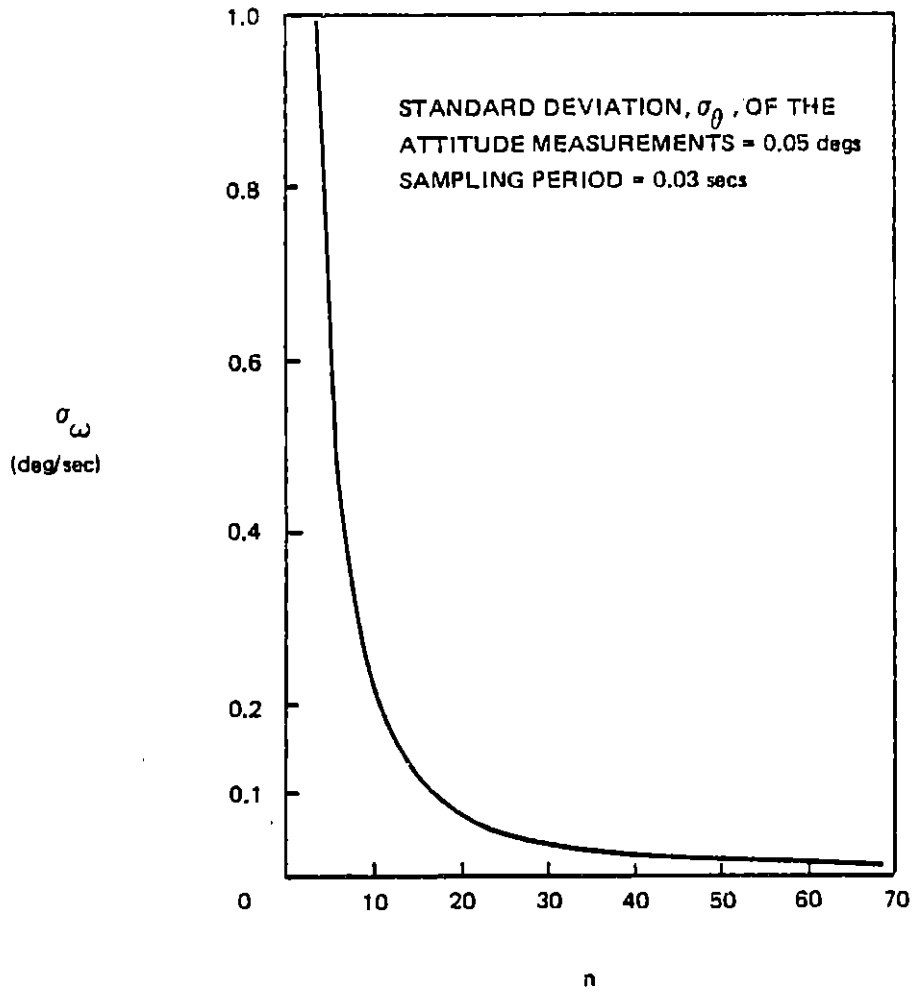

Figure 5.1. Standard deviation of estimated rate vs. number of attitude measurements.

Table 5-2. Estimation periods used in phase space autopilot.

Description of Period	Duration or Estimation Period	Number of Measurements	Stand. Dev. of Rate Est.
Inital estimation period (Independent of Region)	0.24 sec	8	0.2946 deg/sec
Estimation period when attitude error was in Region 4 prior to most recent jet firings	0.54 sec	18	0.0873 deg/sec
Estimation period when attitude error was in Regions 1, 2, or 3 prior to most recent jet firings	1.14 sec	38	0.0285 deg/sec

firings and estimation periods required) on total convergence time. As will be shown in the discussion of simulation results (Chapter 7) the choice of estimation periods allows the control system to effectively attain the desired state. It was not attempted in this study to optimize the choice of estimation periods to minimize the total convergence time. This would require a solution based on consideration of the probability distributions of initial errors, rate estimation errors, and jet firing and mass property uncertainties and would require determination of optimum control law convergence rates.

The choice of a short initial estimation period was based on the need to avoid a long delay in commanding jet firings for the case where the initial angular rate is large and in a direction such that the magnitude of the attitude error vector is increasing. The standard deviation of the rate estimate for the selected 0.24 sec initial coasting period is 0.2946 deg/sec which is approximately 30% of the assumed maximum inital rate of 1 deg/sec for each axis. This degree of inaccuracy is not critical because of the greatly increased accuracy of the succeeding rate estimates.

After the initial estimation period jets are fired to establish a convergence rate (unless the initial attitude error is in the deadband region). The establishment of this convergence rate allows the use of longer rate estimation periods than was used for the initial rate estimation. As shown in Table 5-2, an estimation period of 0.54 sec is used when the attitude error was in Region 4 prior to the most recent jet firings. It can be seen from Figure 5.1 that the choice of 18 measurements for this case corresponds to a point in the rate estimate standard deviation curve where its slope does not increase rapidly. The standard deviation for this case is 0.0873 deg/sec as compared to 0.2946 deg/sec obtained during the initial estimation period.

It was decided to use the same rate estimation period for all cases in which the Region was 1, 2, or 3 preceding the last set of firings. This period was selected as 1.14 seconds, which was computed to give a high expectation of the true rate being within the rate deadband of ±0.1 deg/sec per body axis when the estimated body-angle rates were within this deadband. If the body-angle samples obtained every autopilot cycle of 30 ms are assumed to have a normal distribution with a standard deviation of 0.05 deg (which has been assumed for the AIRS driver band angles), then the rate estimation based on differencing average body-angles over two successive intervals of 1.14/2 sec will have a normal distribution with a standard deviation of 0.0285 deg/sec. Assuming that the true attitude rates have a normal distribution with a standard deviation of 0.05 deg/sec*, it has been computed that the true angular rates will be within ±0.1 deg/sec for 95% of the times that the

---

* This standard deviation value is only a rough estimate of the effects of autopilot action in the presence of estimation errors, jet firings uncertainties, jet minimum impulse and mass property uncertainties. A Monte Carlo simulation approach, which considered variations in initial conditions along withthe various system uncertainties, would be required to obtain a more accurate value for this true-rate standard deviation.

estimated rates are within this deadband. If the rate estimation period were reduced, then the percentage of times within the deadband would also be reduced. (In addition, on a statistical basis, more firings and estimation periods would be required to achieve estimated body-angle rates that are within the deadband.)

CHAPTER 6

SIMULATION DESCRIPTION

6.1 General

The response characteristics of the phase space autopilot concepts described above were investigated using a detailed six-degree-of-freedom simulation of the spacecraft, attitude jets, and inertial measurement unit (IMU). This simulation, which was programmed on the Draper Laboratory's Amdahl 470/V6 computer, varies its integration step size so as to accurately represent any abrupt changes in system characteristics or variables. The nominal value of the integration time interval is 0.005 seconds, and the selected autopilot sampling interval is 0.03 seconds.

6.2 Vehicle Characteristics

The vehicle dimensions, mass properties, jet locations and nominal jet forces were chosen to suitably tax the performance capabilities of the phase space autopilot concept and also to illustrate certain aspects of the postulated control problem. Figure 4.2 shows the vehicle dimensions, center of mass location, and the locations and orientations of the twelve attitude control jets.

The mass of the assumed vehicle is

$$M = 100 \text{ slugs} \tag{6.1}$$

and the vehicle inertia tensor is

$$I_{(slug/ft^2)} = \begin{bmatrix} 3600 & -300 & 200 \\ -300 & 7400 & -40 \\ 200 & -40 & 8200 \end{bmatrix} \tag{6.2}$$

The vehicle rotational dynamics are simulated in terms of the general relationship

$$\underline{\tau} = \frac{d\underline{H}}{dt} + \underline{\omega} \times \underline{H} \tag{6.3}$$

where

$$\underline{H} = I\underline{\omega}$$

$$\underline{\omega} = \text{angular rate vector} = \begin{bmatrix} \omega_x \\ \omega_y \\ \omega_z \end{bmatrix}$$

ω_x, ω_y, ω_z = roll, pitch and yaw rates, respectively

$$\underline{\tau} = \text{net torque vector} = \begin{bmatrix} \tau_x \\ \tau_y \\ \tau_z \end{bmatrix}$$

τ_x, τ_y, τ_z = torques about the roll, pitch and yaw axes, respectively. (Note: x = roll axis, y = pitch axis and z = yaw axis)

The vehicle translational dynamics are simulated in terms of the relationship

$$\underline{f}_I = M \frac{d\underline{V}_I}{dt} \tag{6.4}$$

where $\underline{V}_I$ is the translational velocity—at the vehicle center of mass in inertial coordinates and $\underline{f}_I$ is the total jet force applied to the vehicle transformed to inertial axes.

It should be noted that the jets are configured to provide pure couples about the pitch, roll and yaw axes of the vehicle. This particular feature of jet couples and the general symmetry of the jets are not at all required for the phase space autopilot, which can be accommodated to asymmetrical jet configurations without couples. However, the simplicity of the chosen configuration facilitates an understanding of the autopilot's operation.

6.3 Jet Firing Characteristics

As previously mentioned in Chapter 4, the random variation in the force impulse of each jet is added in the simulation to the nominal or biased impulse versus time curve (which is assumed to be the same for all jets). The dual-slope, straight line approximations of the jet impulse versus time curve, for nominal conditions as well as for extreme biases are shown in Figure 4.4. The choice of the nominal or either of the two biased curves of impulse versus time is an input condition to each simulation run. The effects of random variations in the force impulses of individual jet firings are represented by adding to the chosen nominal or fixed-bias impulse curve a second curve which represents these random effects. This second curve is obtained by multiplying one of the curves in Figure 6.1 by a random variable which is uniformly distributed between -1 and +1. The polarity of the random variable determines which of the two curves in Figure 6.1 is to be employed. A random number generator is called by the simulation to generate a new value of this random variable for each jet firing.

The impulse versus time curves used in this simulation were obtained by scaling experimental jet firing data to the particular nominal force level of 160 lb assumed in this thesis.

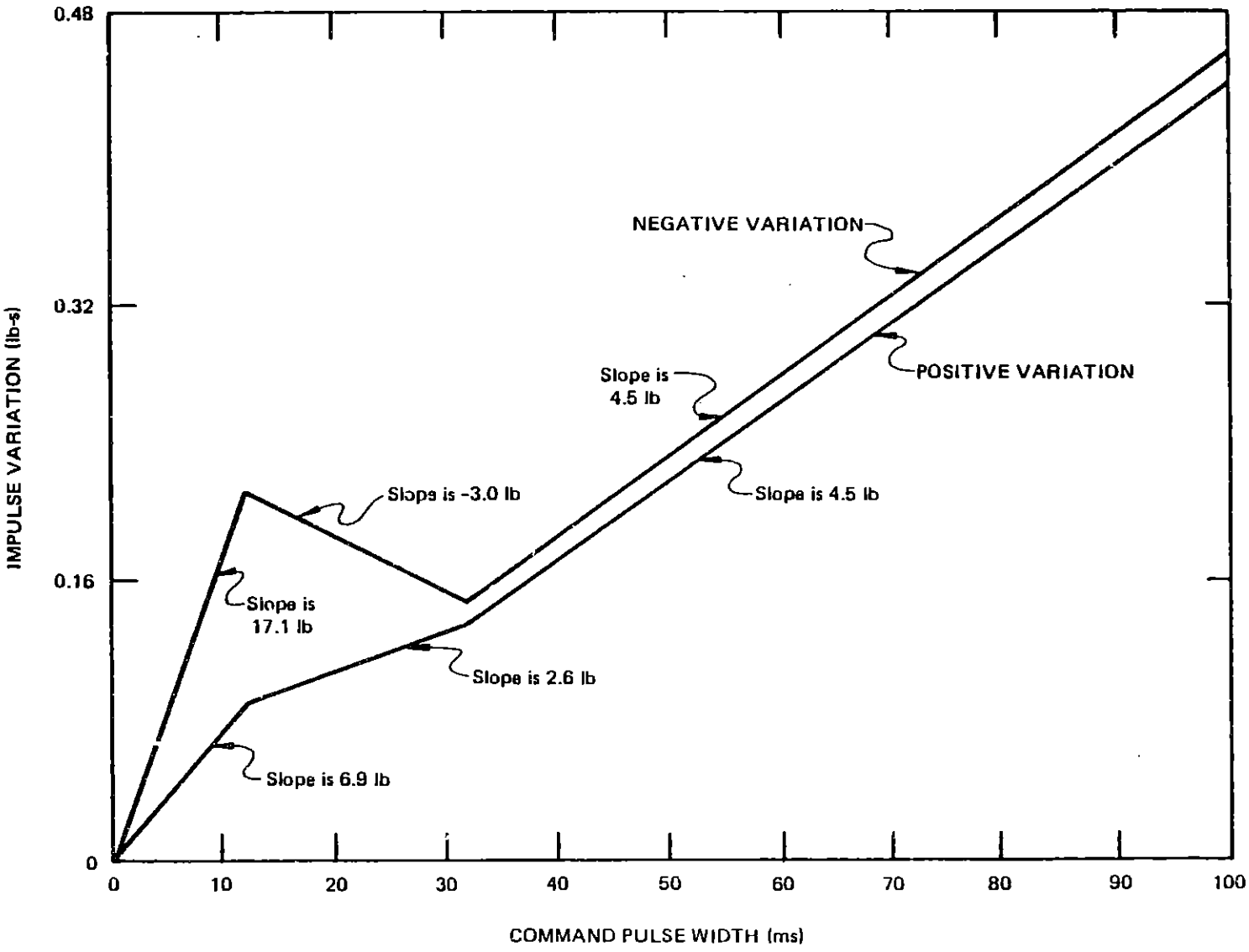

Figure 6.1. Simulation of jet firing uncertainties: impulse variation vs. command pulse width for a 160 lb thrust engine.

6.4 IMU Characteristics

The basic concept of the floated inertial ball, as implemented in the Advanced Inertial Reference System (AIRS), is used in the IMU simulation for this control investigation. The AIRS ball (or "platform") is assumed to be perfectly stabilized, inertially. The attitude measuring system of AIRS is represented in the simulation, with pessimistically large noise levels assumed to illustrate the autopilot's capabilities for estimating angular rate from attitude measurements. The IMU accelerometers are assumed to have the same quantization as the Space Shuttle IMU accelerometers. A random noise of standard deviation equal to twice the quantization level is added to show the autopilot's effectiveness in filtering out noise in its estimation of translational velocity.

The attitude of AIRS is measured by means of printed circuit resolver bands that are mounted on the outer surface of the floated ball and on the inner surface of the spherical shell (or "case") that surrounds the ball. Three orthogonal great circle "driver" bands are mounted on the ball, and one great circle "receiver" band is mounted on the inside of the spherical shell. Each driver band intersects the receiver band at two points, one of which is selected by the IMU electronics for attitude definition. The IMU electronics measure the location of the selected intersection point of any band pair in terms of the angular position of that point along each band from a reference point on the band. These band angles, which are shown in Figure 6.2, are defined as ϕ_1, ϕ_2, ϕ_3 for the three driver bands and as χ_1, χ_2, χ_3 for the receiver band. The intersection of the n^{th} driver band with the receiver band is measured by the angles ϕ_n and χ_n along these bands.

Since only two pairs of band angles are needed for determining the ball-case orientation, the accuracy of attitude measurements may be optimized by rejecting the least accurate pair of band angles, which is the pair associated with the driver band that is most nearly parallel to the receiver band. This band-angle rejection scheme and the AIRS attitude processing logic are represented in the simulation.

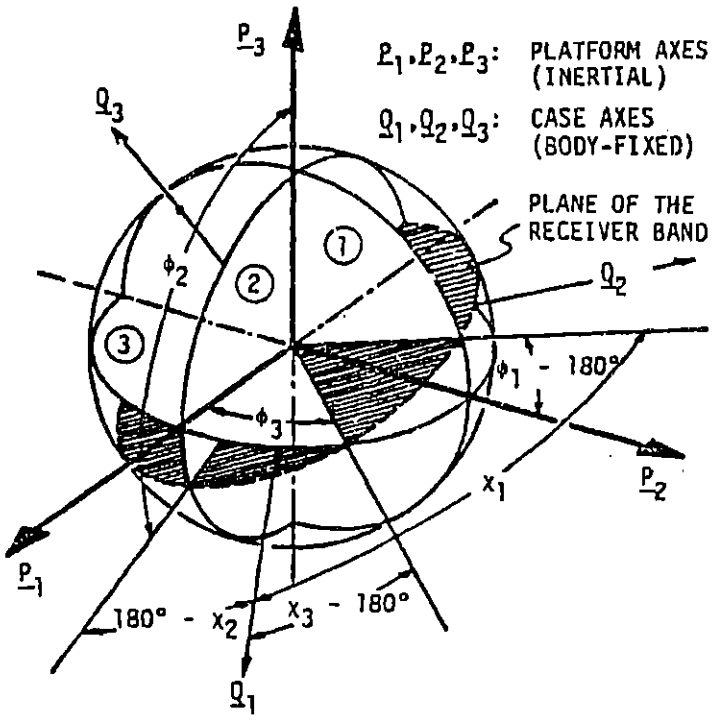

Figure 6.2. Definition of the AIRS band angles.

The simulation assumes that the case axis vectors $\underline{Q}_1$, $\underline{Q}_2$, $\underline{Q}_3$ are related to the body-axis vectors $\underline{X}$, $\underline{Y}$ and $\underline{Z}$ (representing roll, pitch, and yaw axes) by

$$\underline{Q}_1 = \underline{Z}$$

$$\underline{Q}_2 = -\underline{Y}$$

$$\underline{Q}_3 = \underline{X}$$

The relationships for computing the platform-axes-to-body-axes transformation, C_b^P from the measured band angles are given as follows

$$C_b^p = \begin{bmatrix} d_{11} & d_{12} & d_{13} \\ d_{21} & d_{22} & d_{23} \\ d_{31} & d_{32} & d_{33} \end{bmatrix} \tag{6.5}$$

$$d_{1i} = -w \cos \phi_i \cos \phi_j$$

$$d_{2i} = -w \sin \phi_j \cos \chi_i$$

$$d_{3i} = -w \sin \phi_j \sin \chi_i$$

$$d_{1j} = -w \sin \phi_i \sin \phi_j$$

$$d_{2j} = w \cos \phi_i \cos \chi_j$$

$$d_{3j} = w \cos \phi_i \sin \chi_j$$

$$d_{1k} = w \sin \phi_j \cos \phi_i$$

$$d_{2k} = w(\sin \phi_j \cos \chi_j - \cos \phi_j \cos \chi_i)$$

$$d_{3k} = w(\sin \phi_i \sin \chi_j - \cos \phi_j \sin \chi_i)$$

where

$$w = 1/\sin (\chi_i - \chi_j)$$

The subscript, k, is equal to the number of the rejected driver band and the subcripts i and j are the numbers of the retained driver bands. There are three possible combinations for i, j, and k: (1, 2, 3), (2, 3, 1), and (3, 1, 2). The angles ϕ_i and χ_i are the measured angles of the intersection of the i^{th} driver band with the receiver band, and ϕ_i and χ_j are the measured angles of the intersection of the j^{th} driver band with the receiver band.

The matrix C_b^p is used by the autopilot to transform the accelerometer measured velocity vector into body coordinates, to initialize the attitude error vector $\underline{\theta}_e$ and to update $\underline{\theta}_e$ every 15 autopilot cycles.

Numerical values of IMU constants are as follows:

AIRS band angles:

1. Quantization = $360°/2^{16}$.
2. Deterministic errors for driver and receiver angles are as measured in a laboratory mockup of the AIRS attitude system.*
3. Random noise standard deviation is assumed 180 $\widehat{\text{sec}}$ for driver bands and 20 $\widehat{\text{sec}}$ for the receiver band.

IMU accelerometers:

1. Quantization = 0.033 ft/s.
2. Standard deviation of random noise = 0.066 ft/s.

The commanded attitude for the phase space autopilot is specified in terms of a platform-axes-to-commanded-body-axes transformation, $C_b^p\Big|_{com}$. This matrix is used in conjunction with the platform-axes-to-measured-body-axes transformation, $C_b^p\Big|_{meas}$ (designated as C_b^p in Eq. 6.5) to initialize the attitude error vector $\underline{\theta}_e$ and to update it every 15 autopilot cycles. This error computation uses the off-diagonal elements of the error matrix C_{bcom}^{bmeas}, given by

$$C_{bcom}^{bmeas} = C_b^p\Big|_{com} \left[C_b^p\Big|_{meas}\right]^T \tag{6.6}$$

*These deterministic errors are high-harmonic fluctuations which are less than 10 $\widehat{\text{min}}$ in amplitude and have slopes less than 3 $\widehat{\text{min}}/\widehat{\text{deg}}$.

$$C_{bcom}^{bmeas} = \begin{bmatrix} C_{11} & C_{12} & C_{13} \\ C_{21} & C_{22} & C_{23} \\ C_{31} & C_{32} & C_{33} \end{bmatrix} \tag{6.7}$$

The elements of

$$\underline{\theta}_e = \begin{bmatrix} \theta_{e_x} \\ \theta_{e_y} \\ \theta_{e_z} \end{bmatrix} \tag{6.8}$$

are then computed from

$$\theta_{e_x} = (C_{23} - C_{32})/2 \tag{6.9a}$$

$$\theta_{e_y} = (C_{31} - C_{13})/2 \tag{6.9b}$$

$$\theta_{e_z} = (C_{12} - C_{21})/2 \tag{6.9c}$$

These error components are based on a single-rotation-axis definition of the orientation of the measured relative to the commanded body frame. This definition is based on a theorem of Euler, according to which a body may be changed from one orientation to any other orientation by rotating it about a body-fixed axis that is also fixed in the platform reference frame. This axis may be designated by a unit vector $\underline{r}$, whose direction indicates the direction of rotation. Both $\underline{r}$ and the angle α through which the body must be rotated about $\underline{4}$ can be calculated from the elements of the direction cosine matrix relating the two body orientations. In the case where the matrix is C_{bcom}^{bmeas} the values of $\underline{r}$ and α are given by

$$\alpha = \cos^{-1} \frac{1}{2} (C_{11} + C_{22} + C_{33} - 1) \qquad (6.10)$$

and

$$r_x = (C_{23} - C_{32})/ 2 \sin \alpha \qquad (6.11a)$$

$$r_y = (C_{31} - C_{13})/2 \sin \alpha \qquad (6.11b)$$

$$r_z = (C_{12} - C_{21})/2 \sin \alpha \qquad (6.11c)$$

From the last three equations it is seen that the earlier relationships for θ_{e_x}, θ_{e_y}, θ_{e_z} (Eq. 6.9) are based on

$$\theta_{e_x} = r_x \sin \alpha \qquad (6.12a)$$

$$\theta_{e_y} = r_y \sin \alpha \qquad (6.12b)$$

$$\theta_{e_z} = r_z \sin \alpha \qquad (6.12c)$$

Since the commanded body axes are close to the measured body axes in the rolling maneuver, α is small and $\sin \alpha \approx \alpha$. Thus

$$\underline{\theta}_e \approx \underline{r}\, \alpha \qquad (6.13)$$

In between the updating of $\underline{\theta}_e$ based on C_{bcom}^{pmeas} this error vector is updated incrementally every autopilot cycle, by subtracting from $\underline{\theta}_e$ the body angle increment vector $\Delta\underline{\theta}$. This vector is computed from measured AIRS band angle increments, using the relationship

(6.14)

$$\underline{\Delta\theta}_n = B \begin{bmatrix} \Delta\phi_i \\ \Delta\phi_j \\ \Delta\chi_i \end{bmatrix}_n \tag{6.14}$$

where n indicates a particular autopilot sampling instant. Here, the incremental transformation matrix, B, is updated every 15 autopilot cycles, using band angles values ϕ_i', ϕ_j', χ_i', χ_j' which are obtained by adding to the current measured values of each angle one half the difference between the present value and the value measured 15 autopilot cycles previously. The relationship for B is

$$B = \begin{bmatrix} -w \cos \phi_i' \cos \phi_j' & 0 & -1 \\ w^2 \sin \phi_j' \sin \chi_j' & w^2 \cos \phi_i' \sin \chi_i' & 0 \\ -w^2 \sin \phi_j' \cos \chi_j' & w^2 \cos \phi_i' \cos \chi_i' & 0 \end{bmatrix} \tag{6.15}$$

6.5 Autopilot Representation

The equations and parameters of the autopilot in the simulation are as described in previous chapters.

The various values of system constants employed by the autopilot are stored separately from the true system constants, so as to represent the uncertainties in the autopilot knowledge of these constants. The autopilot-stored constants include (1) vehicle mass, (2) vehicle center of mass, (3) vehicle inertia tensor, (4) the two slopes of the nominal jet impulse curve in Figure 4.4, (5) the positions and orientations of the jets, and (6) the IMU position. The simulation neglects computational delays in the autopilot.

CHAPTER 7

SIMULATION RESULTS

Computer plots and tabulated data are presented below for a group of simulation runs which were selected to illustrate general capabilities and specific features of the phase space autopilot. These runs, which are described in Table 7-1, consider the following alternate conditions.

1. Either an ideal system in which there are no IMU errors, no jet firing uncertainties, and no mismodeling of mass properties in the autopilot or an actual system in which all these errors and uncertainties are included. (In the latter the autopilot uses the nominal mass properties of Table 7-2(a) and the vehicle simulation is based on the off-nominal mass properties of Table 7-2(b)).
2. Either the pseudo inverse jet selection or the fixed jet selection routine.
3. Either with or without the parceling of jet firing times. (It should be noted that in those runs where parceling was employed, only those sets of jet firings in which the longest firing time was $\geq$ 0.3 sec were parceled.)
4. Three sets of initial conditions labeled A, B, and C which are described in Table 7-3.

The initial conditions A were chosen to illustrate the performance of the control system in nulling typical initial errors. Initial conditions B, and C were chosen to show the benefits of parceling of jet firing times for "worst case" initial errors.

Table 7-1. Summary of simulation runs

Run Number	Jet Selection Procedure Used	IMU Errors Included	Mass Property Uncertainties and Jet Firing Uncertainties Included	Initial Conditions*	Parceling of Jet Firings Used	Convergence Time (sec)	Total On-time of All Jets (sec)
1	pseudo inverse	no	no	A	no	4.92	5.84
2	fixed jet	no	no	A	no	4.98	6.54
3	pseudo inverse	yes	yes	A	no	4.86	5.51
4	fixed jet	yes	yes	A	no	4.95	6.55
5	pseudo inverse	no	no	B	no	**	17.87
6	pseudo inverse	no	no	B	yes	7.50	13.27
7	fixed jet	no	no	B	no	**	20.45
8	fixed jet	no	no	B	yes	7.08	15.93
9	pseudo inverse	no	no	C	no	6.63	14.29
10	pseudo inverse	no	no	C	yes	6.00	13.88
11	fixed jet	no	no	C	no	8.82	16.14
12	fixed jet	no	no	C	yes	7.47	14.27
13	fixed jet	yes	yes	C	yes	7.20	14.45

* See Table 7-3 for a list of initial conditions

** Did not converge for the 9-second duration of the simulation runs

Table 7-2(a). Nominal vehicle mass properties.

Mass (slugs)		100	
	x	y	z
Center of mass (ft)	4.00	-0.30	-0.30
IMU position (ft)	5.00	1.00	1.00
	I_{xx}	I_{yy}	I_{zz}
	3600	7400	8200
Inertia properties (slug-ft^2)	I_{xy}	I_{xz}	I_{yz}
	-300	200	-40

Table 7-2(b). Assumed off-nominal mass properties.

Mass (slugs)		100	
	x	y	z
Center of mass (ft)	3.95	-0.35	-0.30
IMU position (ft)	5.05	1.00	1.05
	I_{xx}	I_{yy}	I_{zz}
	3672	7548	8364
Inertia properties (slug-ft^2)	I_{xy}	I_{xz}	I_{yz}
	-306	204	-40.8

Table 7-3. List of initial conditions.*

	Attitude Error Vector (deg)			Angular Rate (deg/sec)			Translational Velocity Error (ft/sec)		
	θ_{e_x}	θ_{e_y}	θ_{e_z}	ω_x	ω_y	ω_z	V_{e_x}	V_{e_y}	V_{e_z}
A	1.0	-1.0	1.0	-1.0	1.0	-1.0	-2.0	1.5	0.5
B	1.0	-1.0	1.0	-1.0	1.0	-1.0	4.0	-0.5	6.0
C	1.0	-1.0	1.0	-1.0	1.0	-1.0	-4.0	-0.5	6.0

* Note that $\underline{\theta}_e = \underline{\theta}_c - \underline{\theta}$, that is the attitude error vector is equal to the commanded attitude vector minus the actual attitude vector so that for a constant commanded attitude

$$\dot{\underline{\theta}}_e = -\dot{\underline{\theta}} = -\underline{\omega}$$

Thus, the time derivative of the attitude error vector is the opposite sign of the time derivative of the attitude vector, $\underline{\omega}$.

The convergence times listed in Table 7-1 for each run are the times required to achieve simultaneously the following three conditions.

1. The magnitude of the attitude error vector, $\underline{\theta}_e$ is less than 0.5 deg.
2. The magnitude of each component of the estimated vehicle angular rate vector, $\underline{\omega}_{est}$, is less than 0.1 deg/sec.
3. The magnitude of each component of the translational velocity error vector is less than 0.05 ft/sec.

It should be emphasized that without IMU measurements the convergence times could have been much shorter than indicated here if the control law had been redesigned. However, in order to illustrate the effects of IMU measurements, the same function for the convergence rate, c, and the same length rate estimation coast periods were used in all the simulation runs.

The total on-time of all the jets is the sum of all the on-times of each jet over a complete run and is therefore an indication of the propellant consumed.

Table 7-4 lists, for each simulation run, the effects of successive sets of jet firings on the directions and magnitudes of $\underline{\omega}_c$, $\underline{\omega}_{final}$, $\underline{\theta}_{e_{initial}}$, and $\underline{\theta}_{e_{final}}$. It should be noted that these are acutal rather than measured rate and attitude variables. This means in particular that the commanded rate $\underline{\omega}_c$ is based on the actual attitude error vector $\underline{\theta}_e$ rather than the measured error vector (as in the autopilot implentation). "Initial" refers to the values at the initiation of jet firings and "final" refers to values of these variables at the termination of jet firings. Note that the angle between $\underline{\omega}_c$ and $\underline{\omega}_{final}$ is not defined when $\underline{\omega}_c = 0$ (i.e., when the attitude error is within its deadband).

Ideally the angle between $\underline{\omega}_c$ and $\underline{\omega}_{final}$ should be zero. However, there are three effects which may cause this angle to be finite. First is the effect of measurement errors which result in the autopilot version of $\underline{\omega}_c$ (based on measured $\underline{\theta}_e$) being different from the ideal $\underline{\omega}_c$ in the table (which is based on actual $\underline{\theta}_e$). This difference in autopilot $\underline{\omega}_c$

Table 7-4. Illustrating the effects of the successive sets of jet firings on the directions and magnitudes of $\underline{\omega}_c$, $\underline{\omega}_{final}$, $\underline{\theta}_{e_{initial}}$, and $\underline{\theta}_{e_{final}}$.

Run	Jet Firing	Angle* Between $\underline{\omega}_c$ and $\underline{\omega}_{final}$ (deg)	$\lvert\underline{\omega}_c\rvert$, $\lvert\underline{\omega}_{final}\rvert$ (deg/sec)	Angle Between $\underline{\omega}_{final}$ and $\underline{\theta}_{e_{final}}$ (deg)	Angle Between $\underline{\theta}_{e_{initial}}$ and $\underline{\theta}_{e_{final}}$ (deg)	$\lvert\underline{\theta}_{e_{initial}}\rvert$, $\lvert\underline{\theta}_{e_{final}}\rvert$ (deg)
1	1	0.5	1.72, 1.71	18.6	18.9	2.15, 3.07
	2	0.3	1.79, 1.80	0.8	0.7	2.24, 2.10
	3	0.4	0.94, 0.93	0.5	0.2	1.17, 1.05
	4	---	0.00, 0.01	49.1	111.6	0.02, 0.03
2	1	0.5	1.72, 1.72	13.7	14.1	2.15, 3.33
	2	1.1	1.95, 1.96	0.9	0.5	2.44, 2.27
	3	0.8	0.98, 0.97	1.6	1.1	1.22, 1.03
	4	---	0.00, 0.01	54.5	9.2	0.06, 0.12
3	1	14.1	1.72, 1.68	7.5	15.2	2.15, 2.99
	2	0.9	0.98, 1.05	2.1	1.5	1.23, 1.11
	3	---	0.00, 0.04	64.1	20.8	0.07, 0.12
4	1	13.5	1.72, 1.68	23.3	14.3	2.15, 3.28
	2	0.3	2.01, 2.03	1.5	1.3	2.51, 2.29
	3	10.4	0.92, 0.77	11.8	16.0	1.15, 0.94
	4	---	0.00, 0.04	127.9	12.0	0.20, 0.20

Table 7-4. Illustrating the effects of the successive sets of jet firings on the directions and magnitudes of $\underline{\omega}_c$, $\underline{\omega}_{final}$, $\underline{\theta}_{e_{initial}}$, and $\underline{\theta}_{e_{final}}$. (Cont.)

Run	Jet Firing	Angle* Between $\underline{\omega}_c$ and $\underline{\omega}_{final}$ (deg)	$\lvert\underline{\omega}_c\rvert$, $\lvert\underline{\omega}_{final}\rvert$ (deg/sec)	Angle Between $\underline{\omega}_{final}$ and $\underline{\theta}_{e_{final}}$ (deg)	Angle Between $\underline{\theta}_{e_{initial}}$ and $\underline{\theta}_{e_{final}}$ (deg)	$\lvert\underline{\theta}_{e_{initial}}\rvert$, $\lvert\underline{\theta}_{e_{final}}\rvert$ (deg)
5	1	0.9	1.72, 1.74	132.9	133.8	2.15, 5.53
	2	0.8	4.96, 4.95	3.2	2.5	6.20, 4.74
	3	2.1	0.91, 0.91	145.8	143.7	1.13, 0.40
	4	0.1	1.10, 1.10	3.2	3.3	1.37, 1.35
	5	0.3	0.62, 0.61	0.4	0.2	0.77, 0.71
6	1**	0.6	1.72, 1.72	80.4	80.8	2.15, 1.34
	2**	0.8	1.22, 1.22	8.3	8.1	1.52, 1.50
	3	0.4	0.68, 0.68	0.6	0.6	0.85, 0.79
	4	---	0.00, 0.00	0.6	126.0	0.02, 0.02
7	1	1.1	1.72, 1.74	134.3	135.4	2.15, 6.31
	2	0.8	5.58, 5.58	5.2	5.2	6.97, 4.28
	3	0.6	0.89, 0.89	163.4	163.1	1.11, 1.01
	4	0.3	1.58, 1.59	1.2	1.2	1.98, 1.86
	5	0.4	0.81, 0.81	0.5	0.1	1.01, 0.87

Table 7-4. Illustrating the effects of the successive sets of jet firings on the directions and magnitudes of $\underline{\omega}_c$, $\underline{\omega}_{final}$, $\underline{\theta}_{e_{initial}}$, and $\underline{\theta}_{e_{final}}$. (Cont.)

Run	Jet Firing	Angle* Between $\underline{\omega}_c$ and $\underline{\omega}_{final}$ (deg)	$\lvert\underline{\omega}_c\rvert$, $\lvert\underline{\omega}_{final}\rvert$ (deg/sec)	Angle Between $\underline{\omega}_{final}$ and $\underline{\theta}_{e_{final}}$ (deg)	Angle Between $\underline{\theta}_{e_{initial}}$ and $\underline{\theta}_{e_{final}}$ (deg)	$\lvert\underline{\theta}_{e_{initial}}\rvert$, $\lvert\underline{\theta}_{e_{final}}\rvert$ (deg)
8	1**	0.6	1.72, 1.72	89.1	89.7	2.15, 1.49
	2**	1.0	1.40, 1.40	8.5	8.0	1.76, 1.69
	3	0.5	0.78, 0.78	0.7	0.7	0.98, 0.87
	4	---	0.00, 0.00	90.0	21.6	0.02, 0.06
9	1	0.7	1.72, 1.72	56.3	55.7	2.15, 2.58
	2	1.1	1.76, 1.76	5.3	5.3	2.21, 1.98
	3	0.1	0.84, 0.84	1.6	1.6	1.05, 0.90
	4	---	0.00, 0.00	106.8	14.6	0.04, 0.07
10	1**	0.3	1.72, 1.72	19.6	19.5	2.15, 2.08
	2	0.8	0.97, 0.97	4.1	4.0	1.22, 1.06
	3	---	0.00, 0.00	130.0	31.6	0.08, 0.12
11	1	0.8	1.72, 1.69	75.1	74.5	2.15, 5.44
	2	0.9	4.22, 4.22	44.6	43.5	5.28, 4.37
	3	2.2	0.95, 0.96	29.9	30.1	1.19, 0.49
	4	0.3	0.57, 0.58	0.7	0.8	0.71, 0.73
	5	---	0.00, 0.00	97.7	56.2	0.09, 0.07

Table 7-4. Illustrating the effects of the successive sets of jet firings on the directions and magnitudes of $\underline{\omega}_c$, $\underline{\omega}_{final}$, $\underline{\theta}_{e_{initial}}$, and $\underline{\theta}_{e_{final}}$. (Cont.)

Run	Jet Firing	Angle* Between $\underline{\omega}_c$ and $\underline{\omega}_{final}$ (deg)	$\lvert\underline{\omega}_c\rvert$, $\lvert\underline{\omega}_{final}\rvert$ (deg/sec)	Angle Between $\underline{\omega}_{final}$ and $\underline{\theta}_{e_{final}}$ (deg)	Angle Between $\underline{\theta}_{e_{initial}}$ and $\underline{\theta}_{e_{final}}$ (deg)	$\lvert\underline{\theta}_{e_{initial}}\rvert$, $\lvert\underline{\theta}_{e_{final}}\rvert$ (deg)
12	1**	0.4	1.72, 1.71	42.2	41.9	2.15, 2.60
	2	1.4	1.40, 1.40	7.5	7.4	1.76, 1.63
	3	0.2	0.74, 0.74	0.8	1.0	0.93, 0.85
	4	---	0.00, 0.00	0.5	94.3	0.02, 0.01
13	1**	16.8	1.72, 1.98	75.7	59.3	2.15, 2.88
	2**	1.8	2.25, 2.31	10.5	10.3	2.81, 2.42
	3	9.6	0.93, 0.98	11.3	4.5	1.16, 0.94
	4	---	0.00, 0.05	59.9	79.1	0.26, 0.29

* This angle is not computed when $\omega_c = 0$ (which is the case when the attitude error $\underline{\theta}_e$ is in its deadband.)

** These jet firings were parceled.

produces an $\underline{\omega}_{final}$ whose direction (and magnitude) is different from that of the ideal $\underline{\omega}_c$. Second is the effect of angular rate estimation errors on $\underline{\omega}_{final}$. Here, it should be noted that the rate change request is based on

$$\underline{\Delta\omega}_c = \underline{\omega}_c - \underline{\omega}_{est} \tag{7.1}$$

and that the resulting value of $\underline{\omega}_{final}$ would ideally be given by

$$\underline{\omega}_{final} = \underline{\Delta\omega}_c + \underline{\omega}_{initial} \tag{7.2}$$

or substituting Eq. (7.1) into Eq. (7.2)

$$\underline{\omega}_{final} = \underline{\omega}_c + (\underline{\omega}_{initial} - \underline{\omega}_{est}) \tag{7.3}$$

This last relationship shows that errors between the values of $\underline{\omega}_{inital}$ and $\underline{\omega}_{est}$ translate directly into corresponding errors in $\underline{\omega}_{final}$ (provided, or course, that the jet firings produce exactly the commanded $\underline{\Delta\omega}_c$). The third and last factor influencing the angle between $\underline{\omega}_c$ and $\underline{\omega}_{final}$ is the deviation of $\underline{\omega}_{final}$ from the sum $\underline{\Delta\omega}_c + \underline{\omega}_{initial}$ resulting from inaccuracies in the computation and implementation of jet firings. The jet firing uncertainties, the minimum firing time, the quantization of the jet firing times, and the effects of vehicle motion on the angular rates produced by jet firings all contribute to the angular error between $\underline{\omega}_{final}$ and $\underline{\omega}_c$.

The angle between $\underline{\omega}_{final}$ and $\underline{\theta}_{e_{final}}$ also should ideally be zero. This angle is finite first because of all the factors that caused the angle between $\underline{\omega}_{final}$ and $\underline{\omega}_c$ and second because of the effects of the finite jet firing times in changing $\underline{\theta}_e$ from the initial value on which $\underline{\omega}_c$ was based. If $\underline{\omega}_{final}$ and $\underline{\theta}_{e_{final}}$ are parallel, then $\underline{\omega}_{final}$ would be in a direction to reduce all components of $\underline{\theta}_e$ to zero simultaneously.

The change in the direction of $\underline{\theta}_e$ during a set of jet firings, as shown by the angle between $\underline{\theta}_{e_{initial}}$ and $\underline{\theta}_{e_{final}}$, depends not only on the direction of the jet firings but also on the way in which the firing times differ and on the angular rates at the beginning of the jet firings. The parceling of jet firings tends to reduce this angle between $\underline{\theta}_{e_{initial}}$ and $\underline{\theta}_{e_{final}}$ as well as the angle between $\underline{\omega}_{final}$ and $\underline{\theta}_{e_{final}}$.

The time histories of the vehicle state and autopilot parameters for the runs listed in Table 7-1 are shown in Figures 7.1 through 7.13. The definition of the plotted variables is given in Table 7-5. The plotting routine samples these variables every 0.03 sec and interpolates in between. Note that for Runs 1 through 4, these variables are plotted for 7 sec and for the remaining runs they are plotted for 9 sec regardless of the convergence times.

Computer plots for Runs 1 and 2 are given in Figures 7.1 and 7.2 respectively. Both of these runs were made with the nominal vehicle mass properties and firing characteristics and with no IMU measurement noise or quantization. The pseudo inverse jet selection procedure was used in Run 1 and the fixed jet selection procedure was used in Run 2.

Both runs had an initial firing interval of approximately 1 sec, and during this interval the magnitude of the attitude error vector increased by approximately 50%. The attitude error vector also rotated by more than 14 deg in each case as can be seen in Table 7-4. The translational velocity errors were within the specified limits at the completion of the first burn. Therefore, the second set of jet firings was needed only to establish a new convergence rate which would be parallel to $\underline{\theta}_e$ and which would therefore drive all three components of $\underline{\theta}_e$ to zero simultaneously. It can be seen from the plots that the attitude errors approached zero in a well-behaved manner after the second set of jet firings and that they reached zero at nearly the

same time. The third burn decreased the attitude rates and the final set of jet firings reduced the attitude rates to within the specified limits of 0.1 deg/sec about each body axis.

Although the convergence times for Runs 1 and 2 were comparable, the two jet selections resulted in different time histories during the initial burn. The largest component of the angular rate vector which occurred during the first burn using the pseudo inverse jet selection was -2.02 deg/sec about the x-axis while the largest component of the angular rate vector which resulted from using the fixed jet selection algorithm was -2.42 deg/sec about the z-axis. These different angular rate time histories caused the attitude error time histories to be different for the two runs.

Figures 7.3 and 7.4 show the results of Runs 3 and 4 respectively. These runs include the effects of IMU measurements and jet firing uncertainties. The vehicle mass parameters used to simulate the vehicle response are listed in Table 7-2(b). The autopilot assumed for its computations the nominal vehicle mass properties given in Table 7-2(a). The pseudo inverse jet selection procedure was used in Run 3 and the fixed jet slection procedure was used in Run 4. The convergence times obtained in these two runs were comparable to those obtained in Runs 1 and 2, indicating that the rate estimation and resulting jet firings are sufficiently accurate to make the control system insensitive to the measurement noise levels included as well as to the uncertainties in mass properties and in jet firings considered.

The need for parceling of jet firing times arises when large initial translational velocity errors occur. These large velocities can require a long initial set of jet firings of unequal durations with produce undersirable moments, angular velocity and changes in both the magnitude and direction of the angular error vector $\underline{\theta}_e$. To illustrate the effects of these large initial velocity errors and the benefits of parceling, two sets of initial conditions, B and C, were chosen which contain large initial velocity errors. All but the last of the runs

based on initial conditions B and C were made without any IMU errors, mass property errors or jet firing uncertainties, so as to illustrate the basic dynamic problems alleviated by parceling without any secondary effects to alter the results.

Figure 7.5 illustrates the performance obtained for the initial conditions B using the pseudo inverse jet selection with no parceling of jet firings. The initial burn time (i.e., time of the longest firing jet) was 3.42 sec, and during this time $\underline{\theta}_e$ rotated by 133.8 deg and increased in magnitude from 2.15 deg to 5.53 deg. The large rotation of $\underline{\theta}_e$ was due to the fact that $\underline{\theta}_e$ and $\underline{\theta}_e$ changed sign during the first burn. Although the jet firings produced a $\underline{\omega}_{final}$ that was nearly parallel to $\underline{\omega}_c$, as required by the control law, the rotation of $\underline{\theta}_e$ during the burn resulted in a very large angle of 132.9 deg between $\underline{\theta}_{e_{final}}$ and $\underline{\omega}_{final}$. As a result of this large angle between $\underline{\theta}_{e_{final}}$ and $\underline{\omega}_{final}$ the magnitude of $\underline{\theta}_e$ diverged during the subsequent coast period, increasing from 5.53 deg to 6.20 deg. The peak component of the angular rate vector which occurred during this first burn was -3.82 deg/sec about the y-axis. This run failed to converge in 9 sec.

The computer plots for Run 6 are given in Figure 7.6. This run used the same initial conditions and jet selection procedure as in Run 5, but added a parceling routine which parceled any set of jet in which the longest firing time was $\geq$ 0.3 sec. In this run the first two burns met the 0.3 sec requirement and were parceled. Subsequent burns which were less than 0.3 sec duration were not parceled. The first set of jet firings for Runs 5 and 6 have the same initial conditions, and therefore the same request vector, and differ only in the use of parceling in Run 6. Comparison of the results of these two sets of firings shows that the parceling in Run 6 reduced the peak excursion of ω_y by roughly a factor of 2 (from -3.82 deg/sec to -1.88 deg/sec and resulted in a reduction in the rotation of $\underline{\theta}_e$ (from 133.8 deg without parceling to 80.8 deg with parceling).

The magnitude of $\underline{\theta}_e$ at the beginning of the second burn was only 1.52 deg with parceling compared to 6.20 deg without parceling (for the same initial $|\underline{\theta}_e|$ of 2.15 deg). Run 6 with parceling converged in 7.50 sec, while Run 5 without parceling had not converged by the end of the 9 sec simulation time.

Figure 7.7 and Table 7.4 show that without parceling, the use of the fixed jet slection routine in Run 7 with initial conditions B resulted in an increase in the magnitude of $\underline{\theta}_e$ from 2.15 deg to 6.31 deg and a rotation of $\underline{\theta}_e$ through 135.4 deg during the initial burn. The rotation of $\underline{\theta}_e$ was primarily due to the excursion of the pitch rate, ω_y, which reached a peak value of -5.36 deg/sec. When parceling was used in Run 8, this peak rate was reduced by more than a factor of 2 to -2.45 as shown in Figure 7.8. As a result of the reduction in the ω_y excursion with parceling, the rotation of $\underline{\theta}_e$ was reduced from 135.4 deg to 89.7 deg. The magnitude of $\underline{\theta}_e$ at the beginning of the second burn was only 1.76 deg with parceling compared to 6.97 deg without parceling (for the same initial $|\underline{\theta}_e|$ of 2.15 deg).

Runs 9 through 13 were made using initial conditions C. This set of initial conditions differs only in the sign of the x-component of the translational velocity error vector. Comparing the plots of these runs with those of Runs 5 through 8, it can be seen that this sign change had a major effect on the time histories of the state variables. This can be explained by examining the jet configuration. When V_{e_x} is negative the jets which must be fired to null out V_{e_x} are the symmetrically located jets which have the largest pitch and yaw moments. While these jets are being fired together for translationalvelocity nulling they are not available to be fired individually or as couples with other jets to produce requested changes in angular rate about the pitch and yaw axes. Thus, in effect the ability to produce or control pitch and yaw rates is virtually inhibited while these jets are being used for translation. On the other hand, when V_{e_x} is positive, the nulling of V_{e_x} requires the firing of jets which have only small pitch and yaw moments,

leaving the larger moment jets free to control the angular velocities about the pitch and yaw axes. Thus, the response characteristics for a positive V_{e_x} will be quite different then those for a negative V_{e_x}, even if all other initial conditions are the same. The effects of other conditions in combination with the polarity of V_{e_x} will determine which set of conditions are most difficult to null out.

Runs 9 through 12, made with conditions C, consider the same combinations of the previous for runs—that is, with two jet selections, with and without parceling, and without any IMU errors, mass property errors or jet uncertainties. The improvement in convergence time resulting from the addition of parceling is evident in these latter four runs as it was in the first set of runs. However, it should be pointed out that the non-parceled runs did converge in 6.63 sec and 8.82 sec in Runs 9 and 12 (as shown in Table 7-1), where as they did not converge within the 9 sec of Runs 5 and 7. There are other differences between the two sets of runs which show the strong effects of initial conditions on performance. For example, the runs with parceling converged more quickly for the fixed jet selection than for the pseudo inverse selection in the first set, while the opposite was the case in the second set of runs.

It should be noted that the pseudo inverse jet selection procedure had slightly shorter jet on-times than the fixed jet selection routine in all the comparative runs listed in Table 7-1. However, as will be discussed further in Chapter 8, the pseudo inverse has a very strong disadvantage in the long computation time required relative to the fixed jet selection method. Therefore the reduction in propellant consumption is probably not sufficient in itself to warrant the use of the pseudo inverse technique over the must simpler fixed jet selection procedure.

One additional simulation run was made to illustrate the effects of adding the IMU errors, mass property errors and jet firing uncertainties to the case of Run 12 where the fixed jet selection is employed

with parceling for the initial conditions C. A comparison of Figures 7.11 and 7.12 shows that there are no dramatic differences between the responses for the two cases. Interestingly, the convergence time is less for the case with errors than it is for the case without errors. However, this reduction of convergence time with added errors is probably the result of the particular bias assumed for jet firings and the particular mass property errors assumed rather than the indication of a general trend.

Table 7-5. Definition of plotted variables and labels.

ROLL ERROR (DEG) PITCH ERROR (DEG) YAW ERROR (DEG)	Actual attitude errors in deg
MEAS ROLL ERR (DEG) MEAS PITCH ERR (DEG) MEAS YAW ERR (DEG)	Measured attitude errors in deg
ROLL RATE (DEG/S) PITCH RATE (DEG/S) YAW RATE (DEG/S)	Actual angular rates in deg/sec
EROLL RT (DEG/S) EPITCH RT (DEG/S) EYAW RT (DEG/S)	Estimated angular in deg/sec
LENGTH (DEG)	Magnitude of measured attitude error vector
REGION	Region in which the attitude error lies
FLAG-BURN	0 - no inhibition of jet selection and burn 1 - jet selection inhibited because jets are firing 2 - jet selection inhibited because vehicle is coasting to estimate rate
VEL X (FT/S) VEL Y (FT/S) VEL Z (FT/S)	Translation velocity error along the body axes in ft/sec
X-AACCL (DEG/S-2) Y-AACCL (DEG/S-2) Z-AACCL (DEG/S-2)	Jet-produced angular accelerations about the body axes in rad/sec^2

Table 7-5. Definition of plotted variables and labels. (Cont.)

X-LACCL (FT/S-2) Y-LACCL (FT/S-2) Z-LACCL (FT/S-2)	Jet produced linear accelerations along the body axes in ft/sec^2
JET SELECT #1	Pseudo inverse jet selection policy
JET SELECT #2	Fixed jet selection routine

Figure 7.1. Pseudo inverse jet selection, initial conditions A, no parceling, no uncertainties (in IMU measurements, mass properties, or jet firings).

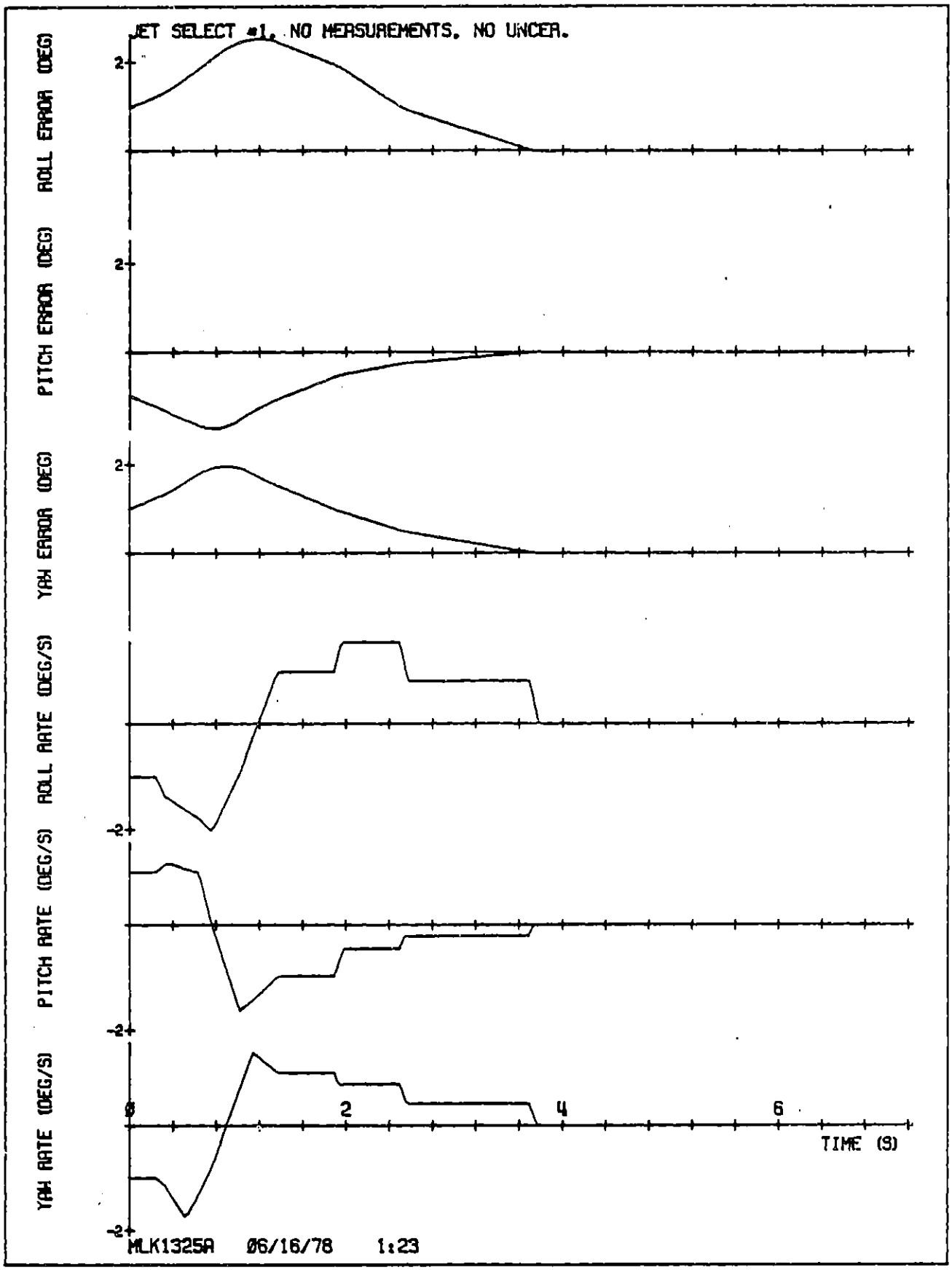

Figure 7.1. (Sheet 1 of 3).

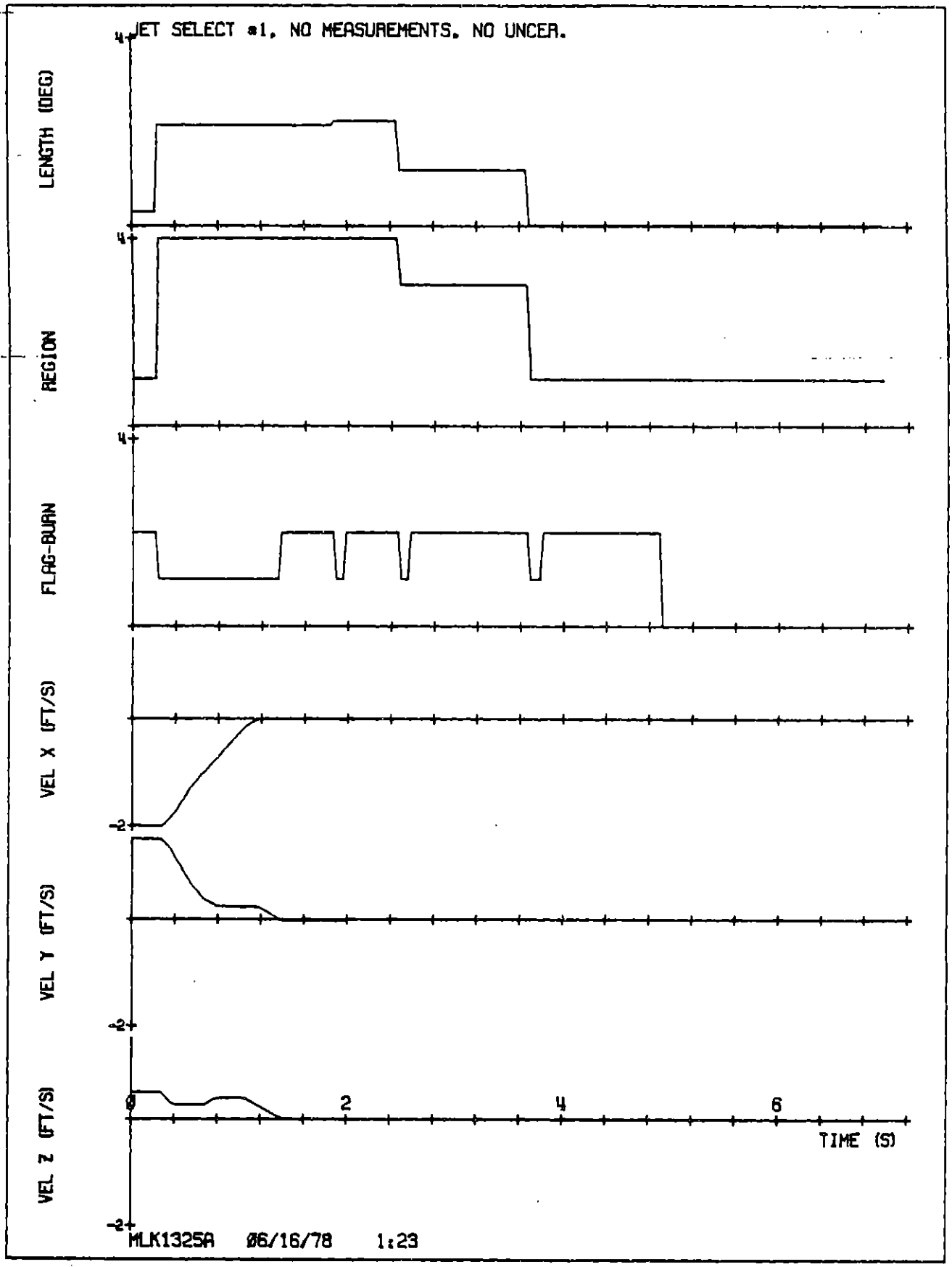

Figure 7.1. (Sheet 2 of 3).

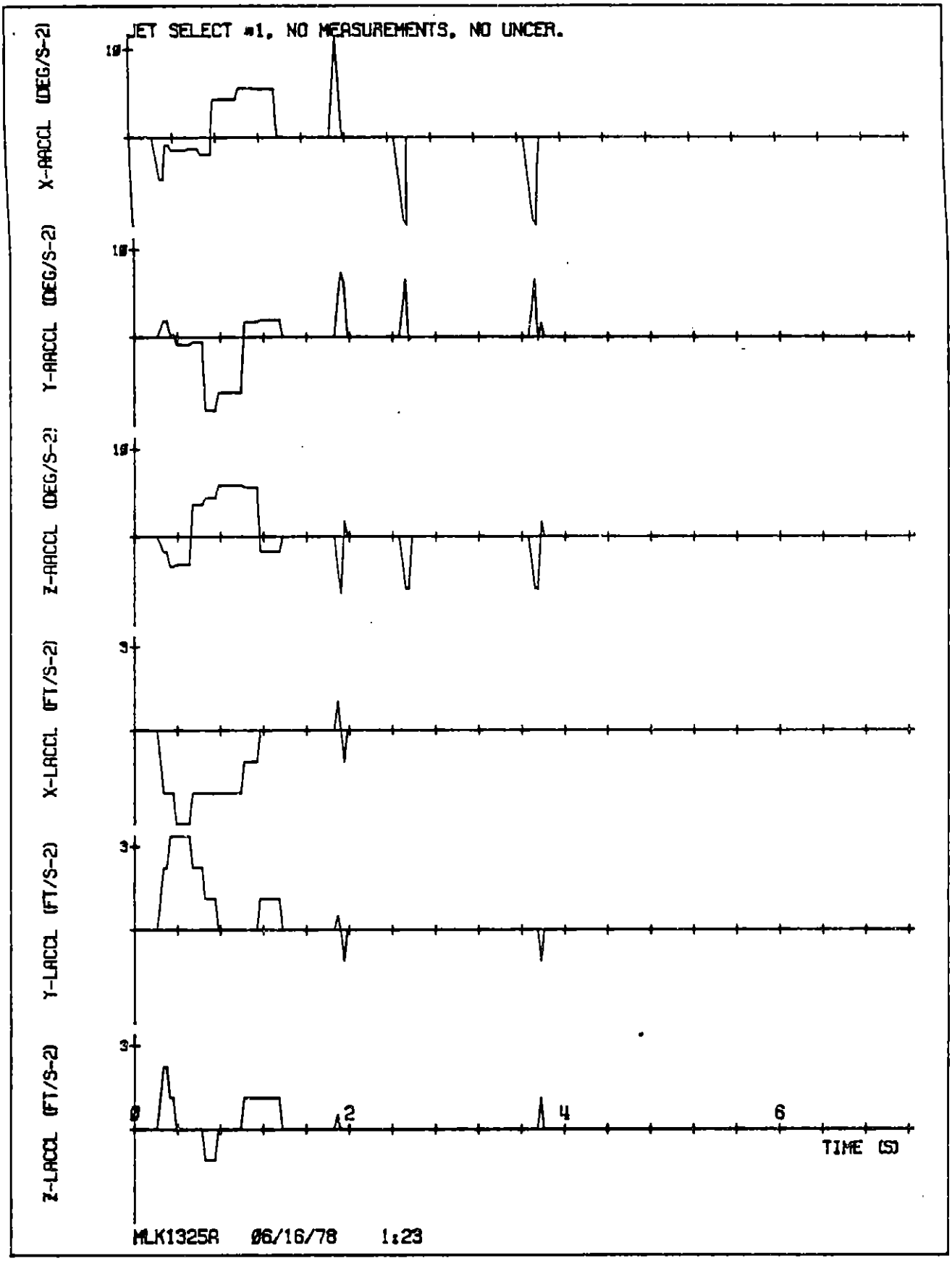

Figure 7.1. (Sheet 3 of 3).

Figure 7.2. Fixed jet selection procedure, initial conditions A, no parceling, no uncertainties (in IMU measurements, mass properties, or jet firings).

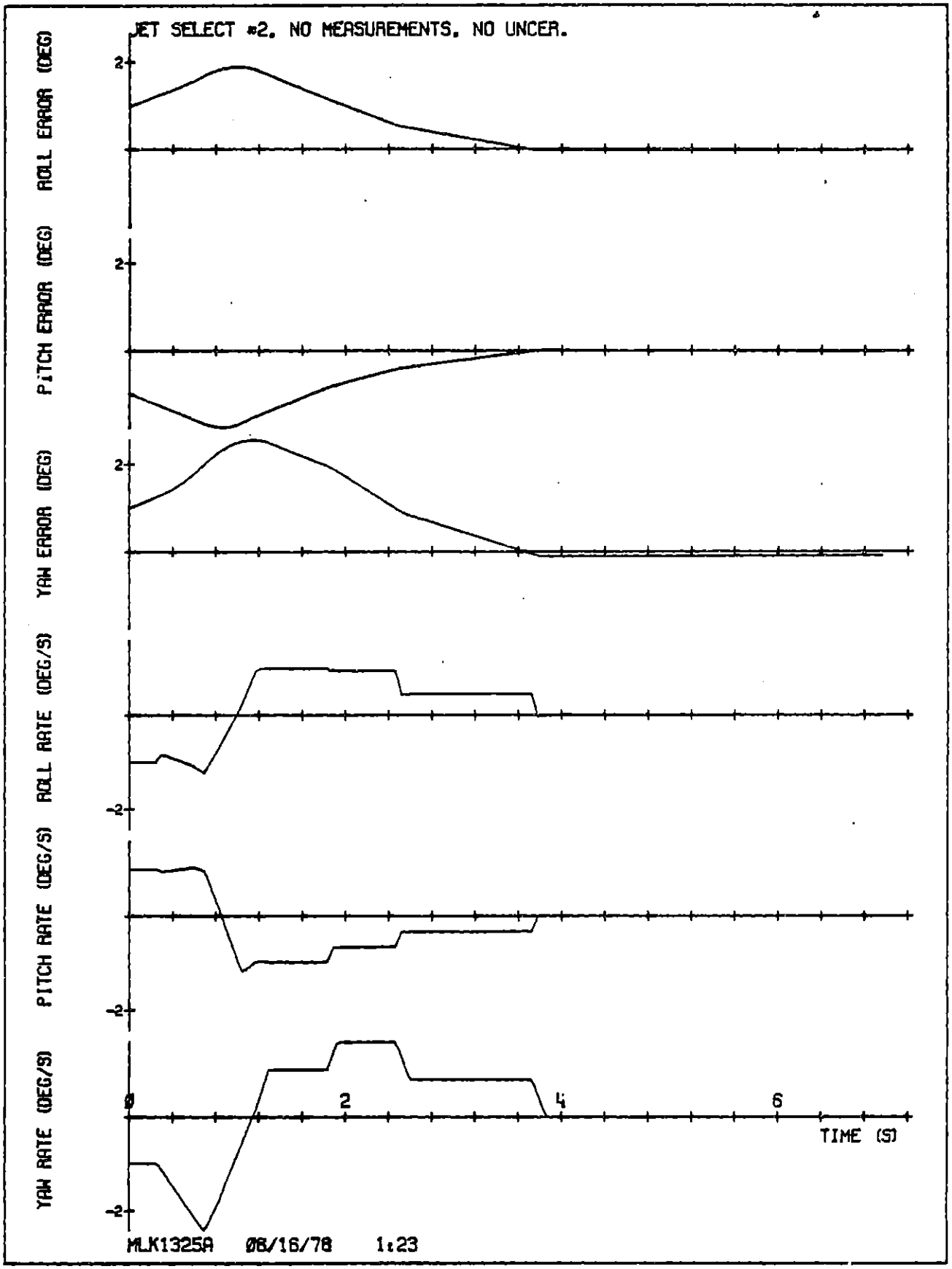

Figure 7.2. (Sheet 1 of 3).

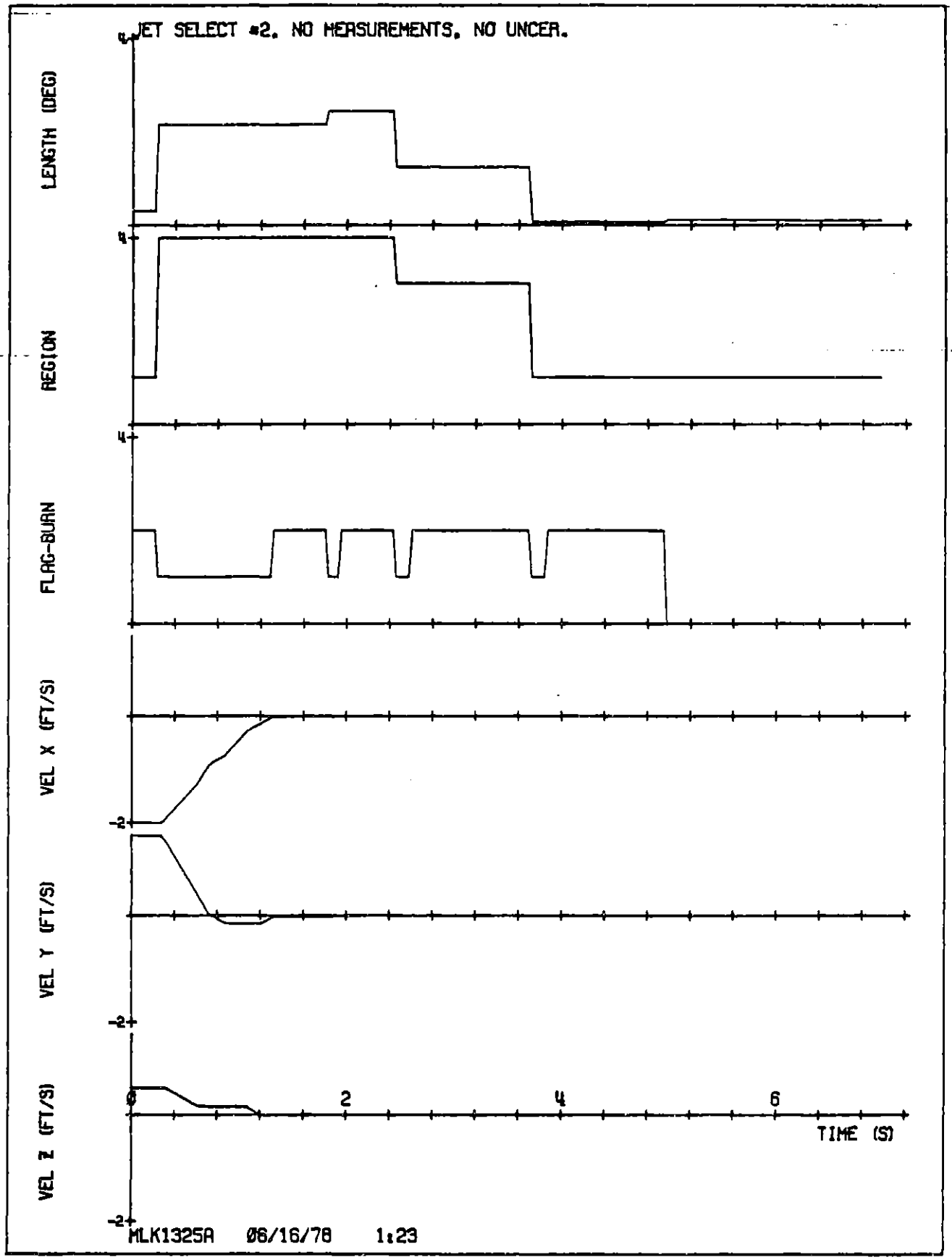

Figure 7.2. (Sheet 2 of 3).

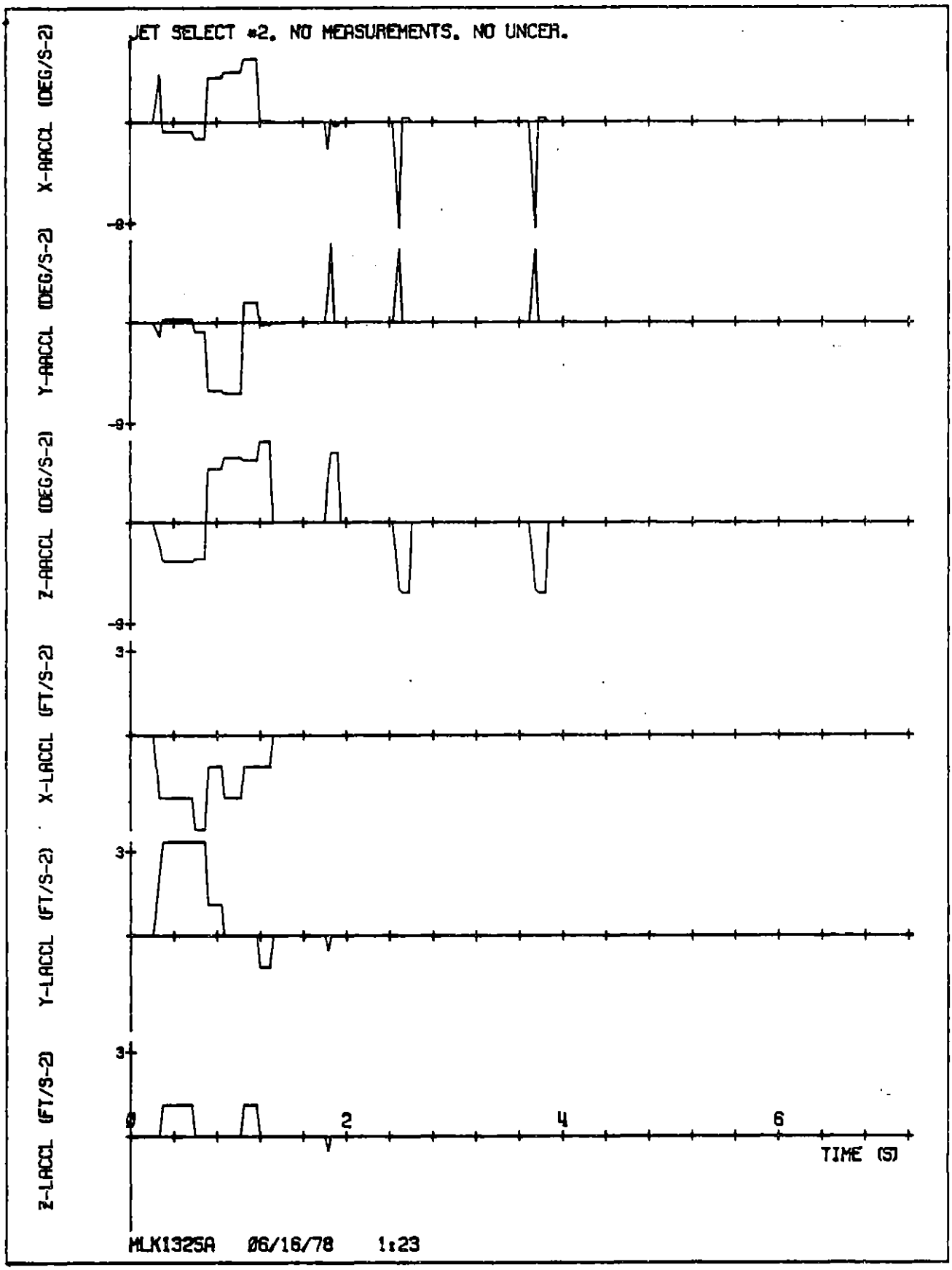

Figure 7.2. (Sheet 3 of 3).

Figure 7.3. Pseudo inverse jet selection, initial conditions A, no parceling, with uncertainties (in IMU measurements, mass properties, and jet firings).

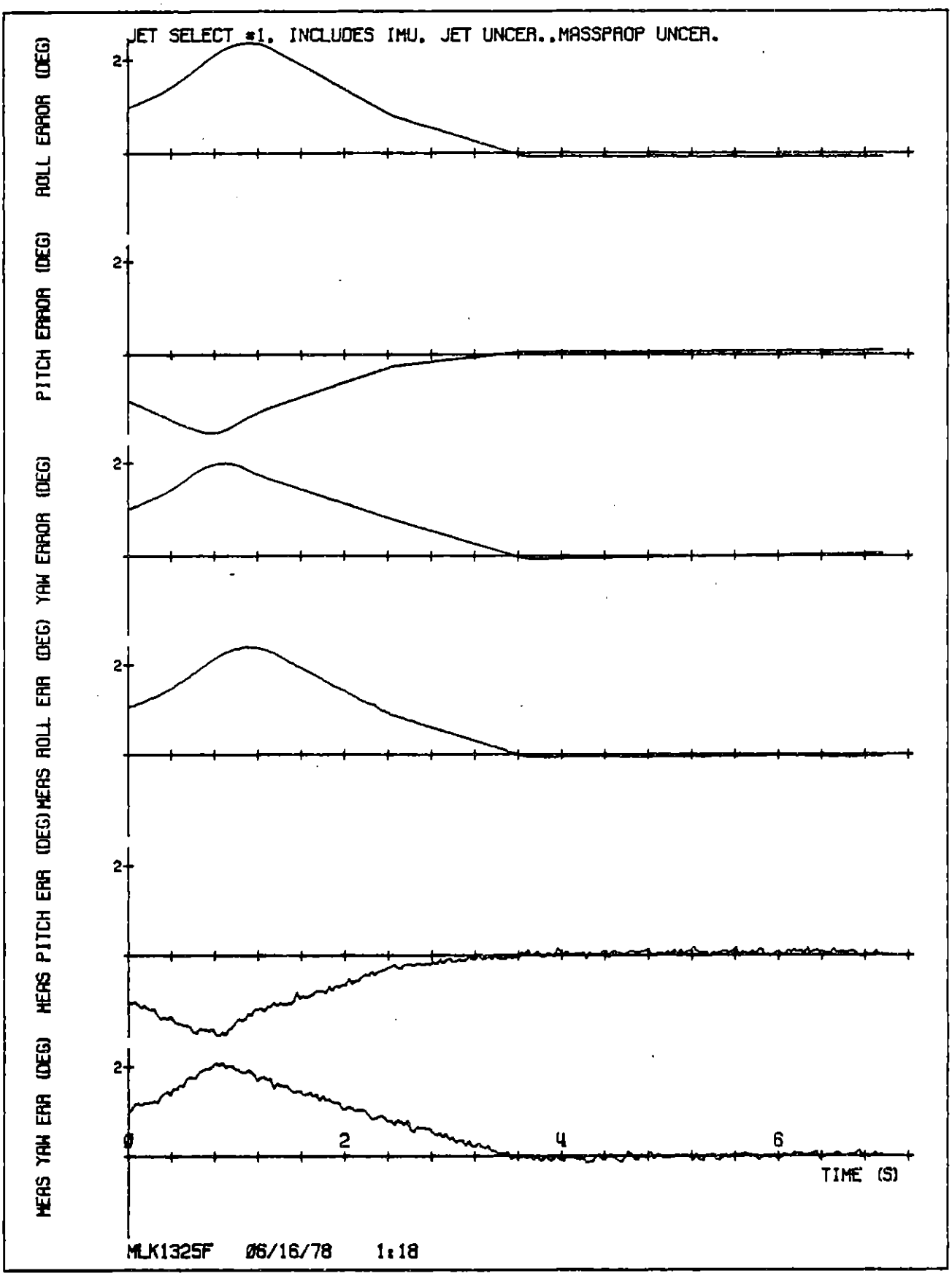

Figure 7.3. (Sheet 1 of 4).

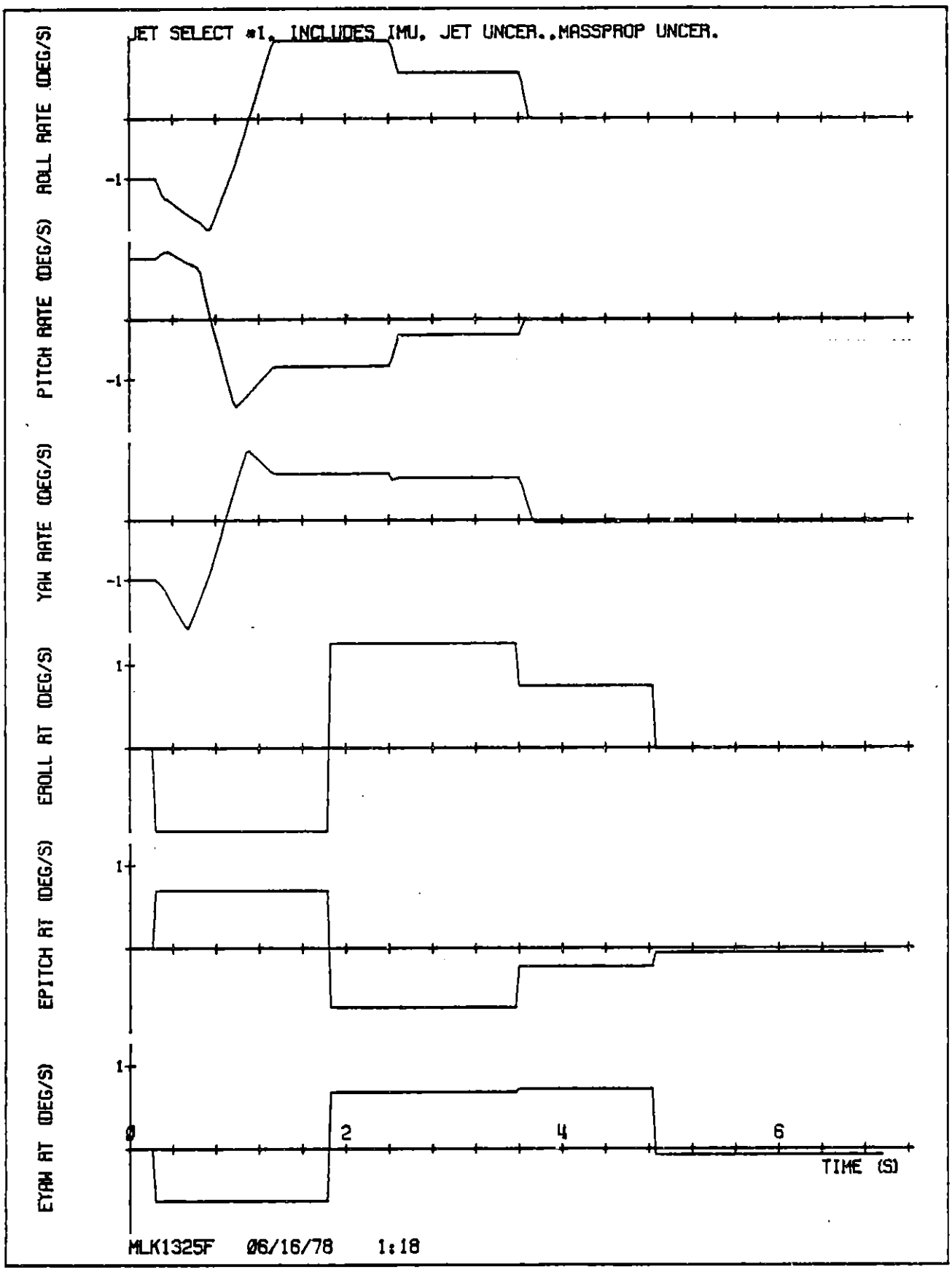

Figure 7.3. (Sheet 2 of 4).

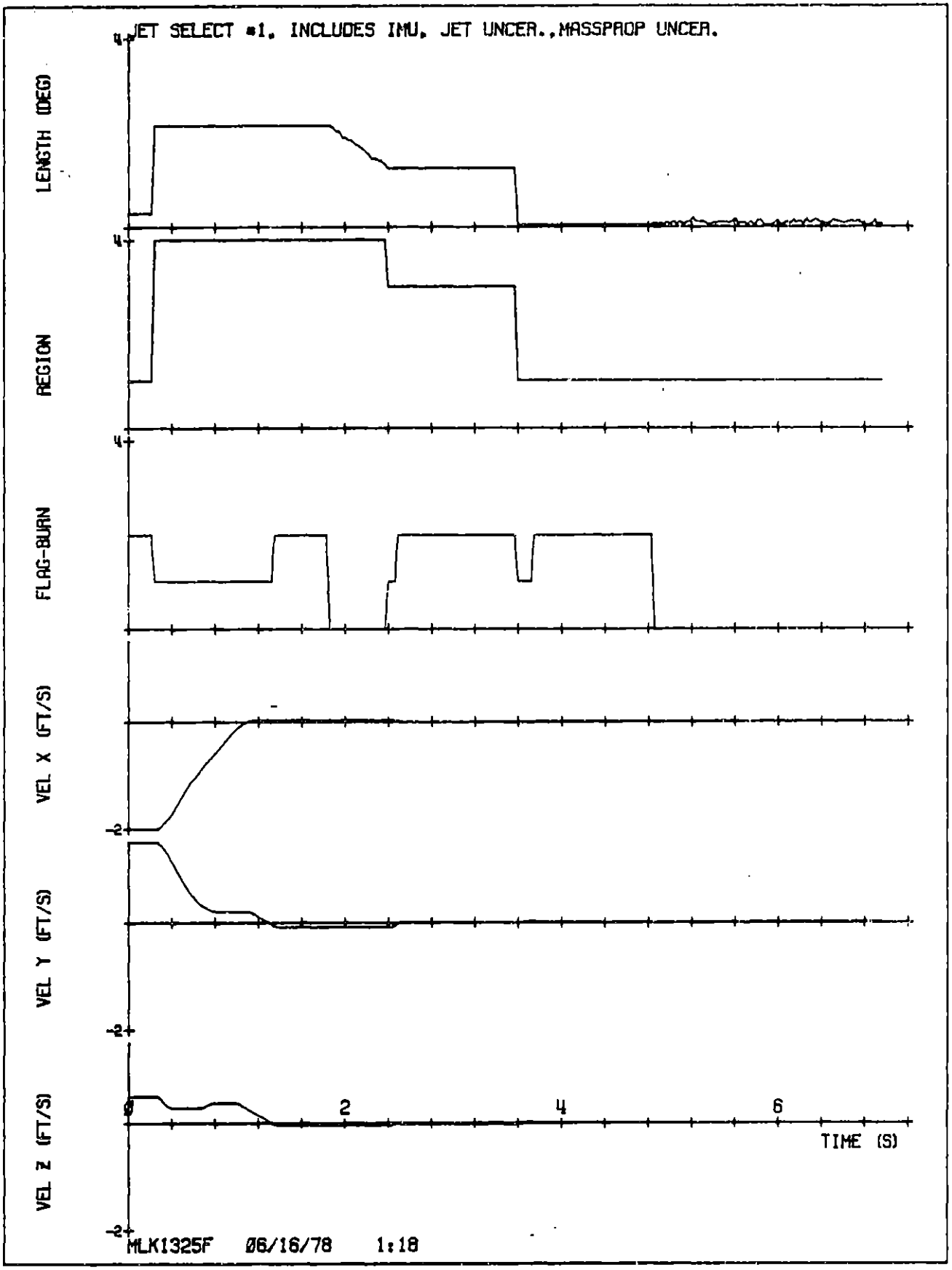

Figure 7.3. (Sheet 3 of 4).

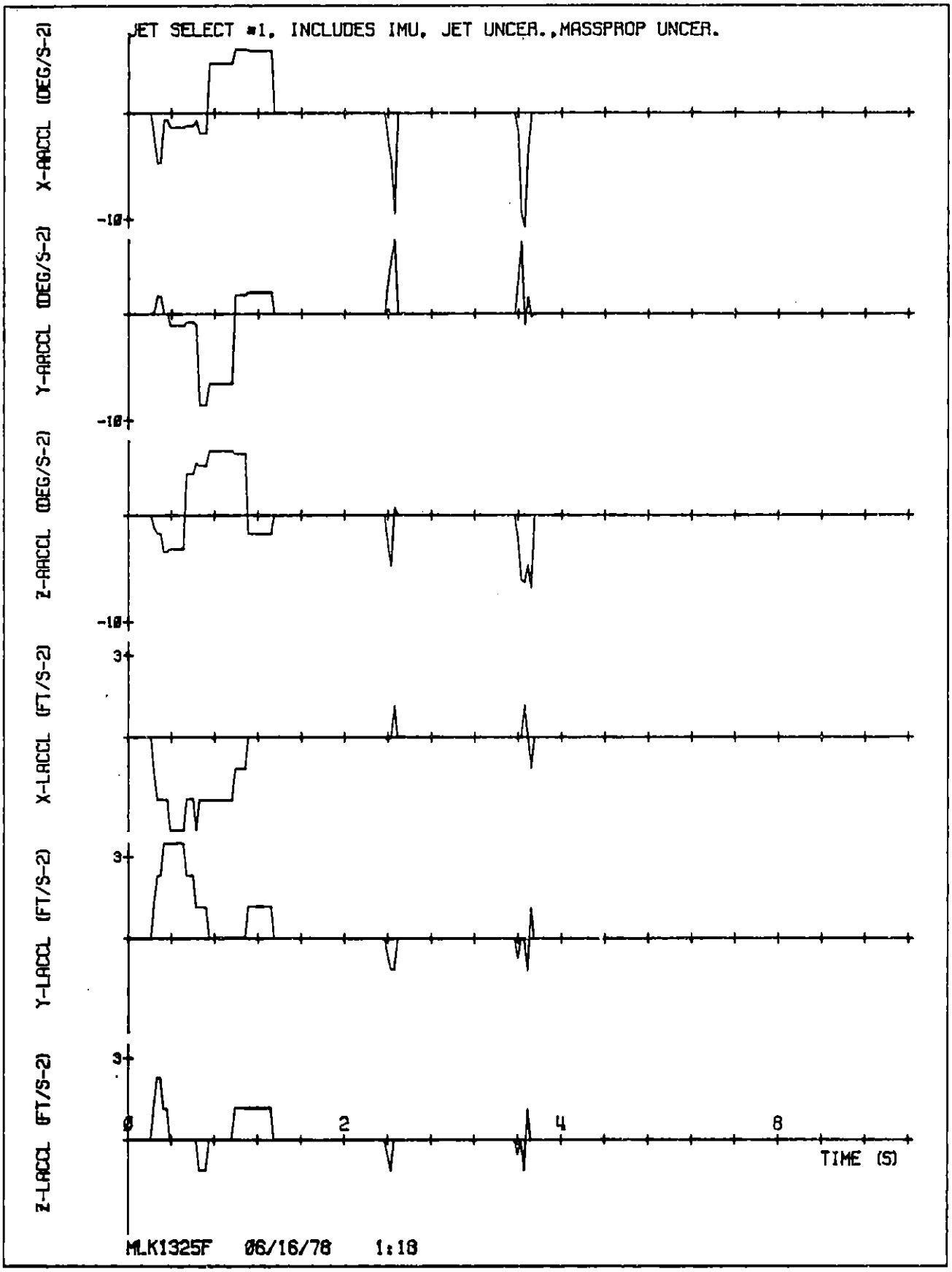

Figure 7.3. (Sheet 4 of 4).

Figure 7.4. Fixed jet selection procedure, initial conditions A, no parceling, with uncertainties (in IMU measurements, mass properties, and jet firings).

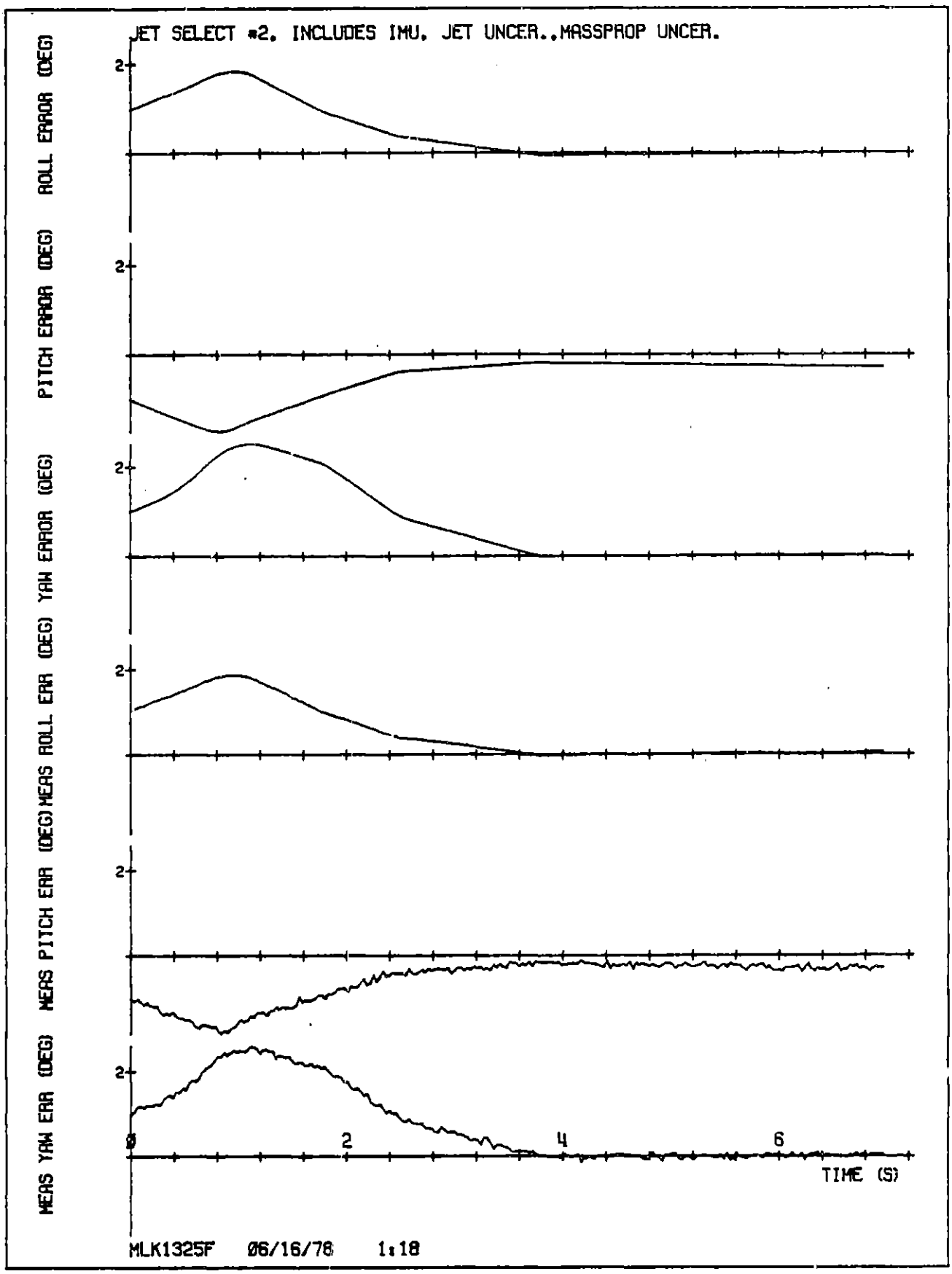

Figure 7.4. (Sheet 1 of 4).

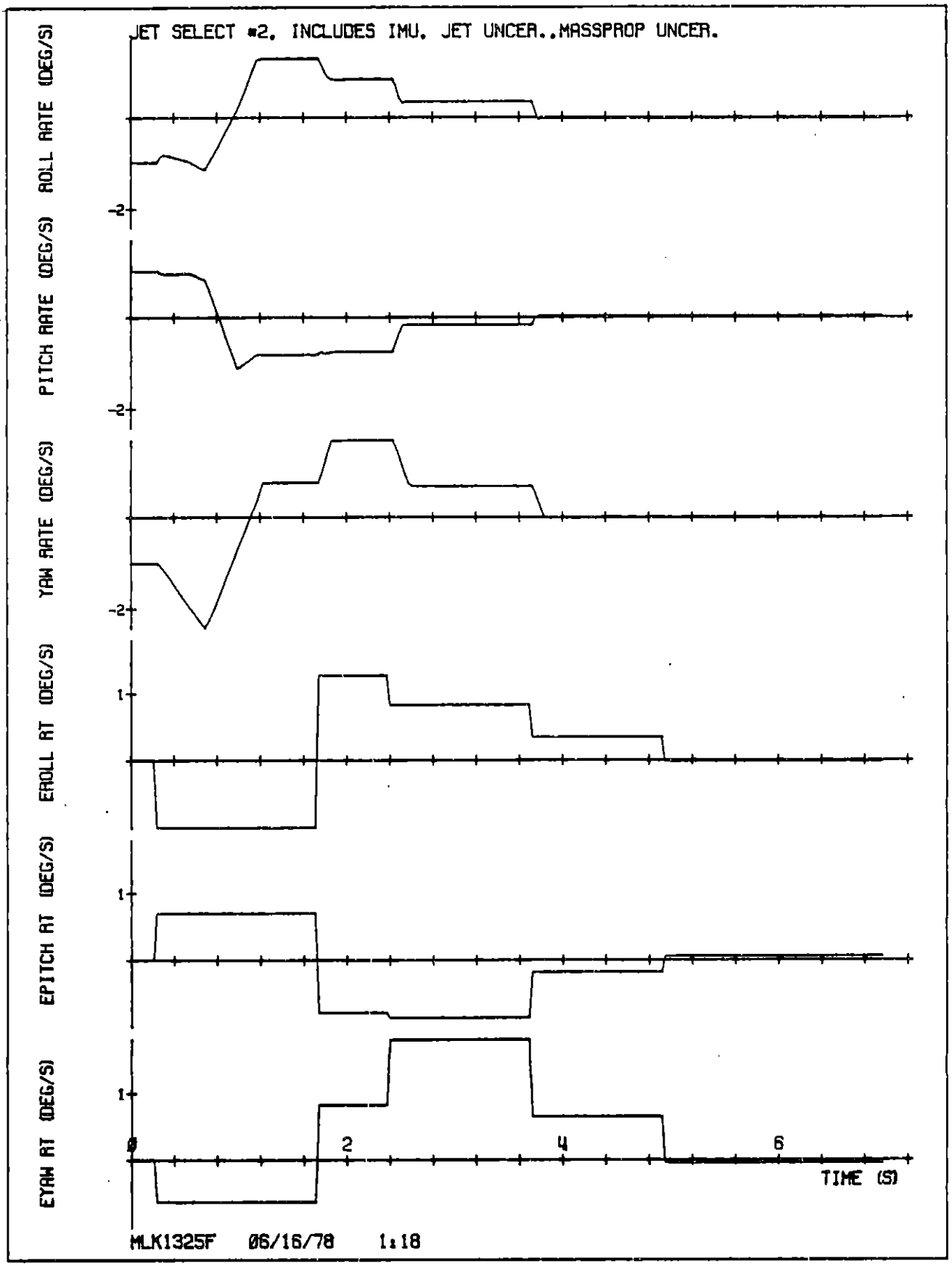

Figure 7.4. (Sheet 2 of 4).

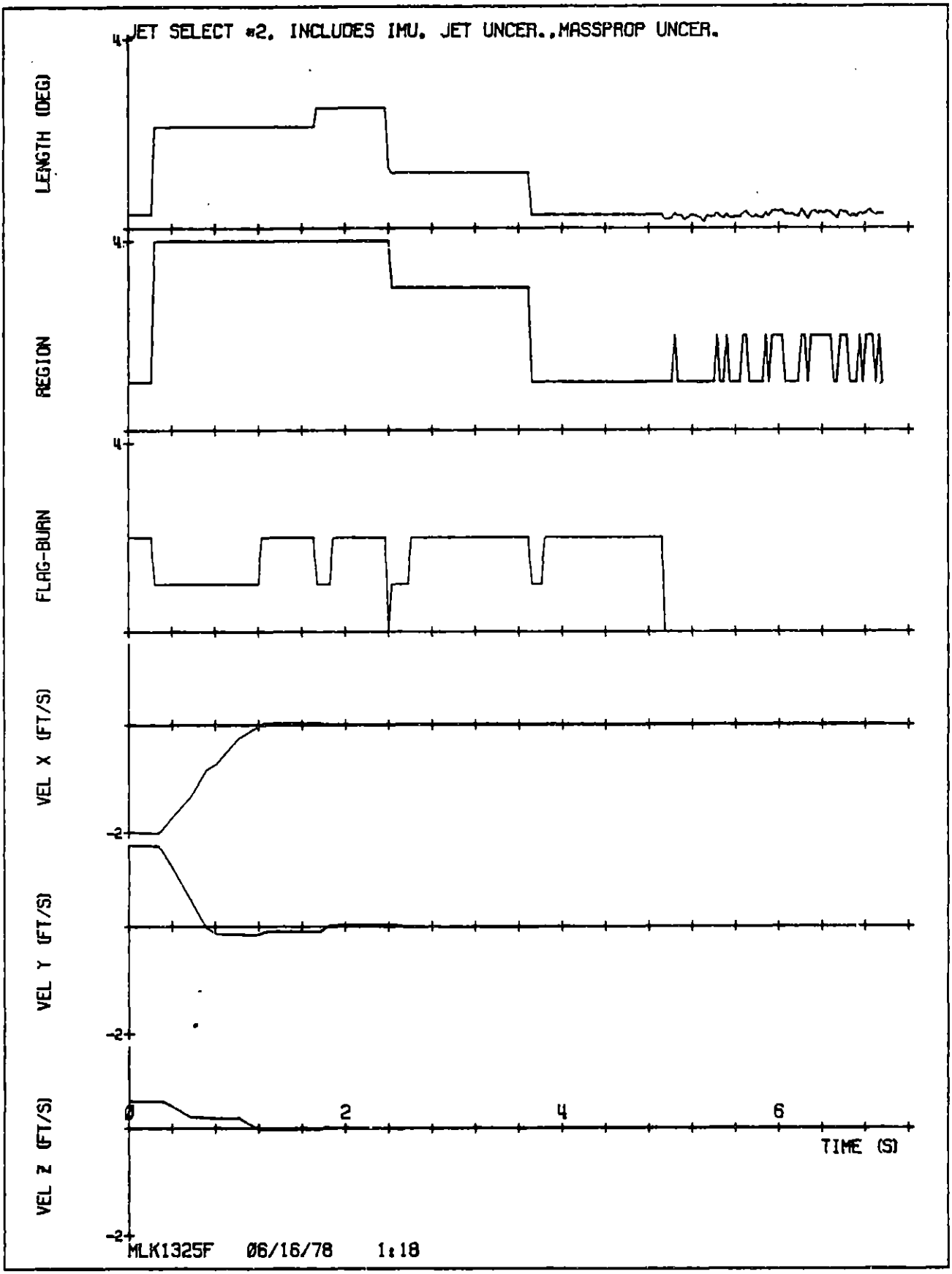

Figure 7.4. (Sheet 3 of 4).

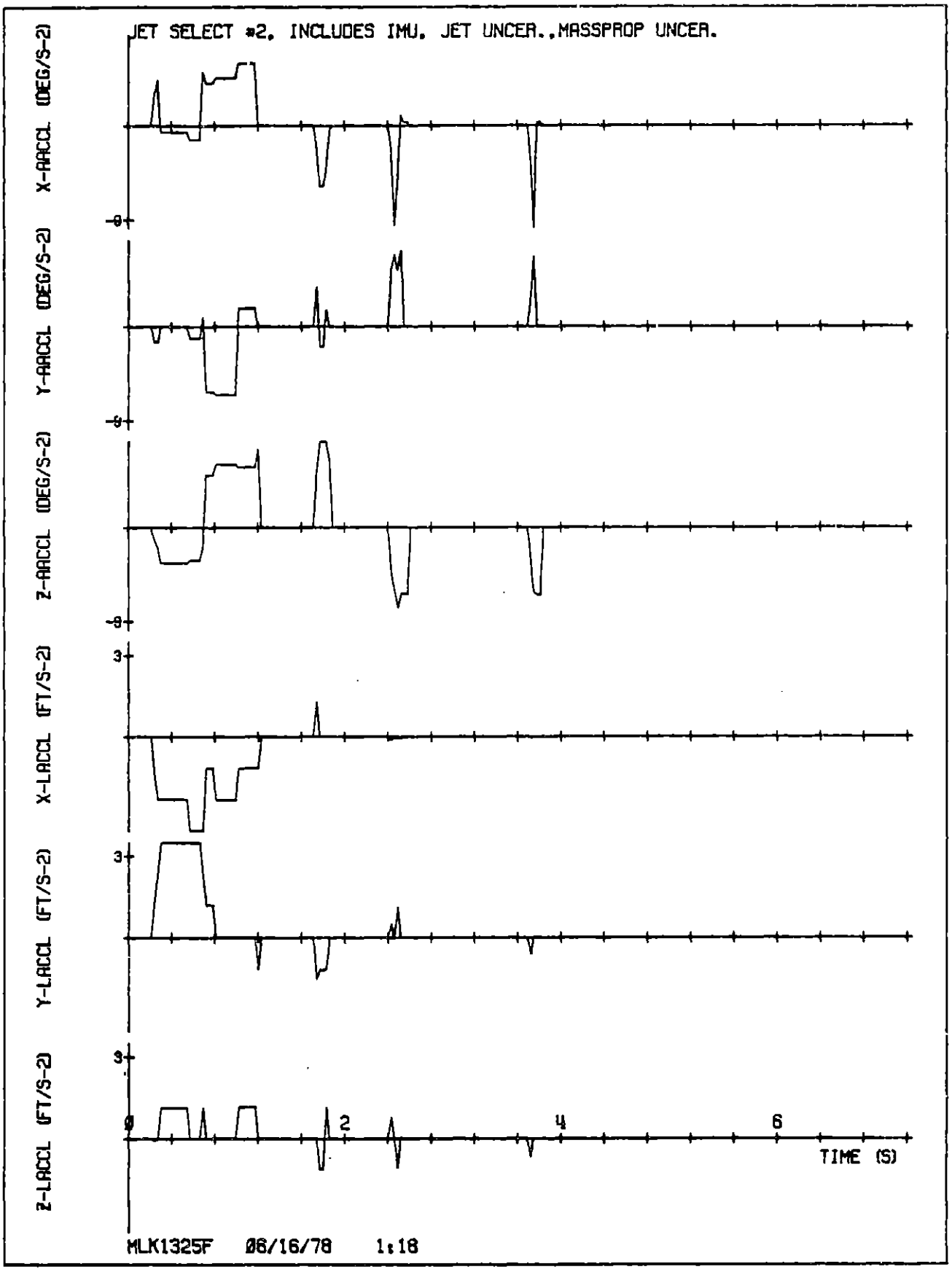

Figure 7.4. (Sheet 4 of 4).

Figure 7.5. Pseudo inverse jet selection, initial conditions B, no parceling, no uncertainties (in IMU measurements, mass properties, or jet firings).

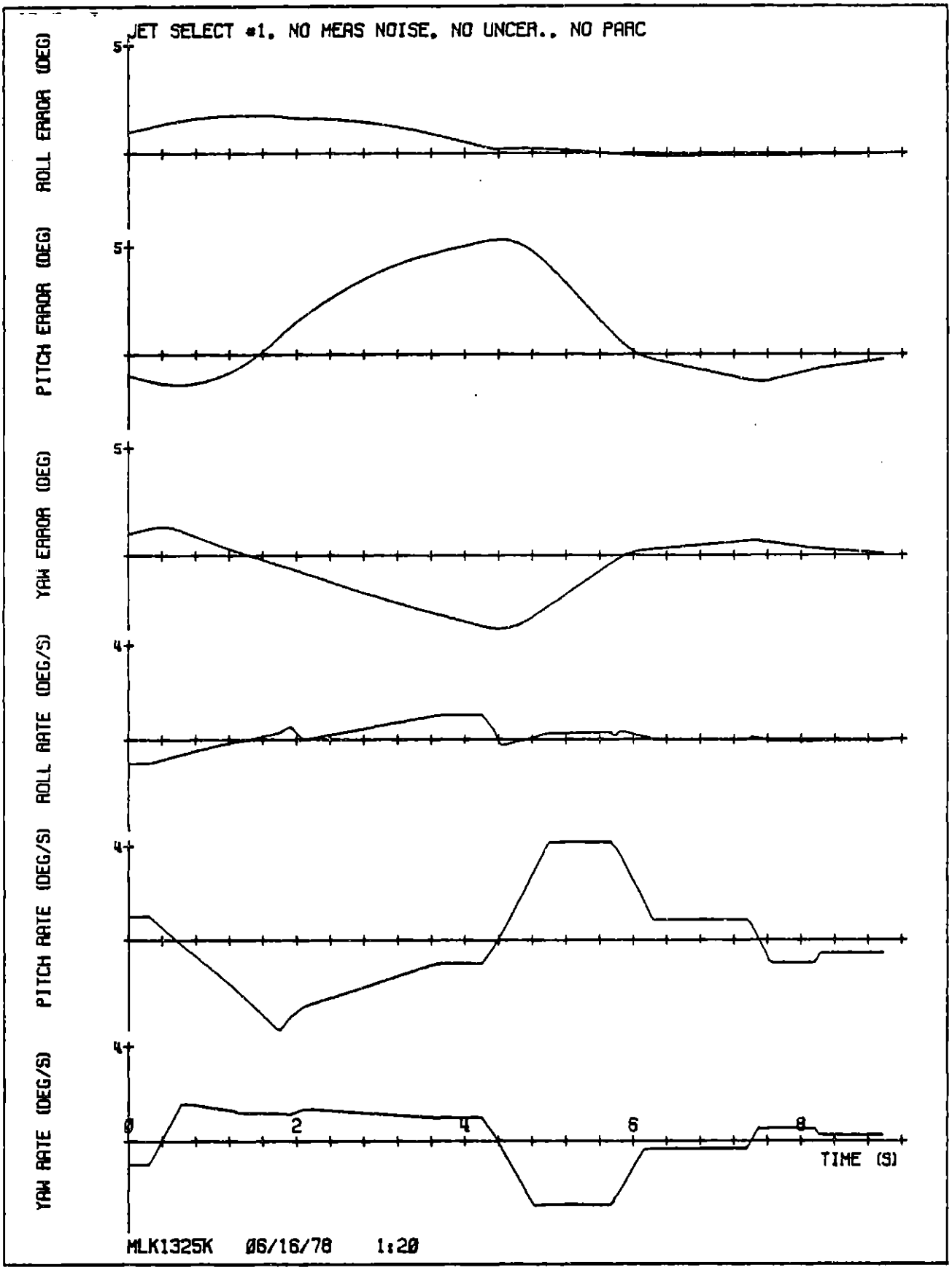

Figure 7.5. (Sheet 1 of 3).

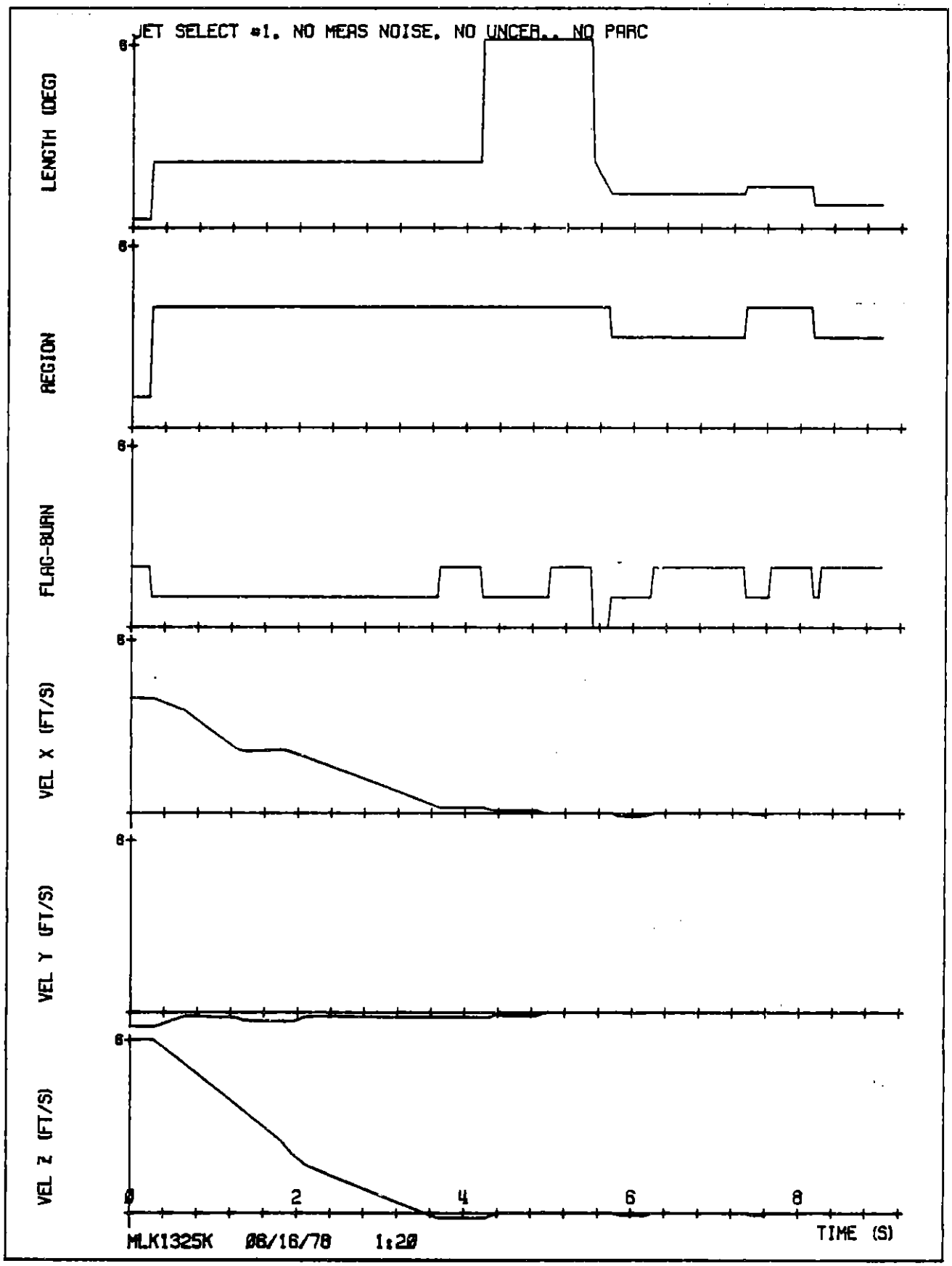

Figure 7.5. (Sheet 2 of 3).

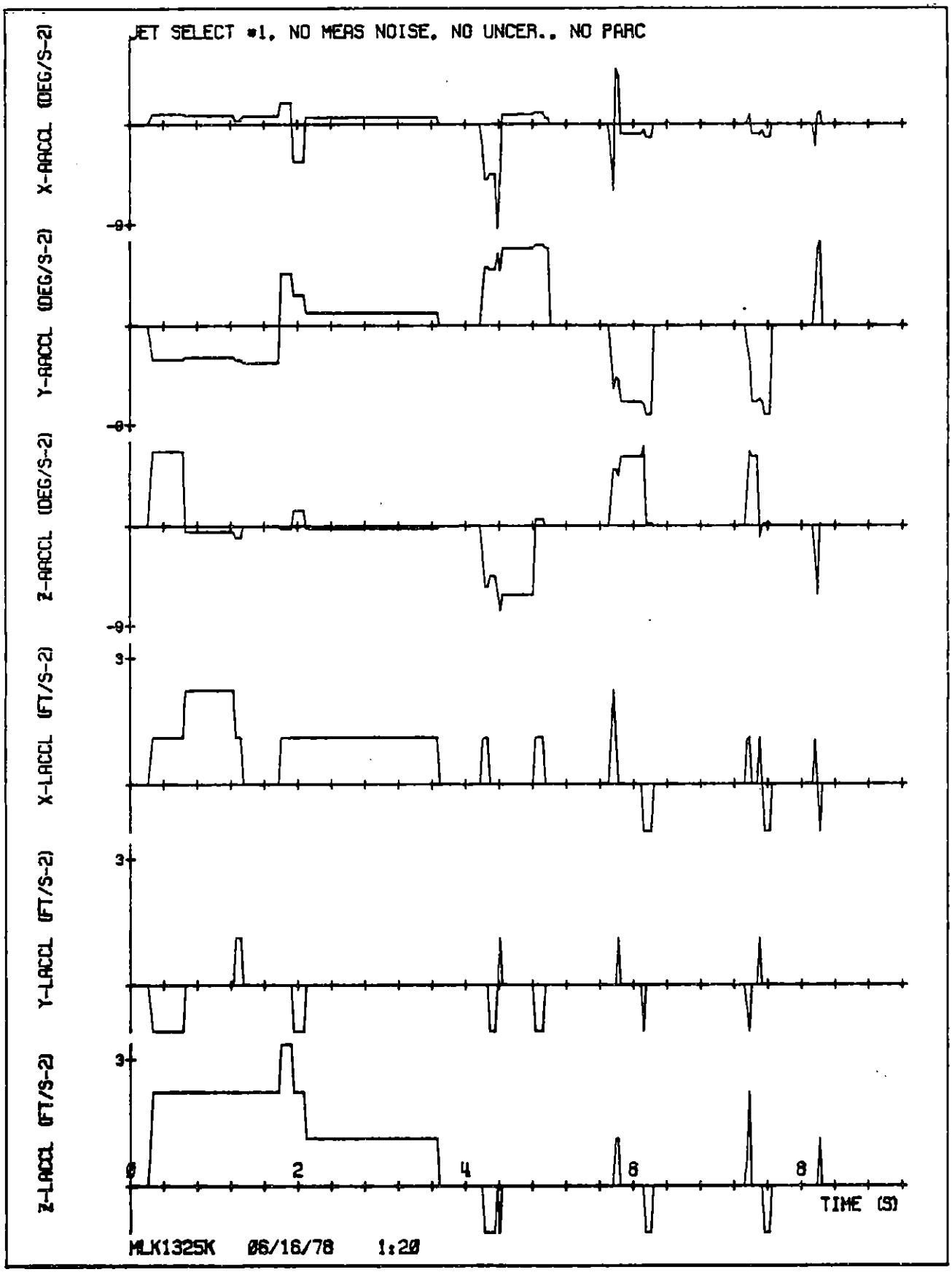

Figure 7.5. (Sheet 3 of 3).

Figure 7.6. Pseudo inverse jet selection, initial conditions B, with parceling, no uncertainties (in IMU measurements, mass properties, or jet firings).

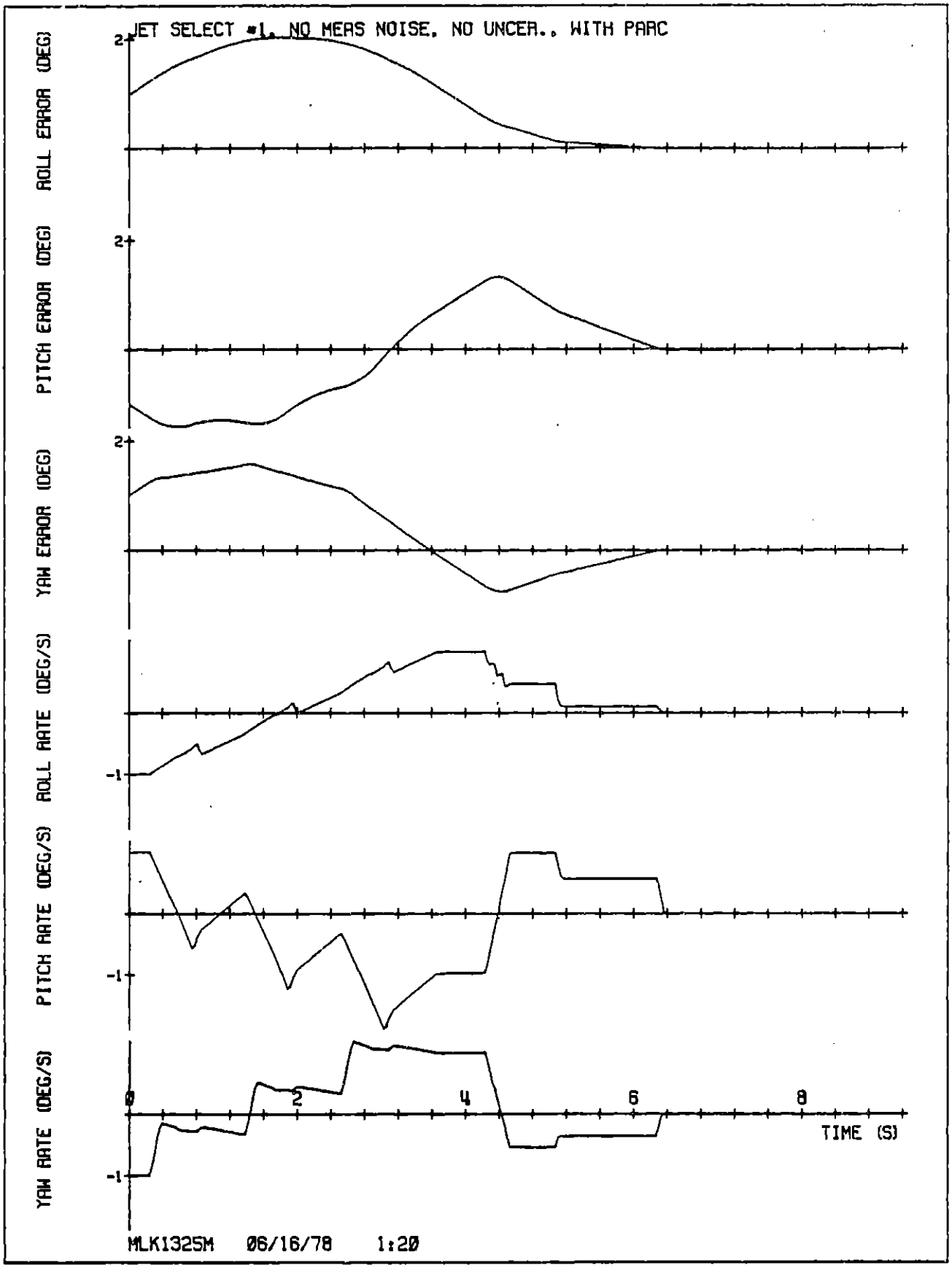

Figure 7.6. (Sheet 1 of 3).

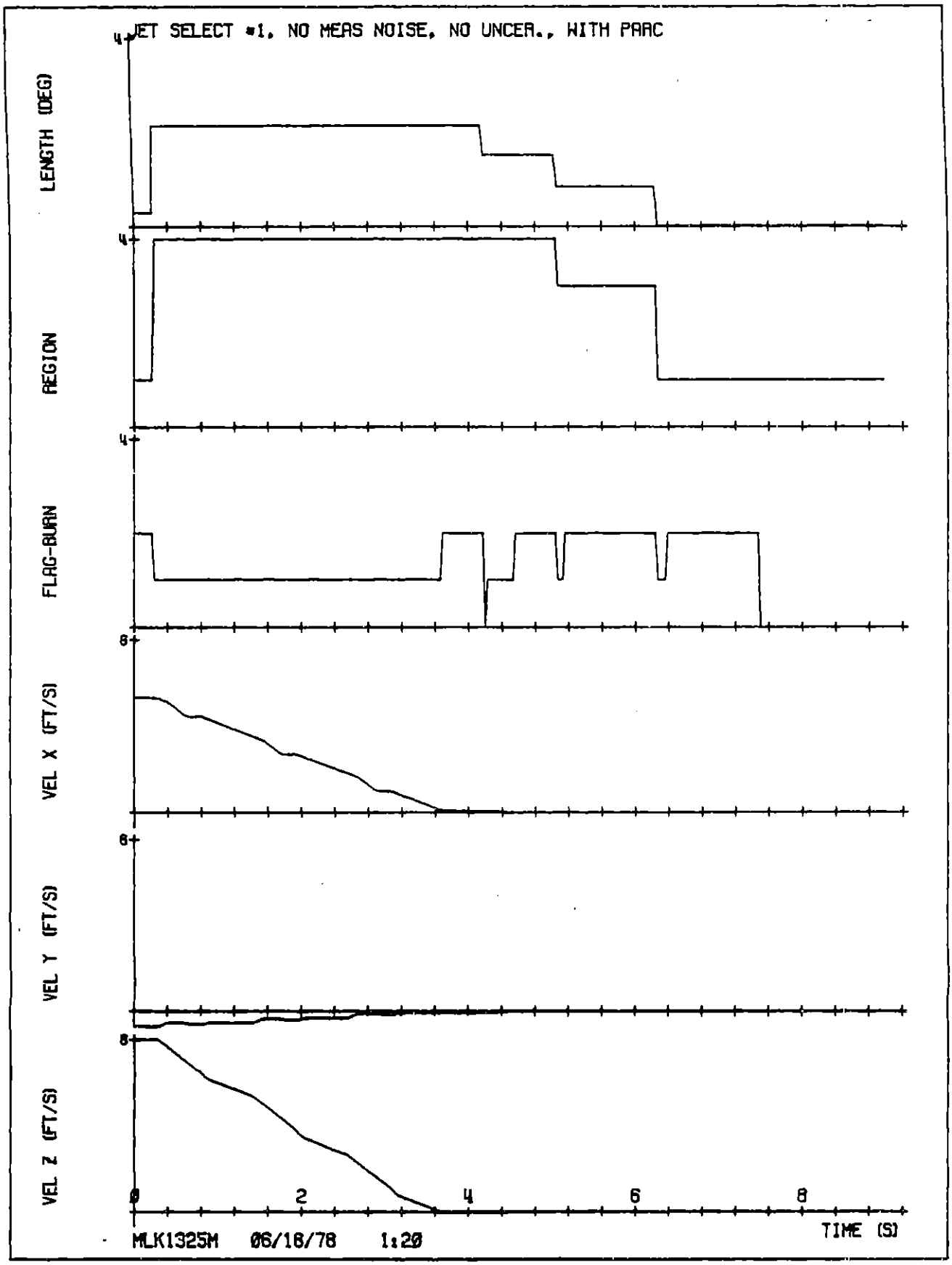

Figure 7.6. (Sheet 2 of 3).

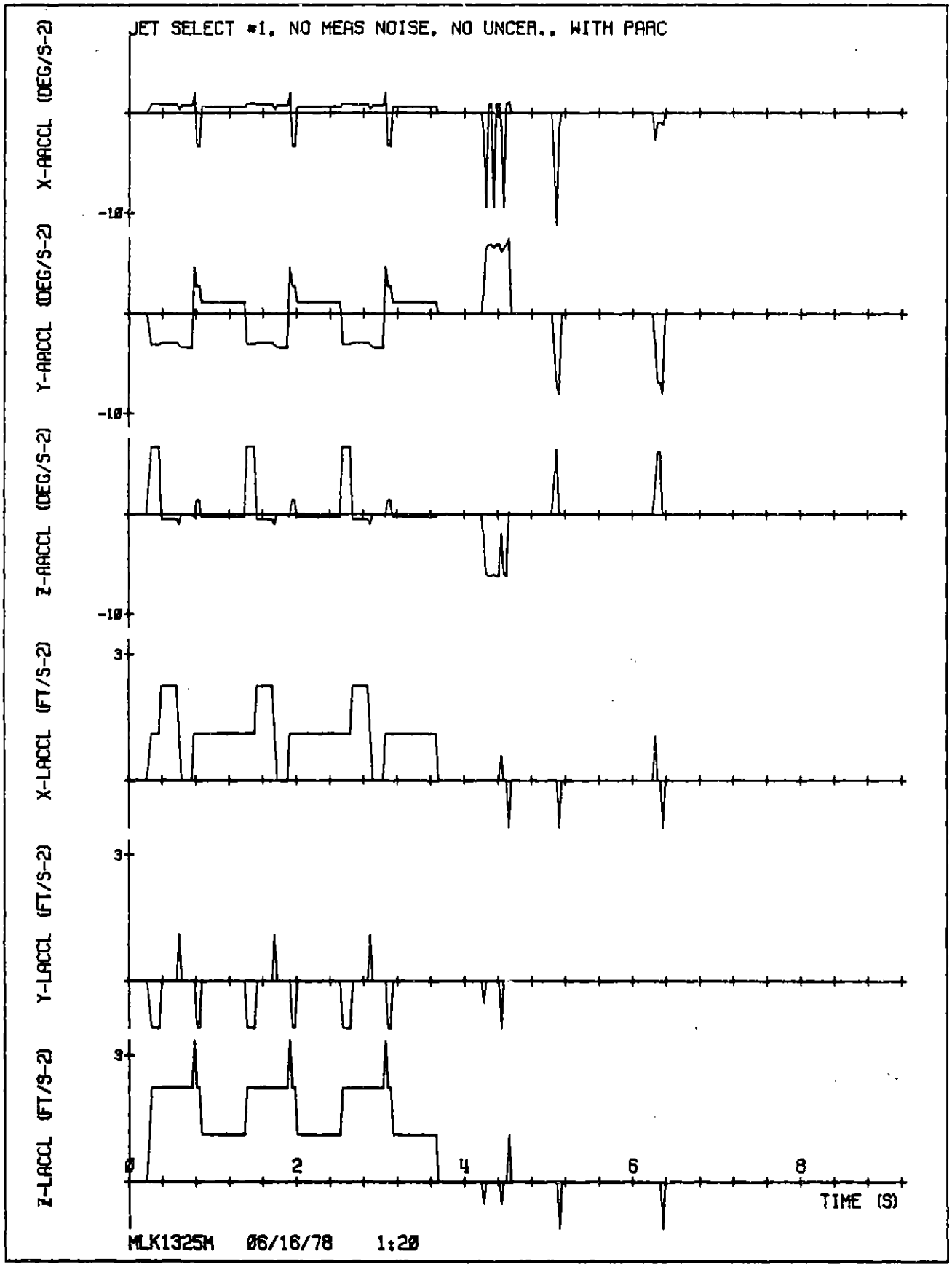

Figure 7.6. (Sheet 3 of 3).

Figure 7.7. Fixed jet selection procedure, initial conditions B, no parceling, no uncertainties (in IMU measurements, mass properties, or jet firings).

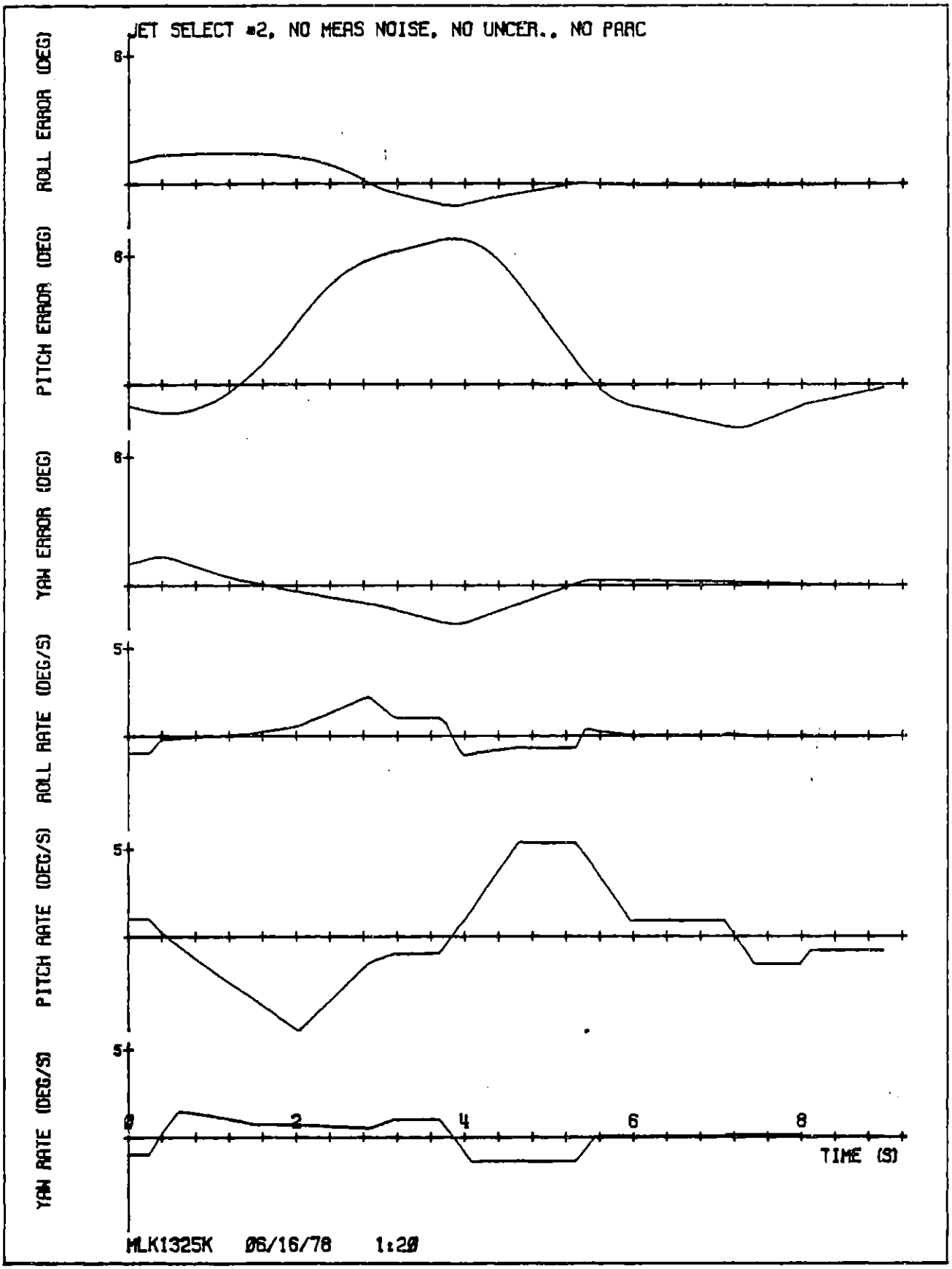

Figure 7.7. (Sheet 1 of 3).

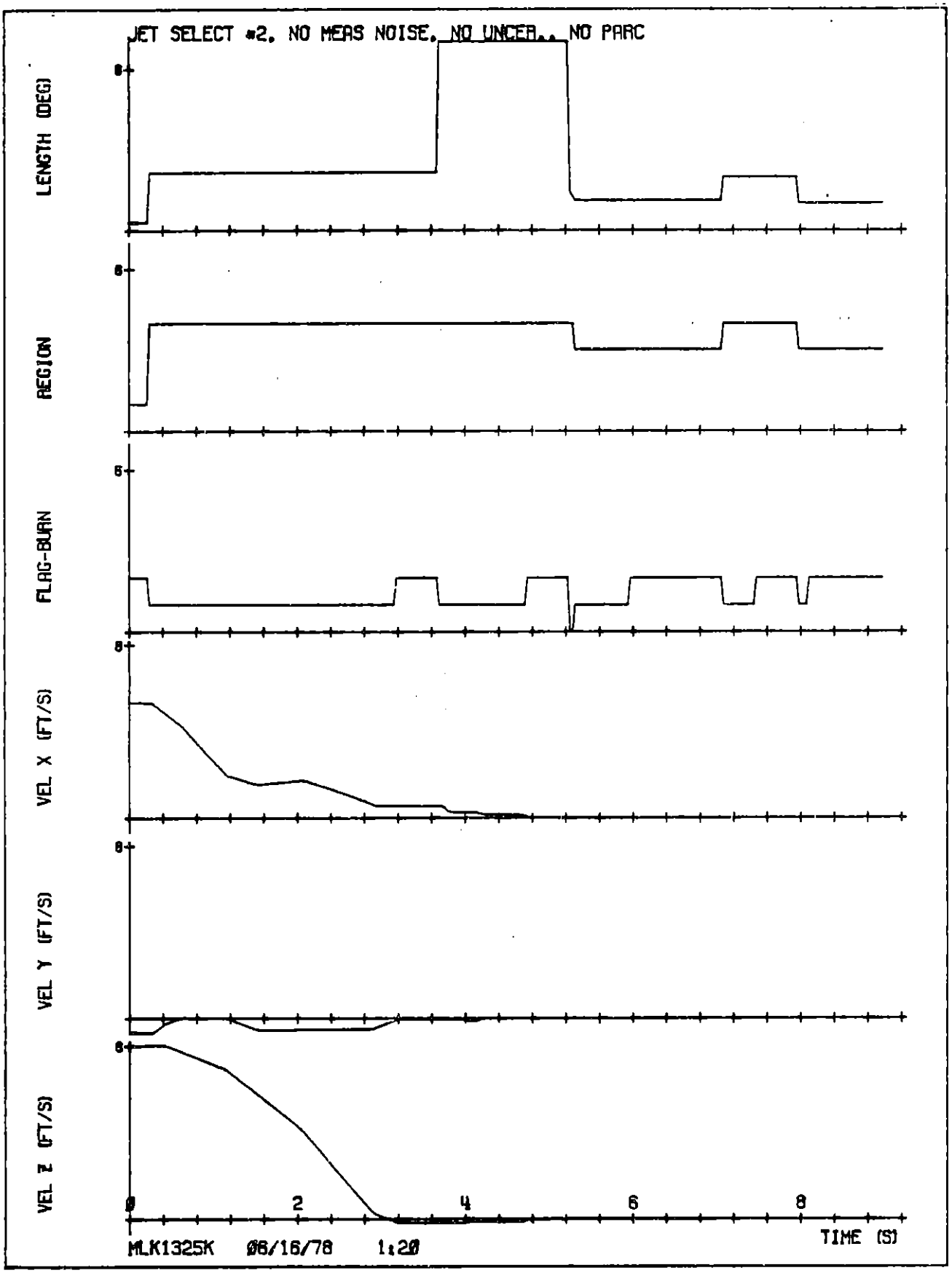

Figure 7.7. (Sheet 2 of 3).

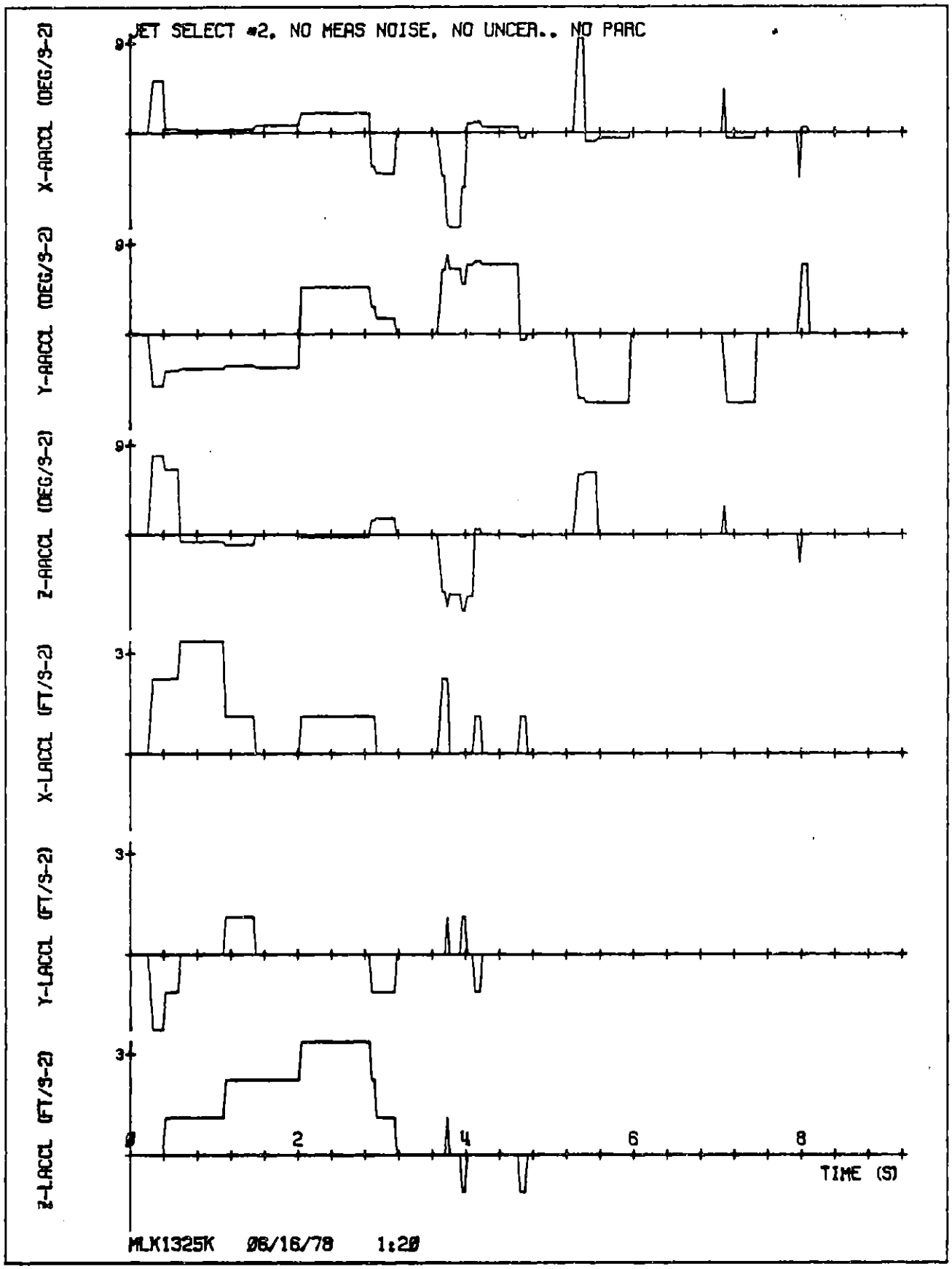

Figure 7.7. (Sheet 3 of 3).

Figure 7.8. Fixed jet selection procedure, initial conditions B, with parceling, no uncertainties (in IMU measurements, mass properties, or jet firings).

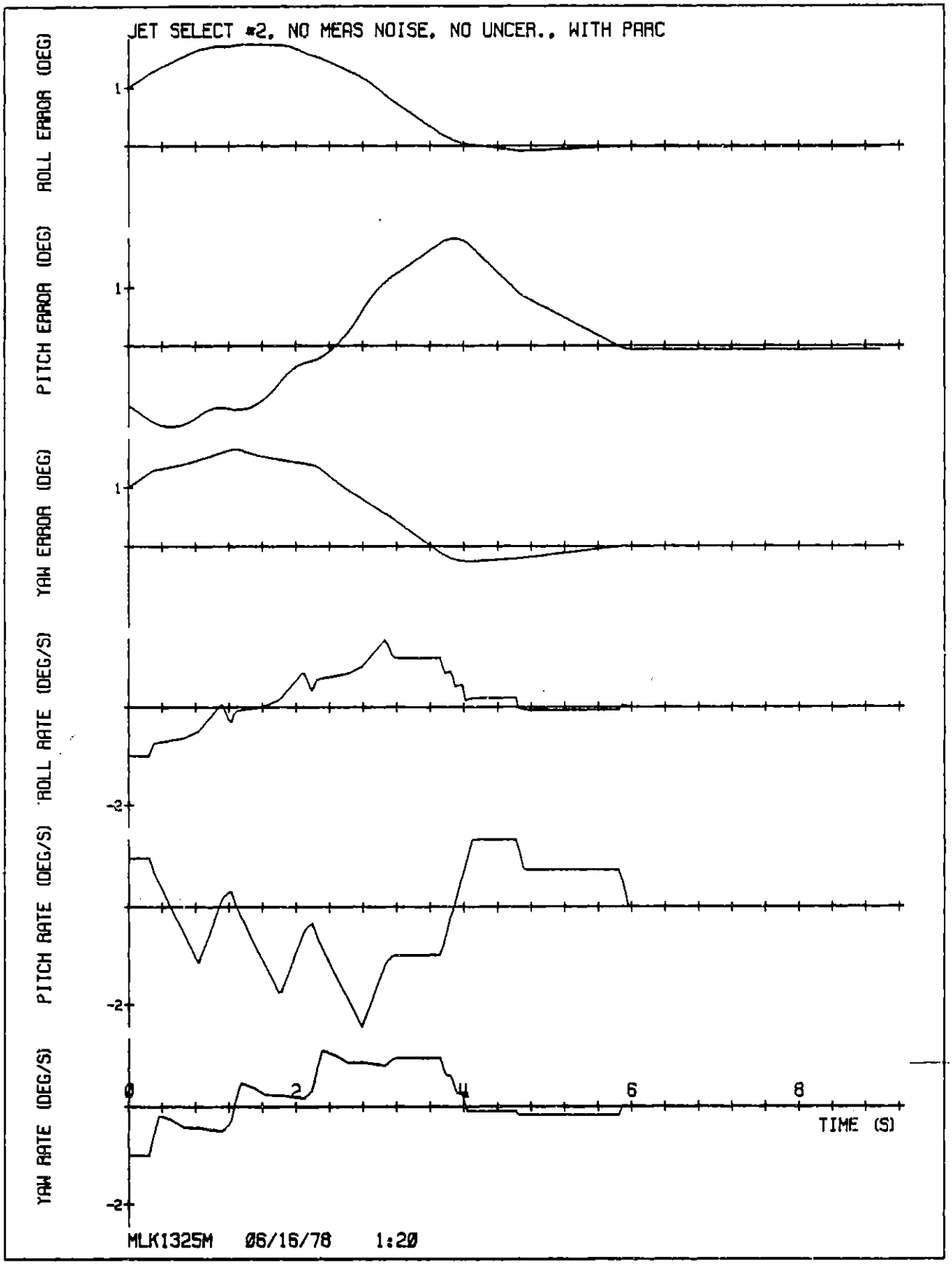

Figure 7.8. (Sheet 1 of 3).

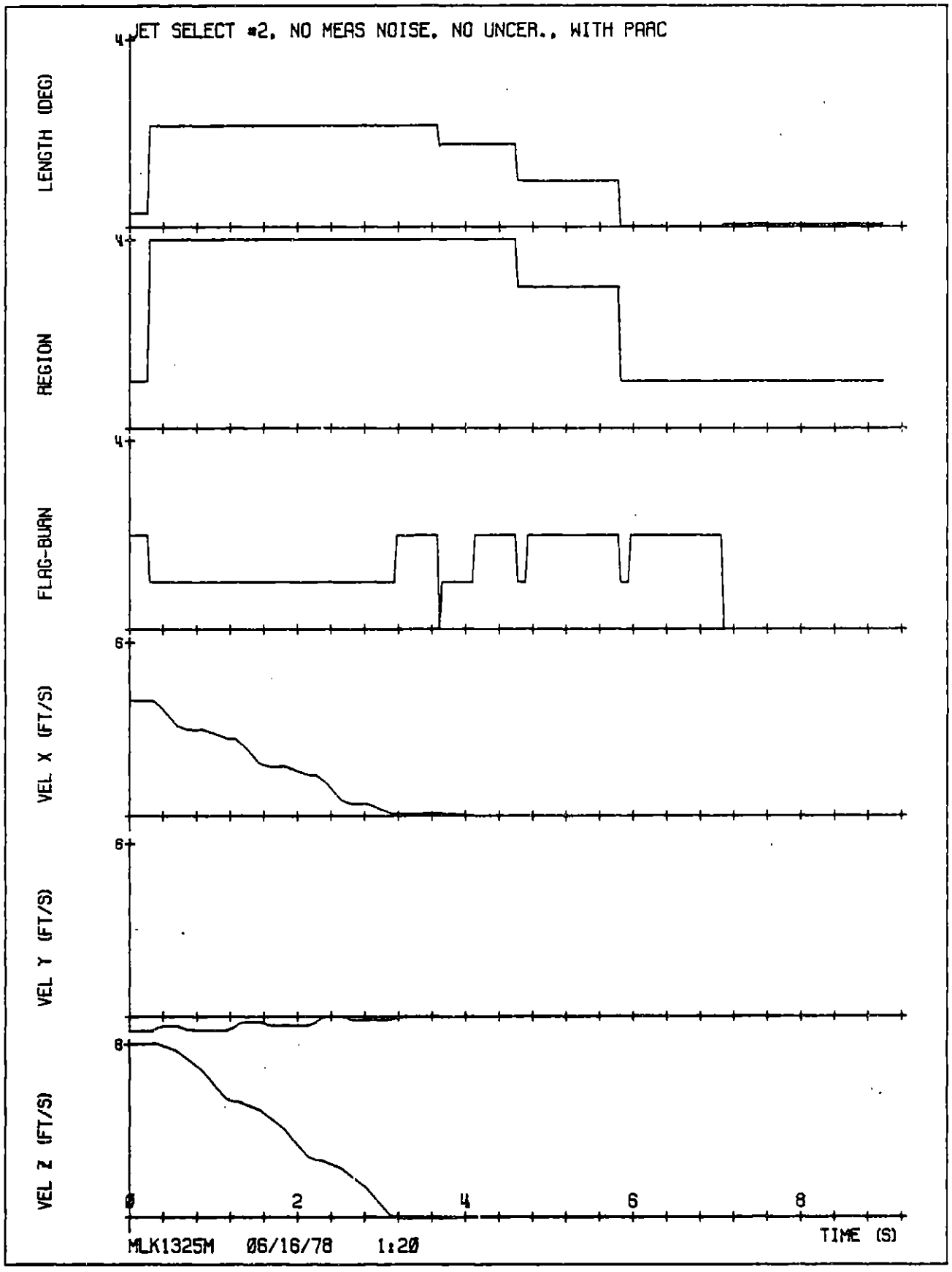

Figure 7.8. (Sheet 2 of 3).

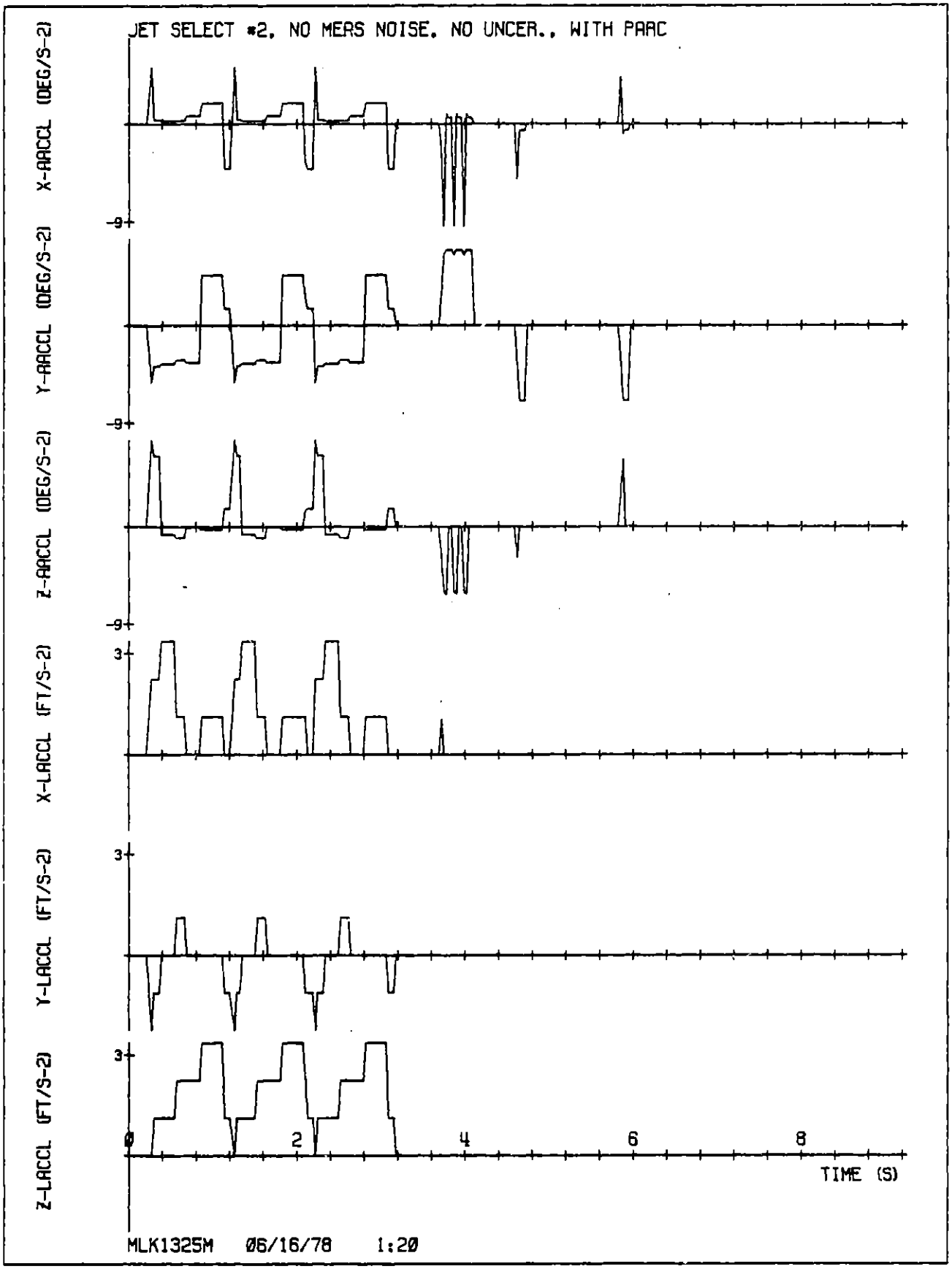

Figure 7.8. (Sheet 3 of 3).

Figure 7.9. Pseudo inverse jet selection, initial conditions C, no parceling, no uncertainties (in IMU measurements, mass properties, or jet firings).

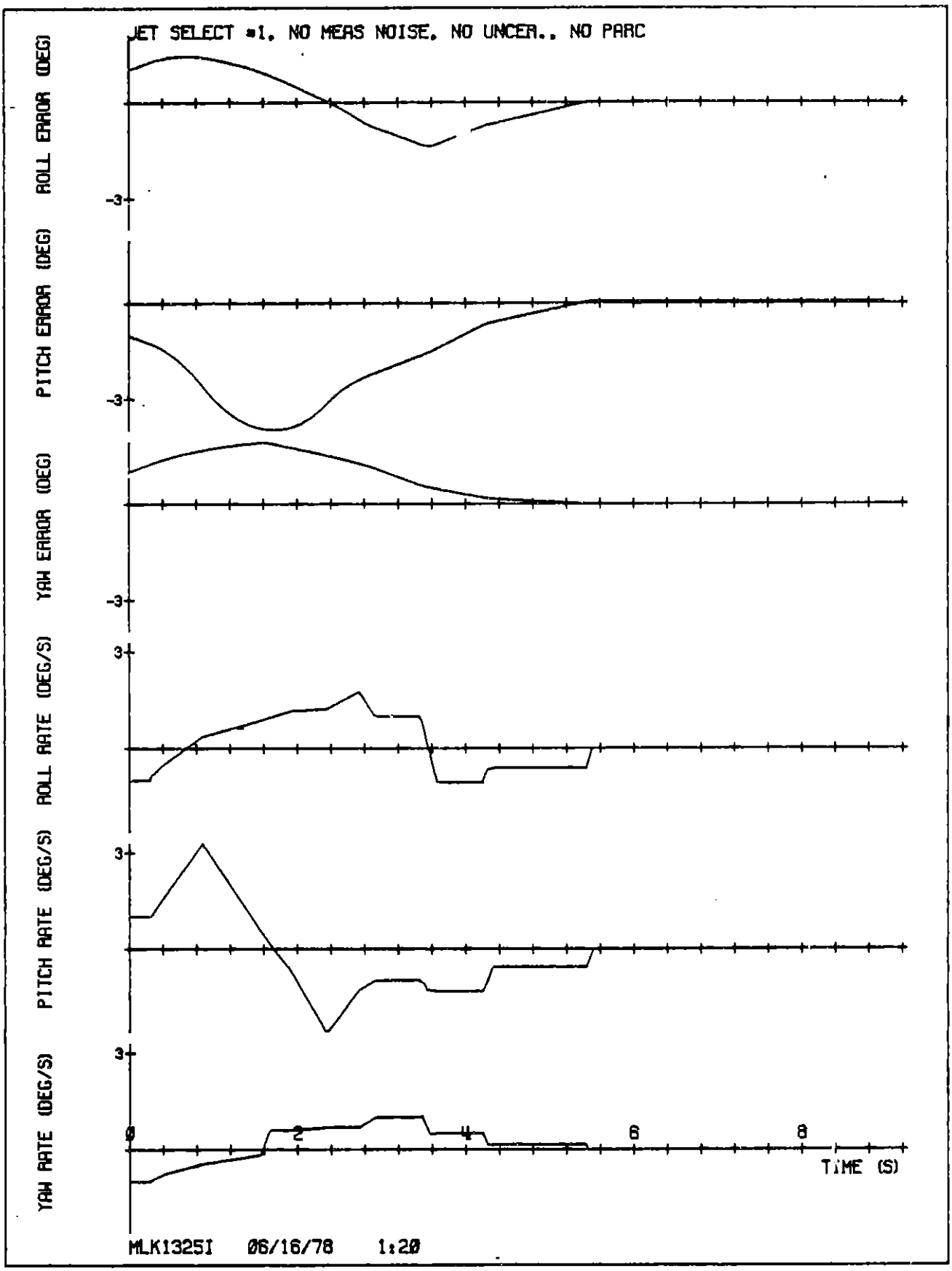

Figure 7.9. (Sheet 1 of 3).

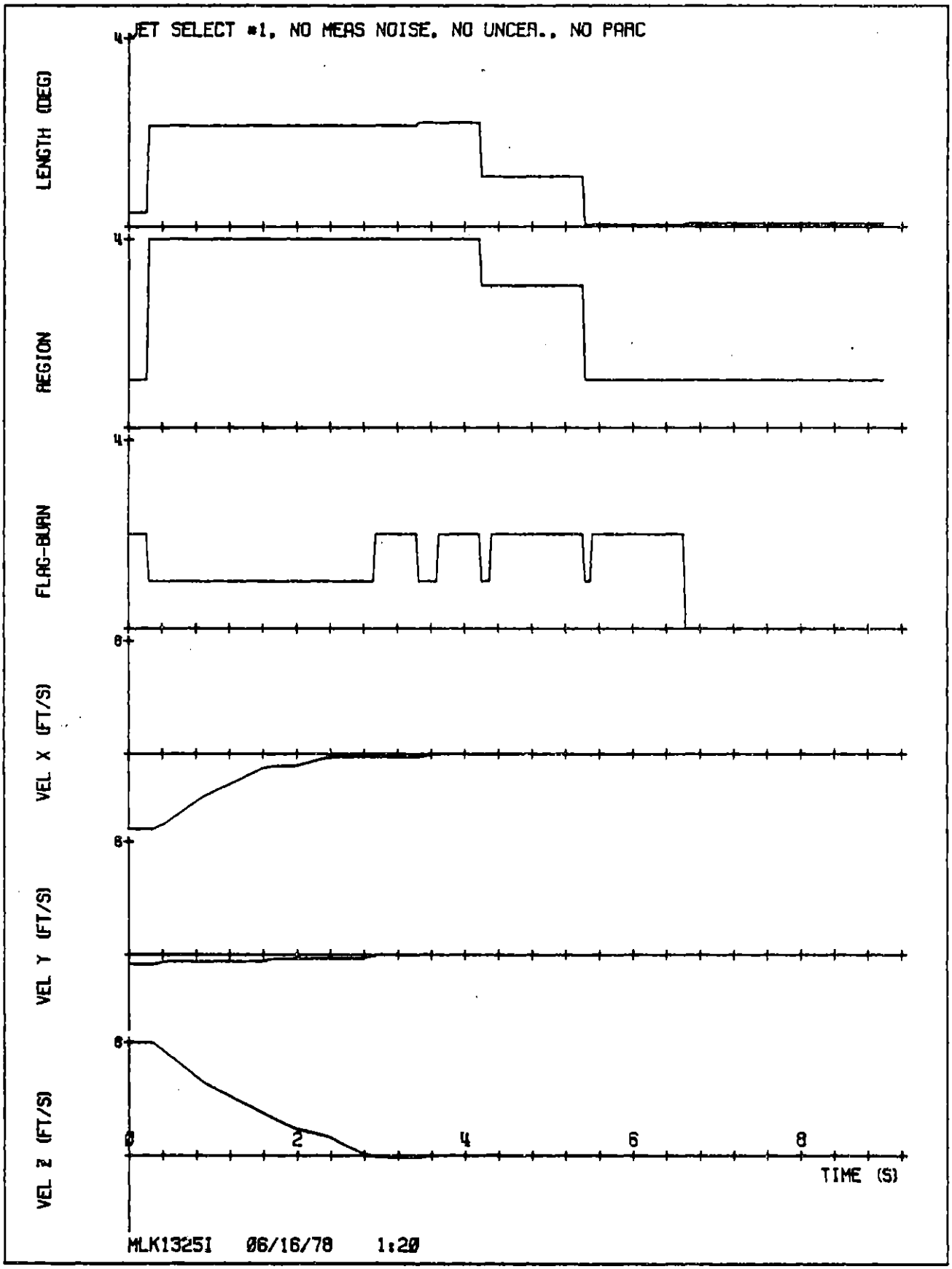

Figure 7.9. (Sheet 2 of 3).

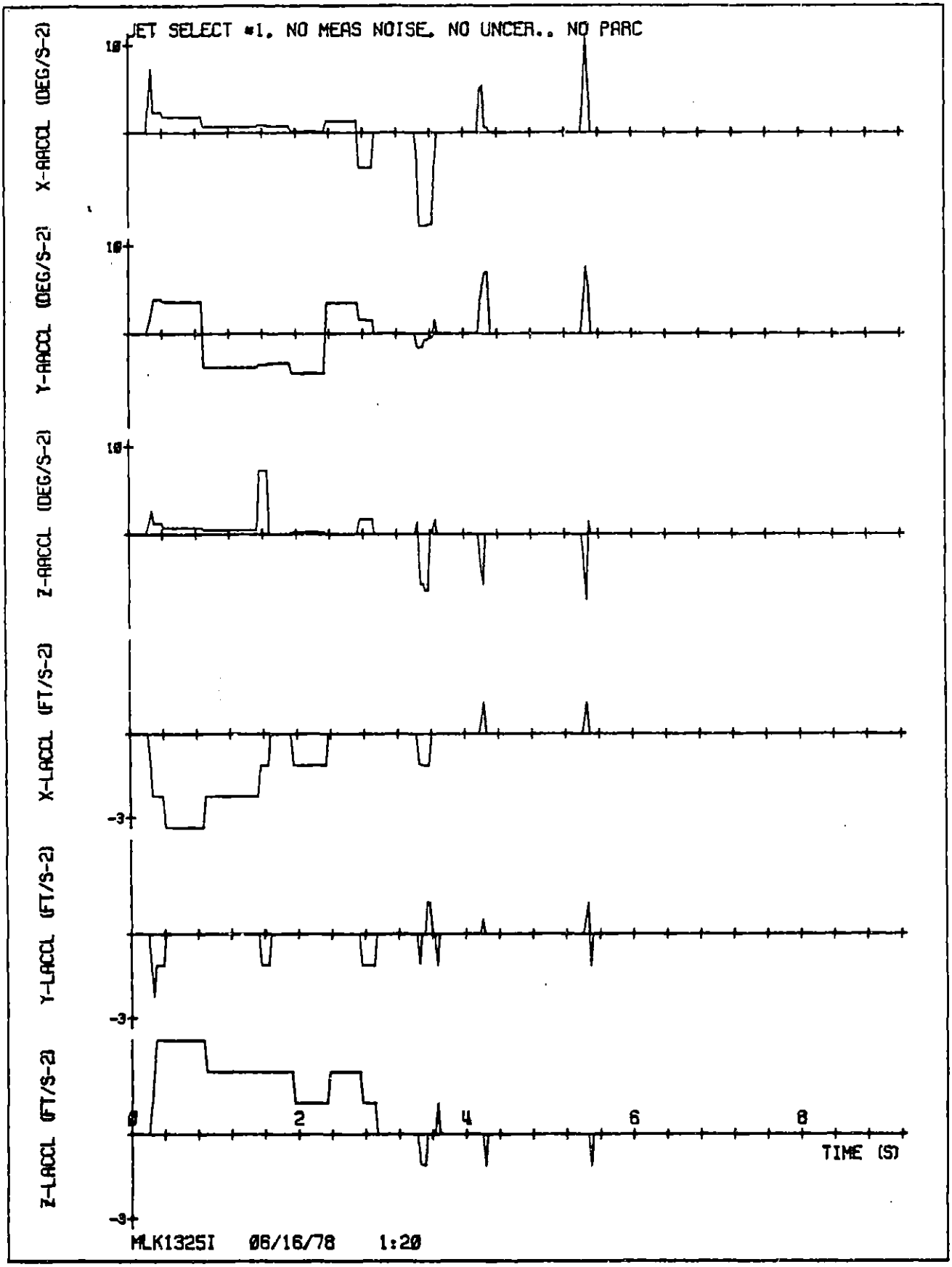

Figure 7.9. (Sheet 3 of 3).

Figure 7.10. Pseudo inverse jet selection, initial conditions C, with parceling, no uncertainties (in IMU measurements, mass properties, or jet firings).

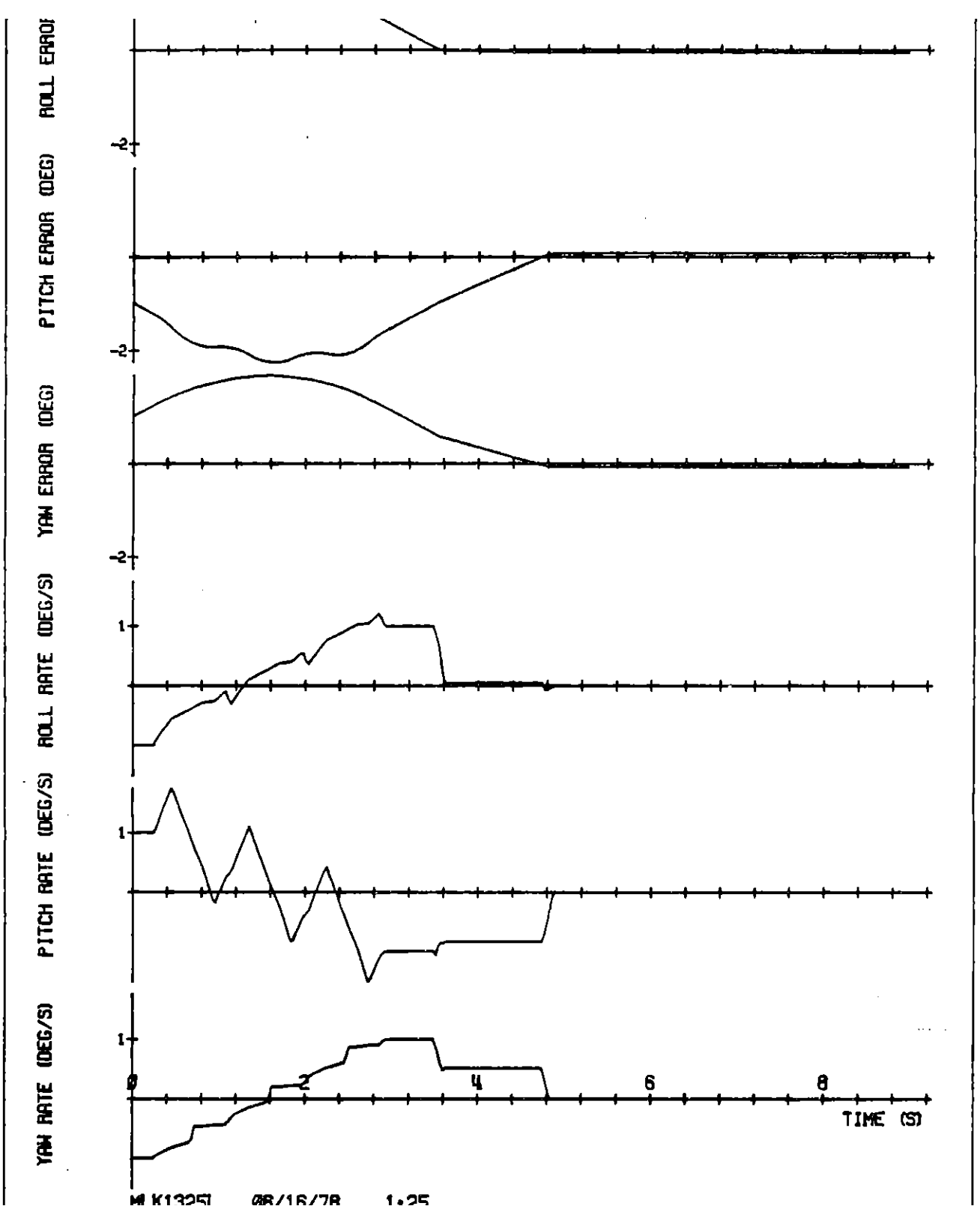
ROLL ERROR
PITCH ERROR (DEG)
YAW ERROR (DEG)
ROLL RATE (DEG/S)
PITCH RATE (DEG/S)
YAW RATE (DEG/S)
-2
-2
-2
1
1
1
0
2
4
6
8
TIME (S)
MK1325I 08/16/78 1:25

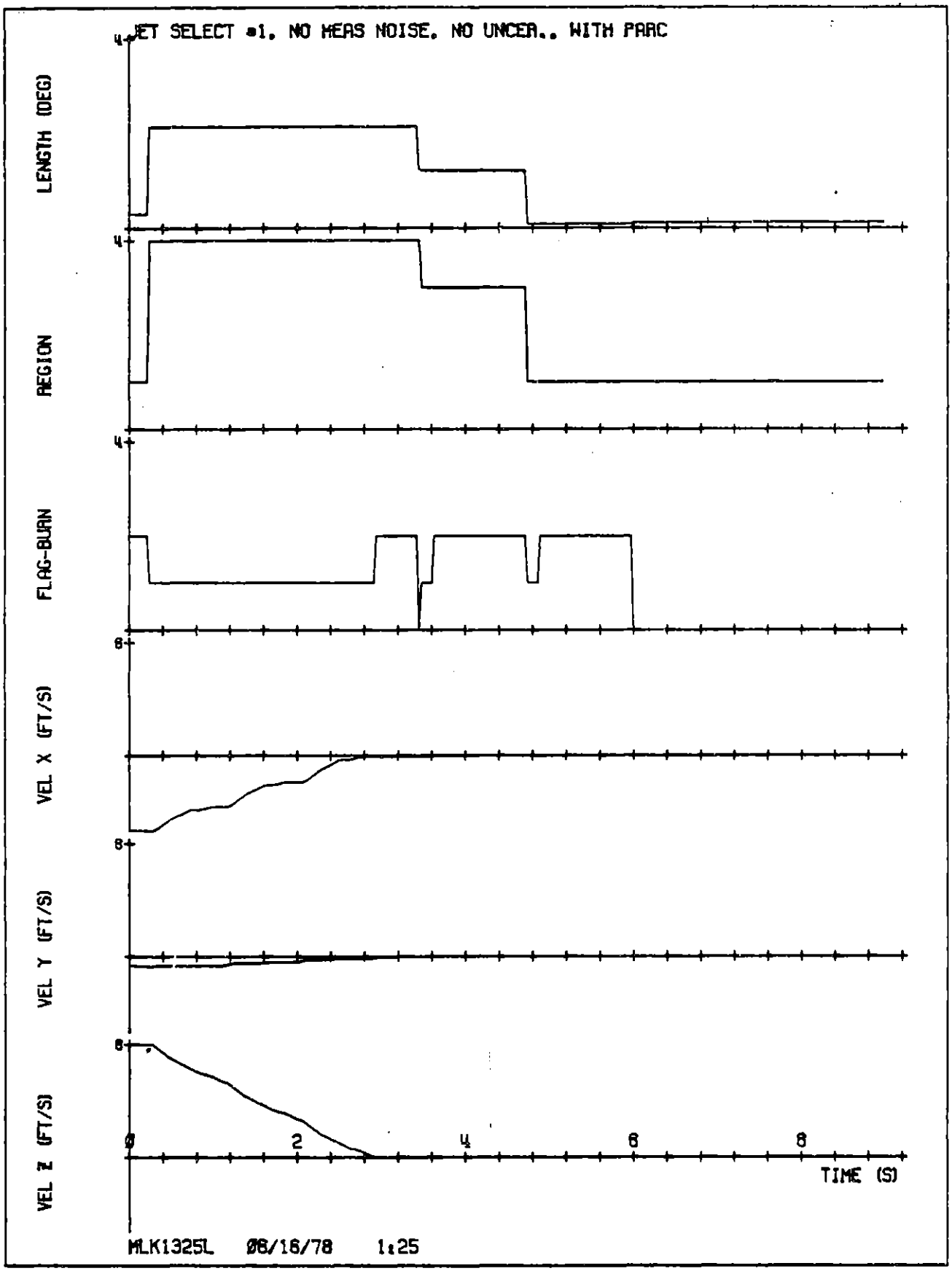

Figure 7.10. (Sheet 2 of 3).

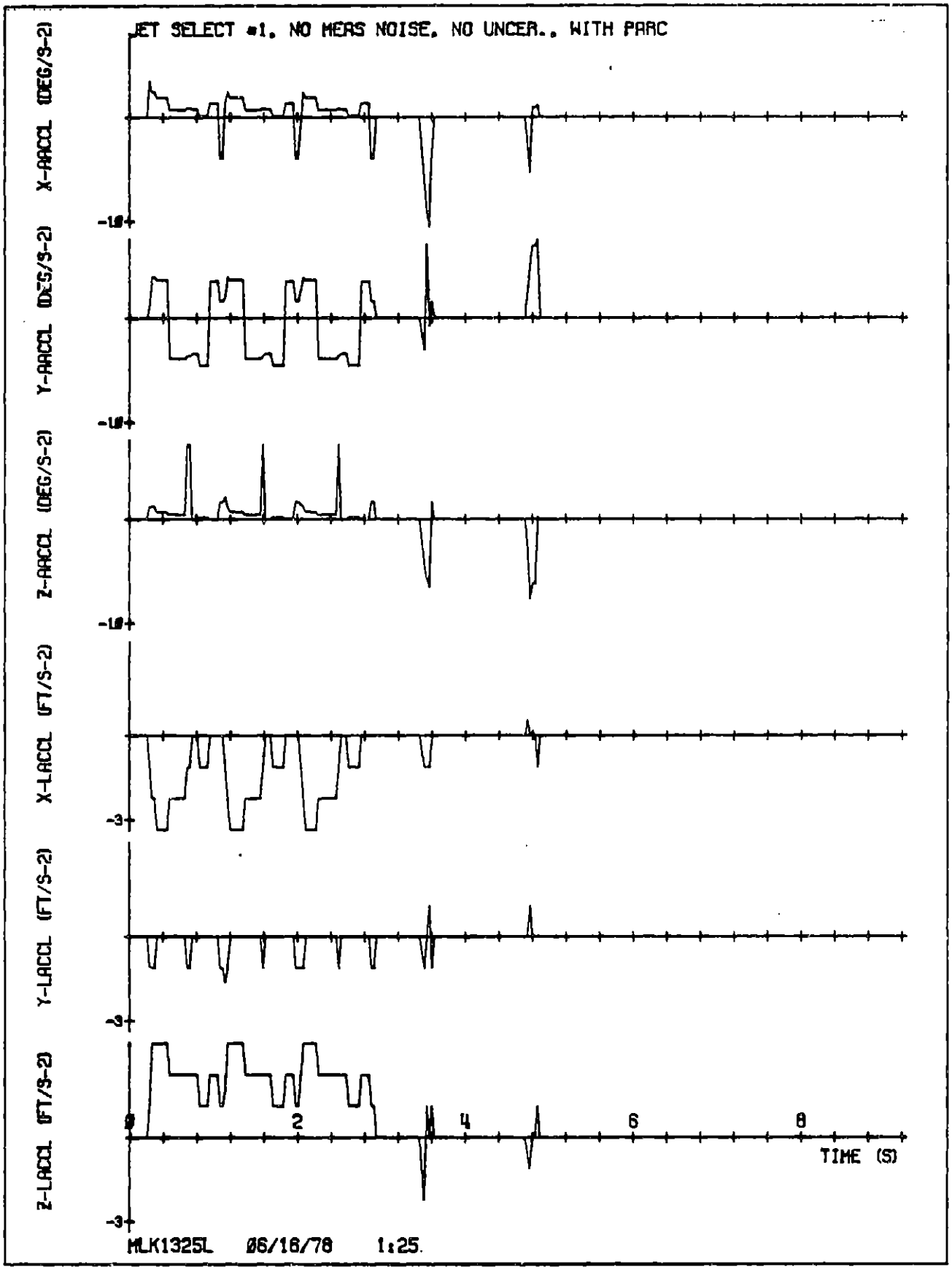

Figure 7.10. (Sheet 3 of 3).

Figure 7.11. Fixed jet selection procedure, initial conditions C, no parceling, no uncertainties (in IMU measurements, mass properties, or jet firings).

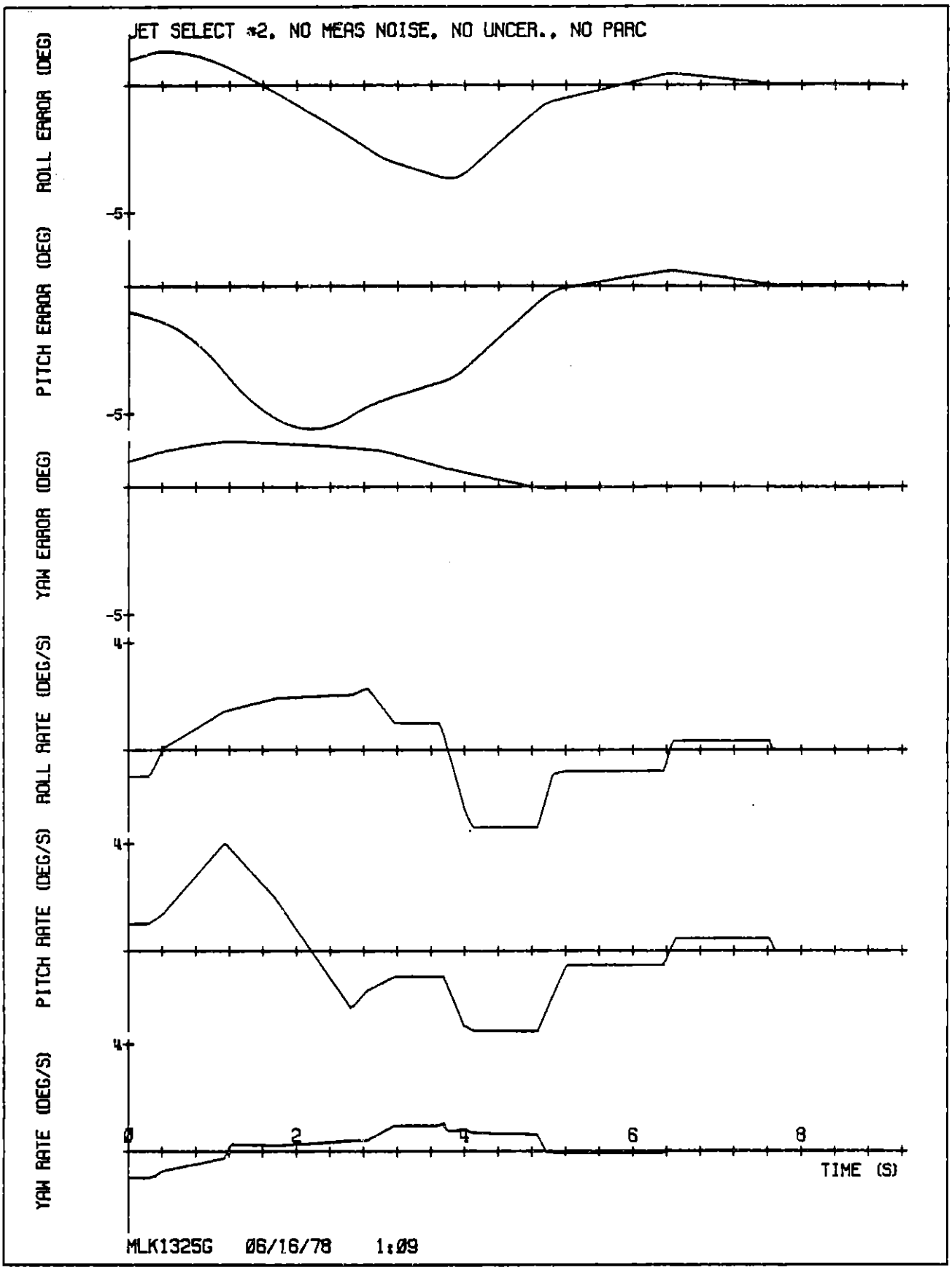

Figure 7.11. (Sheet 1 of 3).

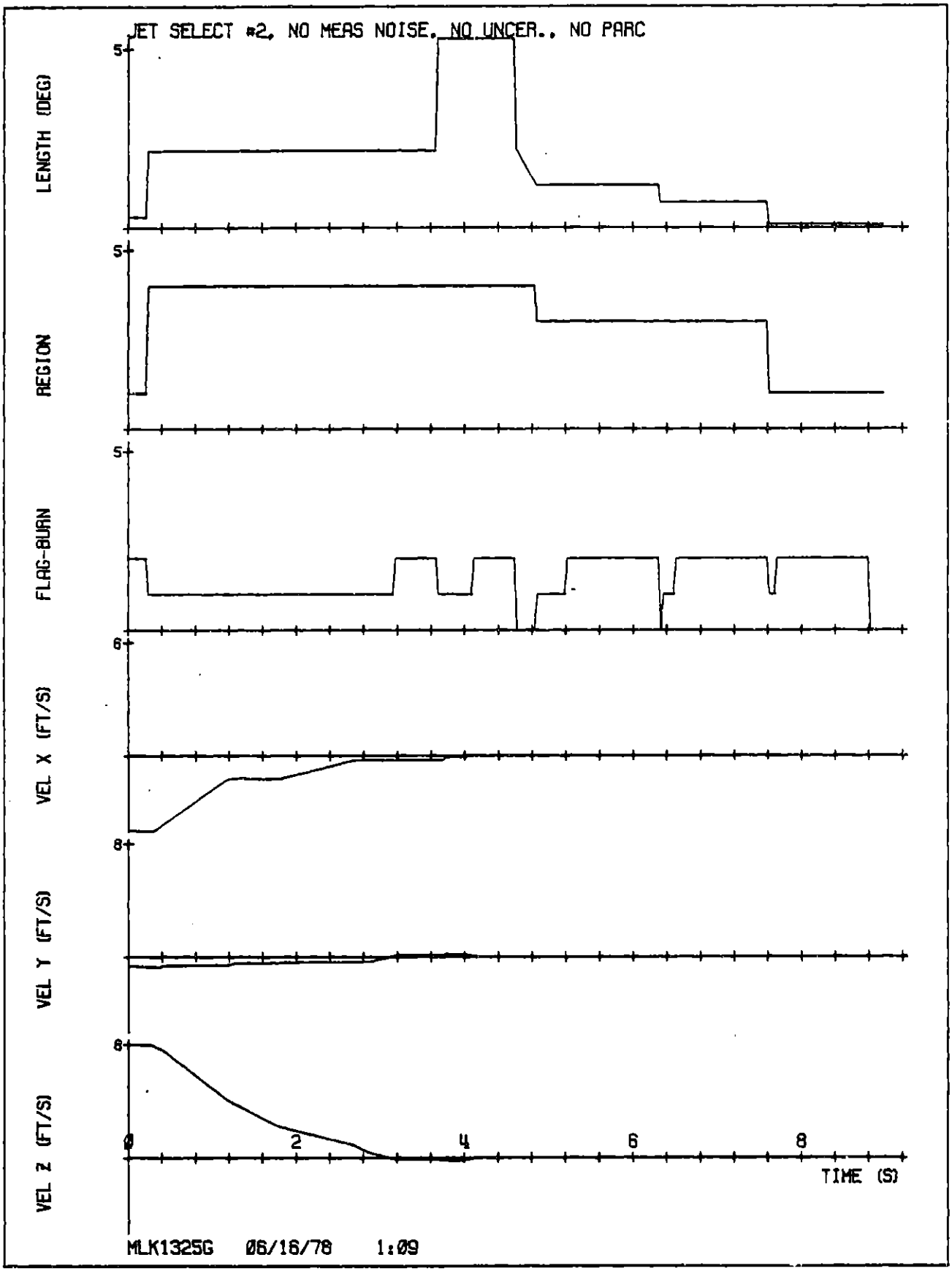

Figure 7.11. (Sheet 2 of 3).

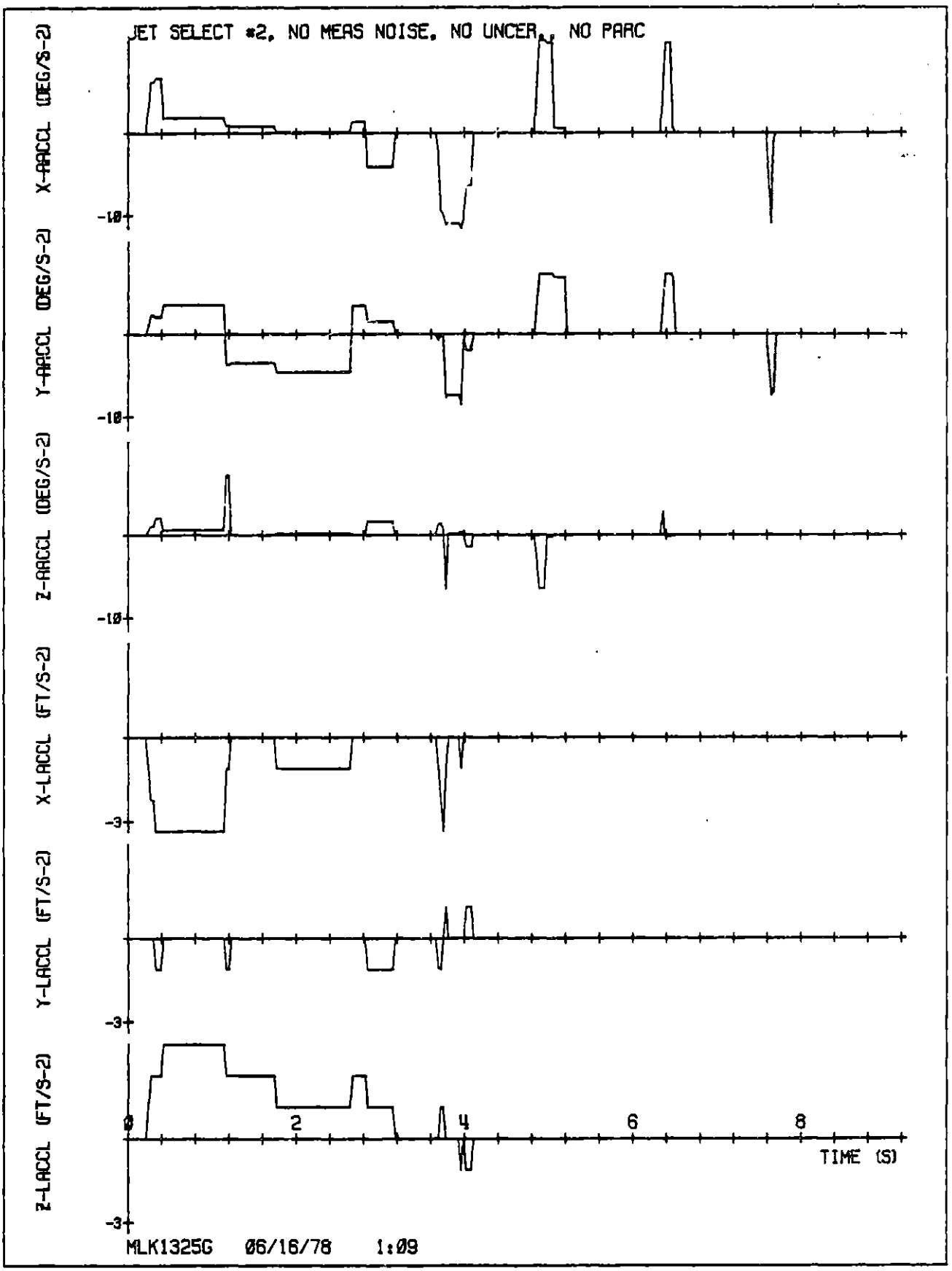

Figure 7.11. (Sheet 3 of 3).

Figure 7.12. Fixed jet selection procedure, initial conditions C, with parceling, no uncertainties (in IMU measurements, mass properties, or jet firings).

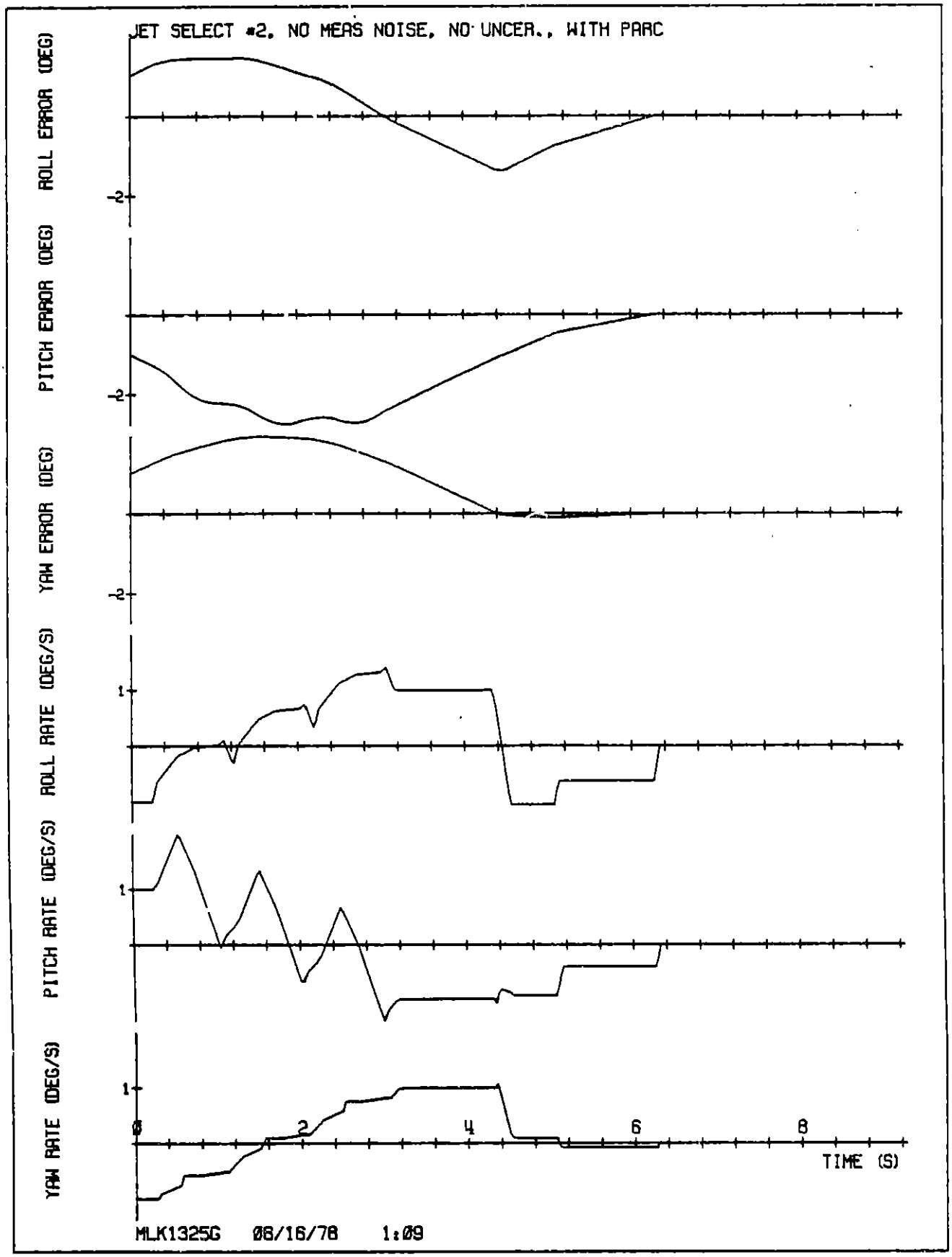

Figure 7.12. (Sheet 1 of 3).

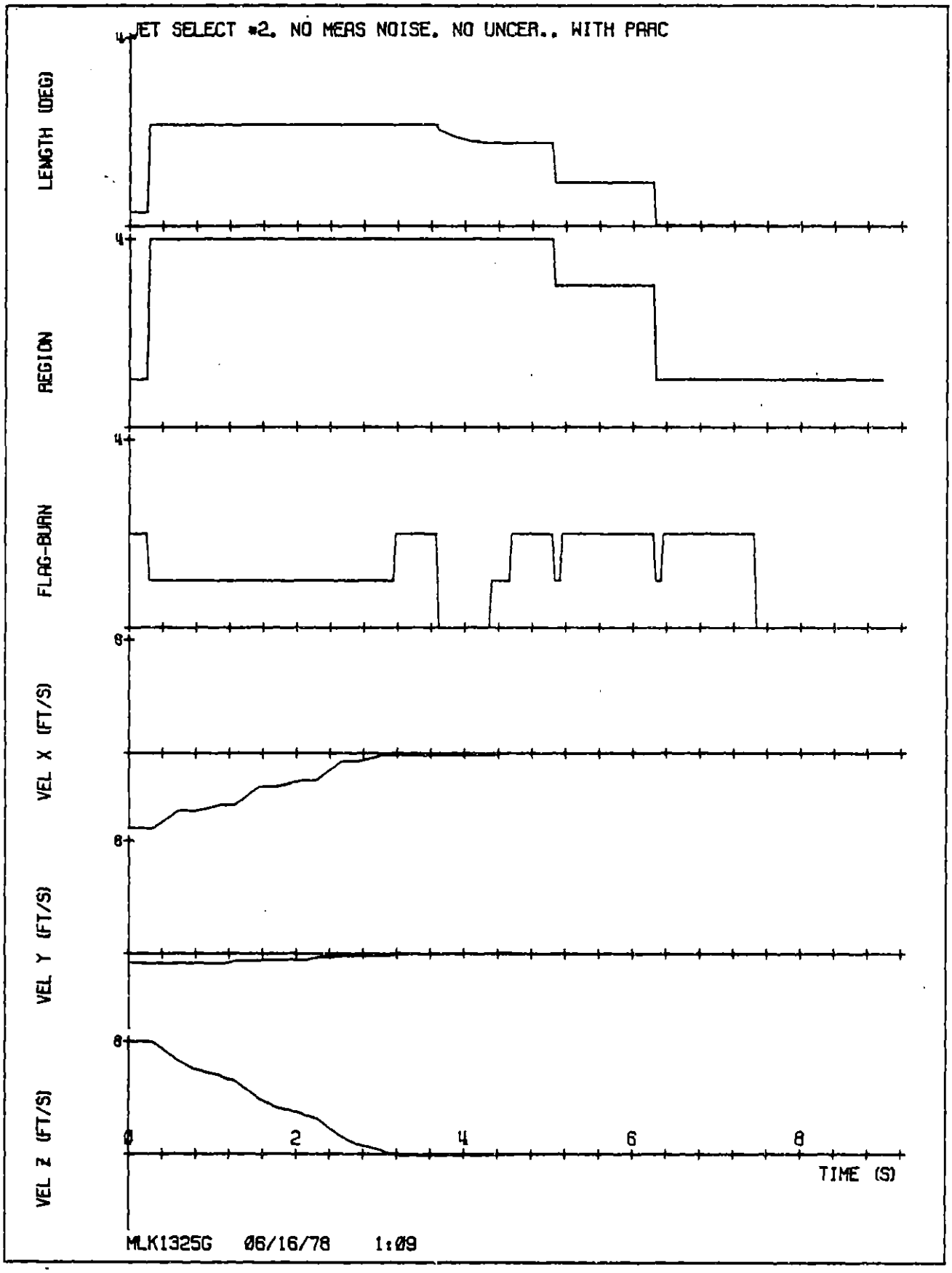

Figure 7.12. (Sheet 2 of 3).

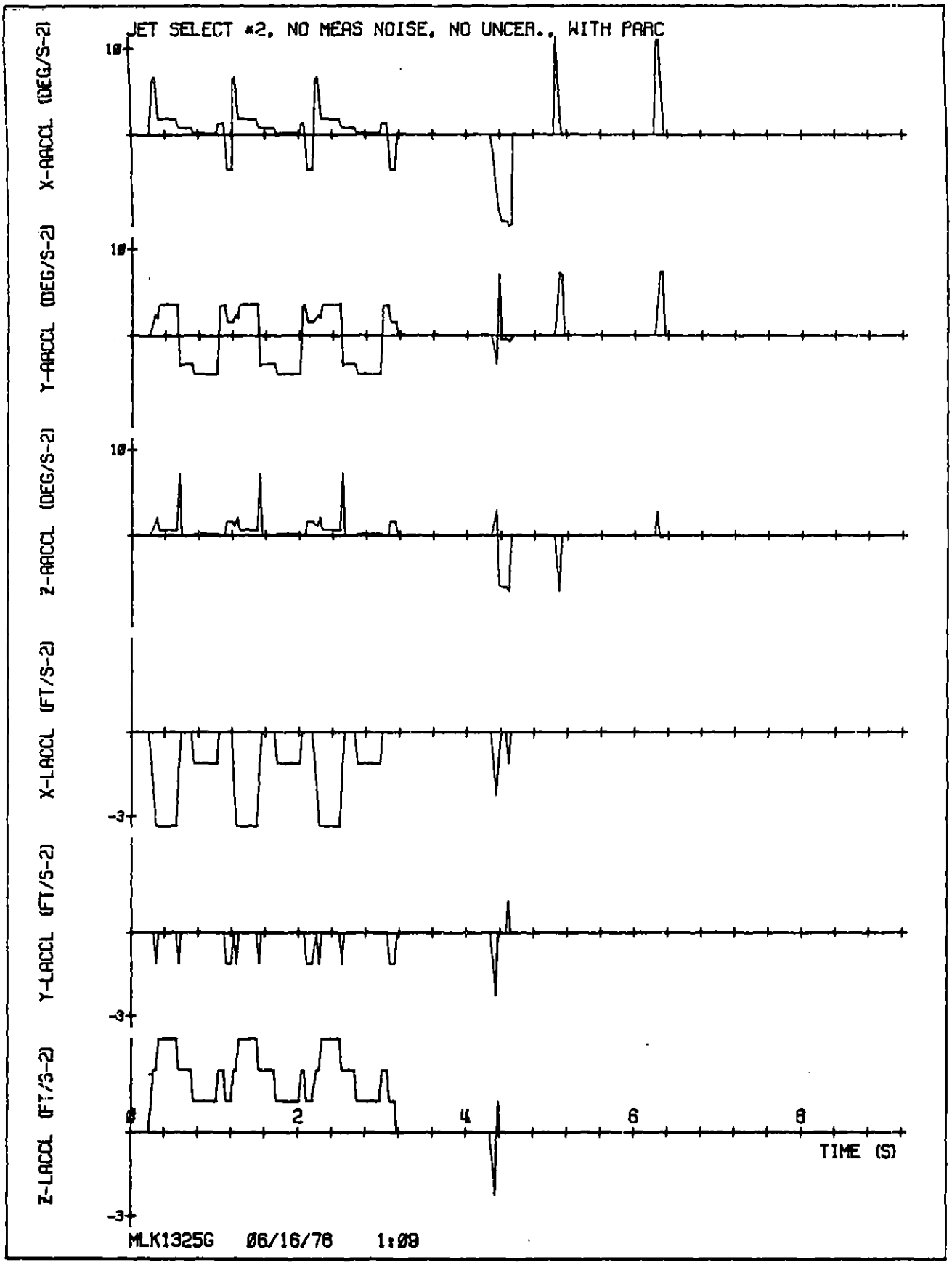

Figure 7.12. (Sheet 3 of 3).

Figure 7.13. Fixed jet selection procedure, initial conditions C, with parceling, with uncertainties (in IMU measurements, mass properties, and jet firings).

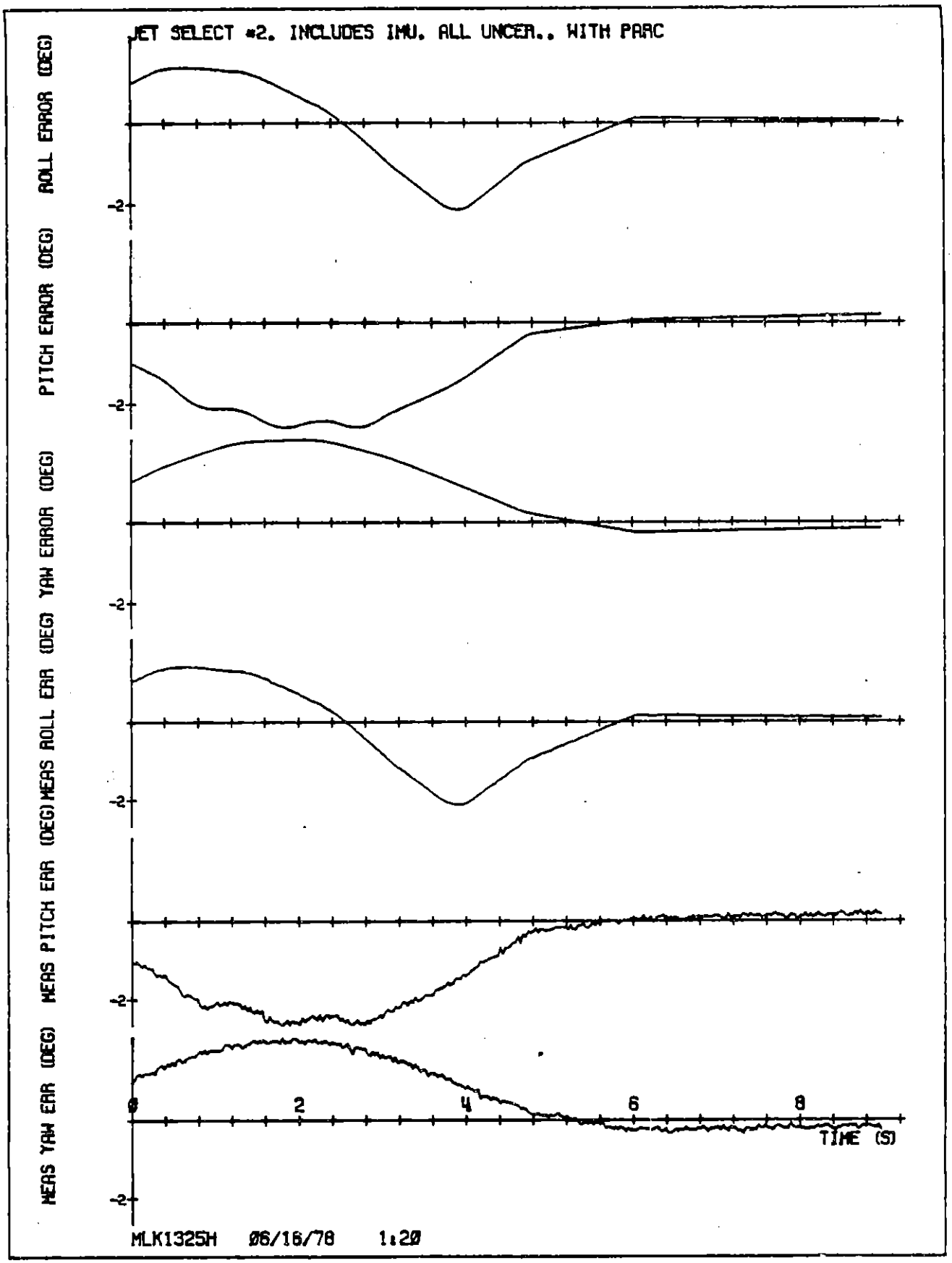

Figure 7.13. (Sheet 1 of 4).

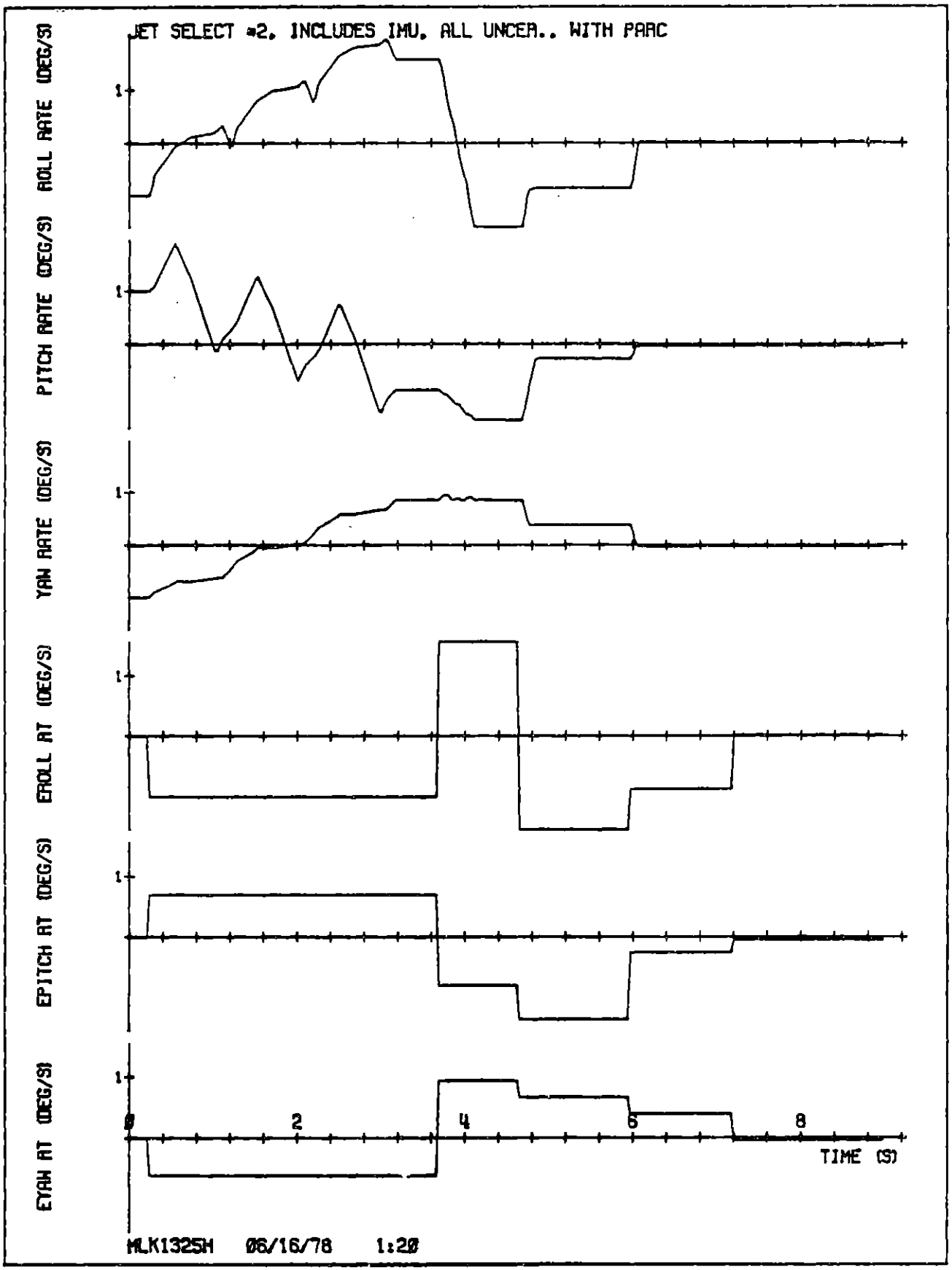

Figure 7.13. (Sheet 2 of 4).

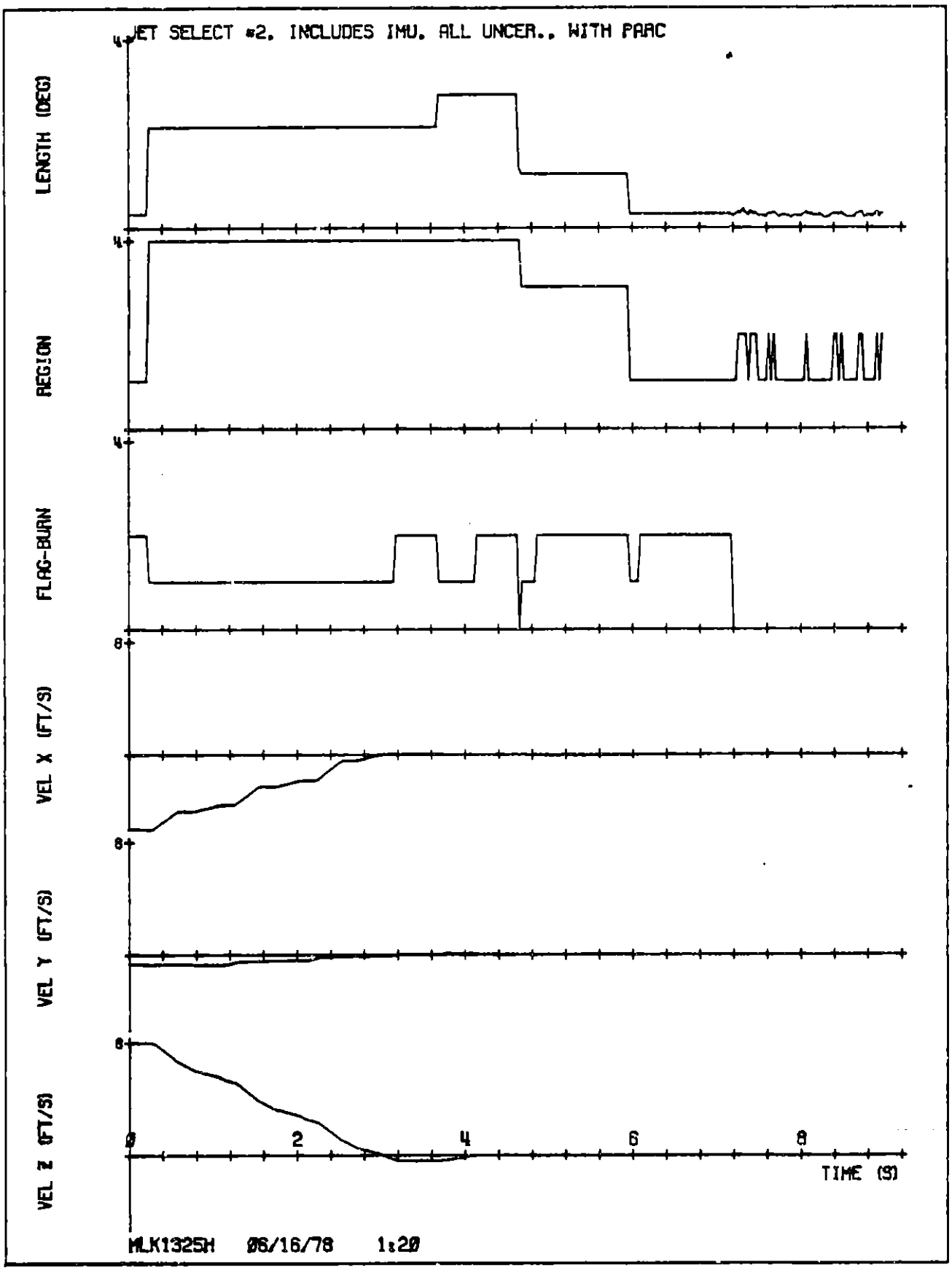

Figure 7.13. (Sheet 3 of 4).

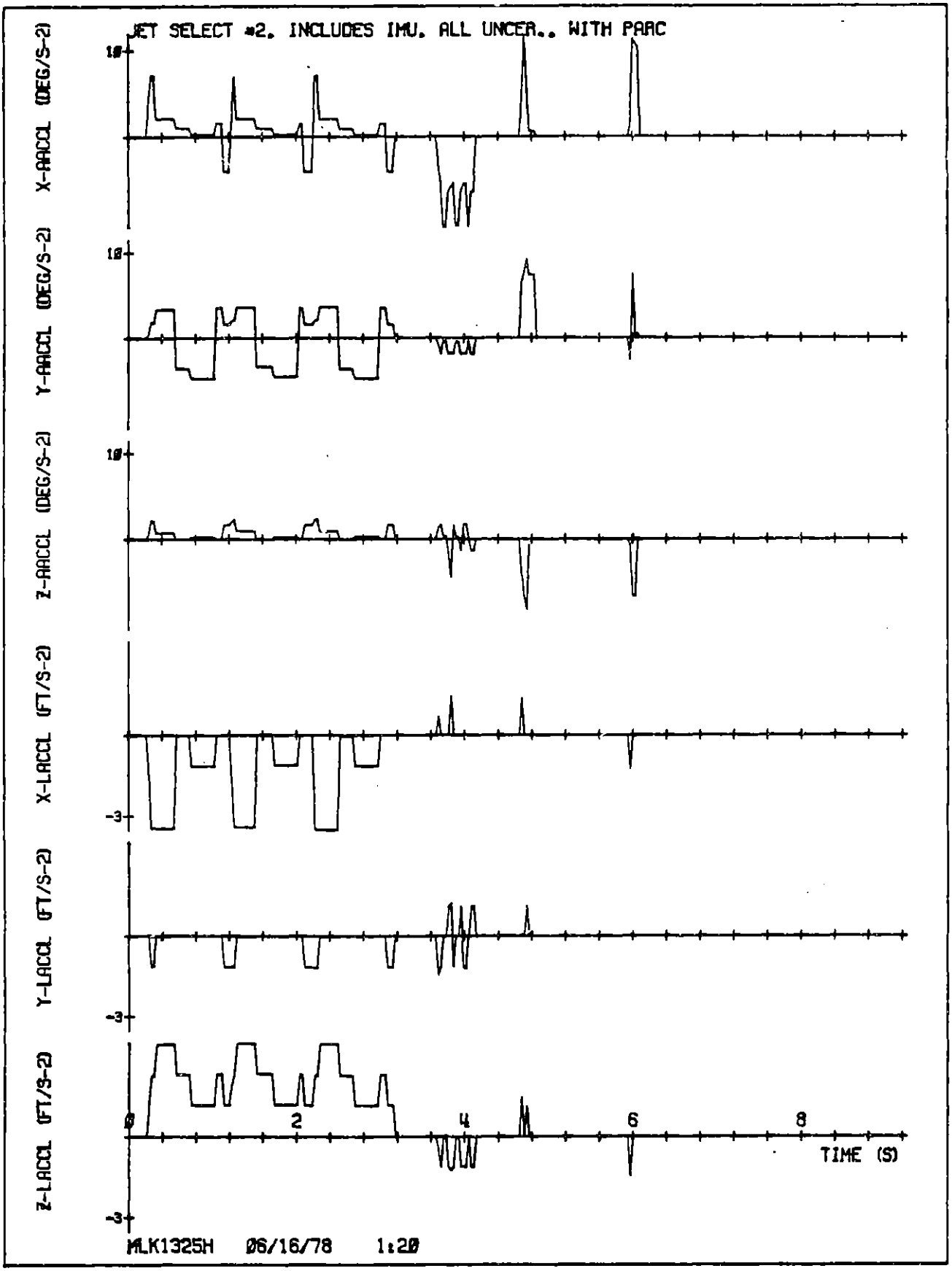

Figure 7.13. (Sheet 4 of 4).

CHAPTER 8

CONCLUSIONS

8.1 General

A phase space control approach which performs the three operations of rate estimation, control law computation, and jet selection separately, in a repeated sequence, has been shown to be well suited to the problem of precisely nulling initial attitude and motion errors of a jet-controlled spacecraft to rapidly achieve a desired end state of constant attitude and constant translational velocity. Some comments are offered below on the three autopilot operations, first on their design, performance, and possibilities for improvement, and second on their suitability for implementation in a modern digital flight computer.

8.2 Design and Performance Aspects

8.2.1 Jet Selection and Implementation of Jet Firing Times

In the simulation runs presented the two jet selection procedures provide comparable performance but the total on-times of all the jets is less for the pseudo inverse than for the fixed jet selection procedure (see Table 7-1).

In those particular cases where large translational velocity change requests require long firing times for some of the jets, the resulting attitude and attitude rate excursions can be quite large. These excursions are slightly larger on the average for the fixed jet selection procedure than for the pseudo inverse. However in either case,

it has been possible to reduce these excursions in attitude and attitude rate by a factor of two or more by parceling the jet firing times. The process of parceling increases the computation time and memory requirements as implemented in the present design. It would be possible to eliminate these requirements by using a different approach. This approach would compute a set of jet firings for one-third of the rate change request vector, $\underline{\Omega}$, and then implement these firings three times in succession without intermediate periods of coasting.

Some benefits might be realized by redesigning the fixed jet selection algorithm to consider all components of the rate change request vector initially and to use different combinations of jets to provide translation depending on the rotational requirements.

Although the pseudo inverse method is more efficient in its utilization of jets than the fixed jet selection routine considered in this thesis, the pseudo inverse method needs improvement in two areas before it can be considered a practical approach for the phase space autopilot. First, the problem of encountering a singular matrix must be resolved—either by eliminating the possibility in the redesign of the pseudo inverse method or by providing an alternative jet selection procedure when the singular matrix occurs (see Section 4.2,). Second, the number of arithmetic operations required for each jet selection must be reduced to make it more competitive with other approaches such as the fixed jet selection routine in the utilization of the flight computer. The present "trial-and-error" approach to selecting the final set of jets in the pseudo-inverse solution should be re-examined with a view to reducing the number of iterations and avoiding the problem of a singular matrix.

8.2.2 Rate Estimation

The effects of each individual source of error in the autopilot were investigated separately and compared to the case where there were no uncertainties at all. However these detailed comparisons are not

presented in this thesis because it was found that the performance of the system was not appreciably more sensitive to the errors when taken all together. The errors in the autopilot modeling of mass properties and jet firings were therefore included with IMU measurement errors in runs made to compare the performance of the system in the presence of all these errors with the performance without these error sources. The coasting periods in which rate estimates were made were kept the same in the comparative simulation runs regardless of whether IMU errors were included. The estimations of angular rate and translational velocity were sufficiently accurate that the convergence times in the presence of IMU errors did not differ appreciably from the convergence times without these errors (see Table 7-1). It is possible that the convergence times might be further optimized by revisions in the lengths of individual rate estimation periods based on detailed Monte Carlo studies.

8.2.3 The Control Law

The choice of the number of attitude error spheres and their radii was somewhat arbitrary, but the design chosen and integrated with the coast-period rate estimation does provide adequate results as shown in Chapter 7. Further optimization of the control law should be carried out simultaneously with the optimization of rate estimation in a Monte Carlo series of runs. One possible revision is to combine Regions 3 and 4 into one region and reduce to two the number of different length estimation periods used.

It should be emphasized that the assumption that the attitude error vector, $\underline{\theta}_e$, does not change in direction or magnitude during jet firings tends to be less accurate for long firings and becomes increasingly more accurate as the firings times approach zero. The first set of jet firings may be of long duration, particularly when the requested changes in translational velocities are large. The resulting $\underline{\theta}_e$ vector at the end of the first set of firings may not be parallel with the angular rate vector, $\underline{\omega}$ established at this time, with the result that

the vehicle may not be moving a direction to null out $\underline{\theta}_e$ during the subsequent coast period. However, it has been found that if the change in $\underline{\theta}_e$ for this initially long burn can be sufficiently bounded (e.g., by parceling jet firing times), then the initial change in $\underline{\theta}_e$ will not adversely affect the autopilot convergence times. The assumption of constant $\underline{\theta}_e$ becomes much better toward the end of the nulling maneuver when the angular rates are small and when the requested changes in angular and translational rates are small (i.e., the jet firing times are short).

The assumptions that the jets produce forces in constant directions in inertial space and that the angular velocity coupling effects are negligible also become progressively better as the attitude error approaches its deadband and the angular rates are reduced.

It might be possible to obtain nearly parallel $\underline{\omega}$, $\underline{\theta}_e$ vectors at the conclusion of a long set of firings by taking into account the anticipated effects of these firings on $\underline{\theta}_e$ when determining the rate change request vector. This might require iteratively performing the computations of the control law and jet selection until a set of jet firings is computed which will result in an almost parallel pair of $\underline{\theta}_e$, $\underline{\omega}$ vectors.

8.3 Computer Implementation

Although the phase space autopilot relationships have been programmed only in a general purpose programming language, it is possible to estimate in a rough way two aspects of the autopilot's implementation in a flight computer. First is the computation time that might be required for autopilot operations in a modern flight computer. Second is the requirement for storage of program constants and variables (not for storage of the program itself). For these purposes a flight computer was assumed which has a single address architecture and which has execution times equal to those of the Honeywell 701P computer, as listed in Table 8-1.

Table 8-1. Assumed execution times.

	Execution Time (μsec)
Load	3.25
Store	3.25
Add or subtract	4.45
Multiply	14.3
Divide	12.85
Change sign	3.25
Absolute value	3.25
Branch	3.00
Modify by increment	3.25

The number of storage locations which need to be committed to specific constants and variables during the operation of the phase space autopilot was estimated to be 71. An additional 39 storage locations were estimated to be required for temporary storage of variables during the various autopilot operations. These estimations do not include the operations for computing mass properties or for determining jet acceleration capabilities. The processing of IMU data to generate the body angle increment vector $\underline{\Delta\theta}$ is also omitted.

One of the very important features of the phase space autopilot is the very low burden which it places on computer time. The estimations of angular rate and translational velocity require very little computation time because they are carried out during coast periods where simple averaging procedures are sufficient for estimation. The control law and jet selection computations are together more complex than the rate estimation computation, but since they are performed less than once a second in typical nulling maneuvers, their impact on average computation-time requirements is quite small.

Estimated computation times for the various phase space autopilot operations are listed in Table 8-2. Here it may be noted that the time which has been estimated for a worst case pseudo inverse jet selection (based on the "one-jet-at-a-time elimination procedure") overshadows all other listed computation times. However, even this large computation time might not be a major drawback in cases such as illustrated in this thesis, where less than one jet selection per second is required. On the other hand, the fixed jet selection routine, which would probably be adequate for many applications, requires very little computation time and also offers a strong advantage of simplicity in implementation. Total computation time estimates given below were made for the case of the fixed jet selection routine.

The total computation time required in Run 4 of Chapter 7, where the fixed jet selection routine is employed without parceling, is computed as follows from the data in Table 8-2:

5 estimation periods × 0.83 ms/period for final pass	=	4.15
115 intermediate estimation passes × 0.13 ms/pass	=	14.95
1 control law pass without jet selection criteria satisfied × 0.14 ms/pass	=	0.14
4 control law passes with jet selection criteria satisfied × 0.77 ms/pass	=	3.08
4 jet section passes × 1.50 ms/pass	=	6.00
Total computation time	≅	28 ms

The nulling maneuver converged in 4.92 sec, which means that the average utilization of the computer for autopilot computations was only 0.028/4.92 = 0.0057 or 0.57%.

The total computation time required in Run 13 of Chapter 7, where the fixed jet selection routine was employed with parceling of the jet firing times in the first two burns is computed as follows from the data in Table 8-2:

5	estimation periods × 0.83 ms/period for final pass =	4.15
115	intermediate estimation passes × 0.13 ms/pass =	14.95
1	control law pass without jet selection criteria satisified × 0.14 ms/pass =	0.14
4	control law passes with jet selection criteria satisifed × 0.77 ms/pass =	3.08
4	jet selection passes × 1.50 ms/pass =	6.00
2	computations of parceled jet firing times × 1.84/ computation =	3.68
	Total computation time ≐	32 ms

This nulling maneuver converged in 7.20 sec, so the average utilization of the computer for autopilot operations was only .032/7.20 = 0.0044 or 0.44%.

It should be pointed out that the largest burden on the flight computer would occur during an autopilot cycle in which the estimated rates were computed, control law computations were performed, jet selection was carried out and the resulting jet firing times were parceled. This would require 4.94 ms. The peak burden is reduced to 3.10 ms when parceling is not performed. The first case might occur only once or twice in a nulling maneuver, and the second case might occur six times. The peak burden (i.e., with parceling) of 4.94 ms is only 16% of a 30 ms autopilot cycle, which would certainly be acceptable. As previously calculated for two simulation runs, the average computation time burden may be only ~ 0.6%.

While these estimations of computation time are very crude, they do show conclusively that the phase space autopilot places a very low computation-time burden on the flight computer.

Table 8-2. Computation time estimates.

Autopilot Operations	Estimated Computation Time (ms)
Estimation of Angular and Translational Velocities	
Intermediate passes	0.13
Final pass	0.83
Control Law	
When criteria for jet selections are:	
Not satisfied	0.14
Satisfied	0.77
Jet Selection	
Fixed Jet selection Routine:	
Unadjusted firing times	0.90 } 1.50
Adjustment of firing times	0.60 }
Pseudo Inverse Jet Selection Procedure	
Unadjusted firing times	100 } 100.60
Adjustment of firing times	0.60 }
Parceling of Firing Times (including adjustment of firing times)	1.84

REFERENCES

1. Guidance System Operations Plan for Manned LM Earth Orbital and Lunar Missions Using Program Luminary 1E, Charles Stark Draper Laboratory Report R-567, February 1971, pp. 3.4-1 to 3.4-48.

2. Guidance System Operations Plan for Manned CM Earth Orbital and Lunar Missions Using Program Colossus 3, (Rev. 14), Charles r Stark Draper Laboratory Report R-577, March 1972, pp. 3.2-1 to 3.2-49.

3. Bergmann, E.V., A New Spacecraft Autopilot, Charles Stark Draper Laboratory Report T-628, May 1976.

4. Bergmann, E.V., "Pseudo Inverse Jet Select", Charles Stark Draper Laboratory Memo, September 1977.

5. Zadeh, L., and DeSoer, C.A., Linear System Theory: The State Space Approach, New York, McGraw-Hill, 1963.

6. D'Amario, L.A., and Stubbs, G.S., A Single-Rotation-Axis Digital Autopilot Design which Compensates for Nonlinear Rotational Dynamics in Rapid Attitude Maneuvers of a Space Vehicle, Charles Stark Draper Laboratory Report P-377, December 1976.